공학박사학위논문

A study on the fabrication of fluorescent sensors using molecularly imprinted nano-sized particles and fibers

분자인식 나노재료를 이용한 형광센서 제조에 관한 연구

2016년 2월

서울대학교 대학원

재료공학부

김 영 도

A study on the fabrication of fluorescent sensors using molecularly imprinted nano-sized particles and fibers

분자인식 나노재료를 이용한 형광센서 제조에 관한 연구

지도교수 장 지 영

이 논문을 공학박사 학위논문으로 제출함
2015년 10월

서울대학교 대학원
재료공학부
김 영 도

김영도의 공학박사 학위논문을 인준함
2015년 12월

위 원 장 조 원 호 (인)

부위원장 장 지 영 (인)

위 원 박 종 래 (인)

위 원 안 철 희 (인)

위 원 임 순 호 (인)

Abstract

A study on the fabrication of fluorescent sensors using molecularly imprinted nano-sized particles and fibers

Youngdo Kim

Department of Materials Science and Engineering

Seoul National University

Molecular imprinting has been considered as a practical way to produce materials with molecular recognition properties due to its ease of use and low cost. In this study, the fluorescent sensors based on molecularly imprinted nanomaterials were developed using various fluorescent materials as a signal transducer.

Firstly, a highly sensitive molecularly imprinted fluorescent sensor was prepared by using a CdSe quantum dot (QD) as a signal transducer and a mesoporous silica nanoparticle as an imprinting material. Bisphenol A (BPA) was chosen as a model template, which is known as an endocrine disruptor. Binding sites were selectively formed between the pores and CdSe QDs were encapsulated in the pores of the mesoporous silica. QD-encapsulated, molecularly imprinted mesoporous silica particles (QD-MIMS) exhibited excellent molecular recognition properties in terms of both sensitivity and selectivity. Owing to the proximity of the binding sites to the QDs, a significant, concentration-sensitive fluorescence quenching was observed in the presence of BPA. QD-MIMS showed a linear Stern-Volmer relationship for BPA and its analogs. QD-MIMS had a much larger quenching constant for BPA (by more than ten times) than for BPA analogs, demonstrating the high selectivity of QD-MIMS.

Secondly, a molecularly imprinted polymer-based fluorescent sensor was fabricated through an organogelation process. The sensor was comprised of a molecularly imprinted nanofiber as a receptor and a CdSe/ZnS quantum dot as a signal transducer. Histamine was selected as a model template. An organogelator with two different polymerizable groups, an acrylate and a diacetylene was successfully synthesized. As a functional monomer for complexation with the template, an acrylate having a carboxyl group was used. The QD and template-containing organogel formed in *n*-decane was polymerized in the presence of a photoinitiator and a cross-linker by UV irradiation to produce highly cross-linked organogel nanofibers. The template molecules were removed by extraction with methanol/acetic acid (9:1 v/v) to give the QD-incorporated, histamine imprinted organogel nanofibers (QD-HIOGNF). QD-HIOGNF showed high molecular recognition properties toward histamine in respects to both sensitivity and selectivity. The fluorescence intensity of QD-HIOGNF decreased sensitively as the concentration of histamine increased. QD-HIOGNF could be reused for sensing after removing the bound analytes.

Thirdly, a facile and versatile sensing assay of diethylstilbestrol (DES) was developed by fabricating a molecularly imprinted fullerene-silica nanocomposites (MIFSNCs). Fullerene encapsulated in a microemulsion with the aid of the non-ionic surfactant was incorporated into the silica network by the sol-gel reaction of triethyl orthosilicate and a triethoxysilane-DES complex as silica precursors. MIFSNCs exhibited a fast kinetic binding and high molecular recognition properties in terms of both sensitivity and selectivity. MIFSNCs showed a notable fluorescence quenching under all given concentrations of DES. On the other hand, non-imprinted fullerene-silica nanocomposites (NIFSNCs) showed only a few amount of quenching for the concentrations of DES.

Lastly, a molecularly imprinted mesoporous silica in which the tetraphenylethylene based AIE active chromophore was selectively introduced into the inner pore of the silica network was prepared. DES was chosen as a target molecule and connected to the triethoxysilane moieties *via* the thermally reversible urethane bonds. DES-selective imprinted cavities which have two-point binding sites were successfully formed between the pores of the silica framework by the sol-gel reaction and subsequent removal of DES. The AIE chromophore-grafted, DES imprinted mesoporous silica nanoparticles (TFPE-DIMS) showed a specific binding ability for the target template and a fast kinetic binding profile. The degree of fluorescence quenching of TFPE-DIMS was concentration-sensitive. The sensitivity and selectivity of TFPE-DIMS were estimated by the Stern-Volmer equation. TFPE-DIMS displayed a much larger Stern-Volmer quenching constant for DES than for DES analogs with a high molecular imprinting factor. TFPE-DIMS also showed a great recovery of its initial fluorescence intensity even after several extraction and rebinding cycles.

Keywords: Molecular imprinting, mesoporous silica, organogel, fullerene, quantum dot, fluorescence, luminescence, sensor.

Student Number: 2011-30182

Contents

List of Schemes

List of Figures

Figure V-5. Small angle XRD patterns of (a) DIMS-NH_2 and (b) TFPE-DIMS.

Figure V-6. (a) Fluorescence spectra of TFPE-DIMS and TFPE in DMSO. The spectrum of DIMS-NH_2 is measured for comparison. Concentration of AIE chromophore (TFPE): 10^{-5} M. Excitation wavelength (λ_{ex}): 350 nm. (b) Photographs of dispersions of TFPE-DIMS and DIMS-NH_2, and solution of TFPE in DMSO; photographs taken upon irradiation with a UV light of 365 nm.

Figure V-7. (a) UV-vis absorption spectrum of TFPE; (b) emission spectrum of TFPE-DIMS dispersed in methanol (λ_{ex} = 350 nm).

Figure V-8. (a) Kinetic binding profile of emission spectra of TFPE-DIMS (100 μg mL^{-1}) in the presence of DES (500 ng mL^{-1}) recorded after incubating for constant periods of time in methanol (λ_{ex} = 350 nm); (b) Plot of the maximum fluorescence intensity with respect to incubation time.

Figure V-9. Fluorescence emission spectra of (a) TFPE-DIMS (100 μg mL^{-1}) and (b) TFPE-NIMS recorded after 10 min stirring upon a gradual increase on the concentration of DES in methanol (λ_{ex} = 350 nm).

Figure V-10. (a) Cross-selectivity profile for DES and structurally related analogs in TFPE-DIMS (100 μg mL^{-1}) measured after 10 min stirring with an increase on the concentration of DES, DN, BPA and 4BP in methanol. Degree of quenching calculated as Quenching (%) = $(1 - F/F_0)100$. Stern-Volmer plots estimated from (b) TFPE-DIMS and (c) TFPE-NIMS.

Figure V-11. Estimated Stern-Volmer quenching constant (K_{SV}) of TFPE-DIMS and TFPE-NIMS in relation to different analytes. For all the experiments, the excitation wavelength was 350 nm.

Figure V-12. Reversible fluorescence quenching and reuse cycles upon the repeated extraction and rebinding of DES in the dispersion medium of TFPE-DIMS.

Chapter I.

Introduction

I-1. Molecular Imprinting

I-1-1. Principle of Molecular Imprinting

Since the development of host-guest chemistry,[1] the interest in the molecular recognition, binding process, control of chirality has grown. Among the related studies, a molecular imprinting is a feasible strategy to synthesize an artificial host, mimicking the natural receptor. During the process of the molecular imprinting, tailored recognition sites were formed in cross-linked polymeric matrices. Molecularly imprinted polymers (MIPs) have been widely investigated due to their applications in broad fields including separation, sensing, enzyme-like catalysis, solid-phase extraction and so on.[2-5]

Compared to the biological receptors, MIPs have several advantages. MIPs can be prepared quite easily by a large scale synthesis. Because of the rigidity of cross-linked structure, MIPs showed a moderate physical/chemical stability and inertness to the external environment. Moreover, they could be applied by chemical modification with ease to improve their binding properties. However, conventional MIPs prepared by a bulk polymerization had major shortcomings such as low sensitivity and poor site accessibility.[6-8]

MIPs were fabricated as the following procedures (Figure I-1). Firstly, (a) the model template was complexed with functional monomer *via* covalent or non-covalent bonding.

(b) The resulting complexes underwent the subsequent polymerization with suitable cross-linkers to form the cross-linked polymeric network. Lastly, (c) the template molecules were removed to generate the binding sites.

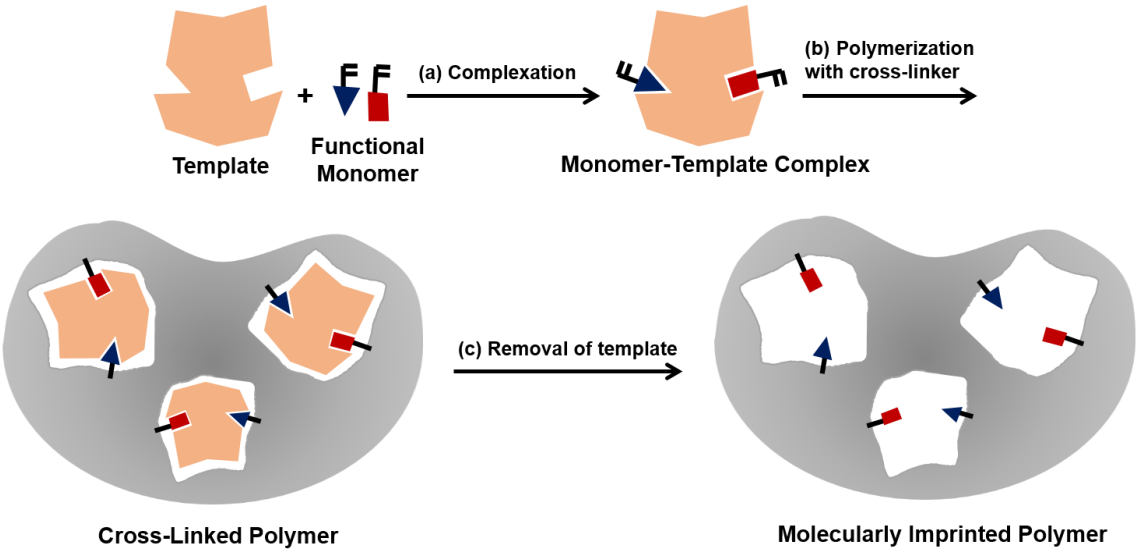

Figure I-1. Schematic procedure of the preparation of molecularly imprinted polymer.

The covalent imprinting technique was early developed by Wulff *et al.*[9] A boronate ester as a covalent linkage was used to form a template-functional monomer complex (Figure I-2a). They also used ketal and Schiff base formation to link the template and functional monomer by a covalent bonding (Figure I-2b and I-2c).[10,11] The covalent approach involved a stable covalent linkage between the template and monomer. This is why a fairly homogeneous cavity can be formed after the extraction of the template molecule. The functional group left in the cavity can interact with a target analyte during the rebinding process. However, the extraction of the target template usually required rather harsh conditions. The number of proper covalent bondings which are reversible was also limited.

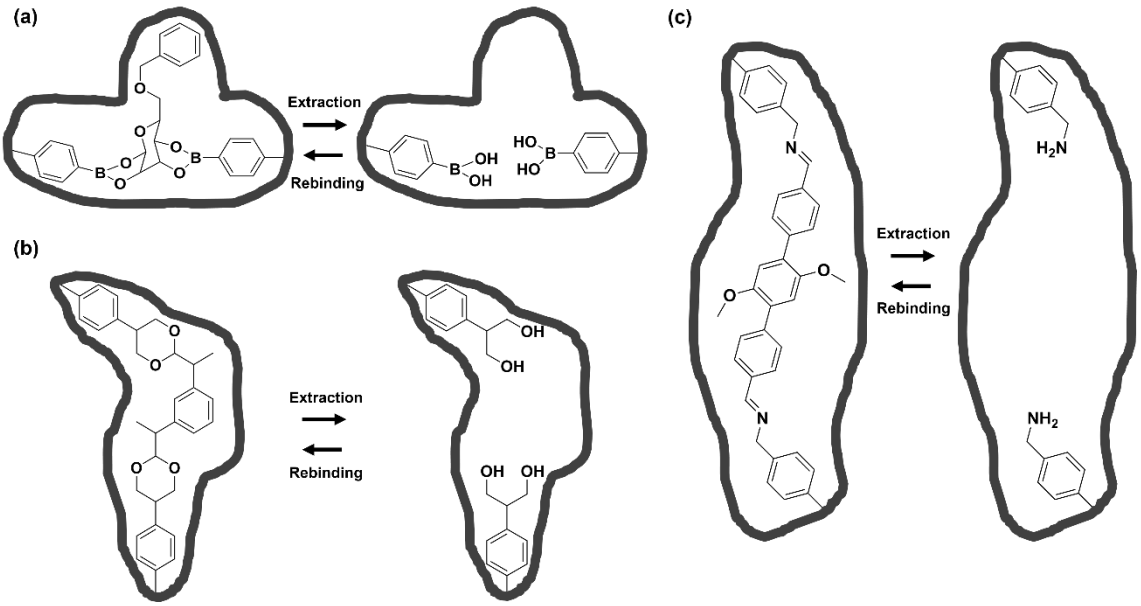

Figure I-2. Schematic designs of covalent imprinting approach based on (a) boronate ester, (b) ketal and (c) Schiff base.

The non-covalent imprinting method was pioneered by Mosbach and co-workers.[12,13] This approach used the template-functional monomer complex obtained from non-covalent interactions such as hydrogen bonds, ionic interactions, hydrophobic interactions, and metal-ion chelating interactions. For instance, guanidine-functionalized molecularly imprinted silica xerogels were investigated by Alam group.[14] As described in Figure I-3, the guanidine groups functionalized on xerogel surface could allow an efficient two-point hydrogen bonding with phenylphosphoric acid used as a template. The complex was simply formed by mixing the template and functional monomer in the appropriate solvent, which brings about a relatively low stability of the complex. In addition, an excess amount of functional monomers was usually used to retain the complex structure. Therefore, it was hard to achieve the structural homogeneity in imprinted sites. However, the non-covalent technique showed much more flexibility in terms of fabrication due to the wide range of functional monomers and template

molecules available as well as the absence of a laborious chemical synthesis.

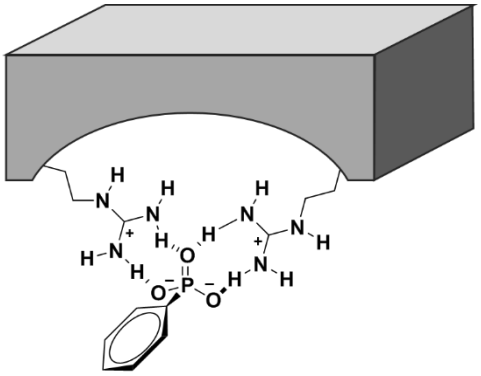

Figure I-3. Schematic design of non-covalent complex based on the guanidine groups.

Subsequently, several studies reported mixed covalent-noncovalent approaches which encompass the advantages of both methods. Suslick group designed a monomolecular imprinting system comprised of the Fréchet-type phenyl-benzyl ether-based dendrimers and polyhydroxylated tetraphenylporphyrins as the functional monomer and the template, respectively (Figure I-4).[15] The multiple hydroxyl groups containing porphyrin template can covalently conjugated with the dendron by *N*,*N*′-Dicyclohexylcarbodiimide-mediated esterification. The subsequent removal of porphyrin template produced an imprinted structure able to act as multipoint non-covalent recognition sites.

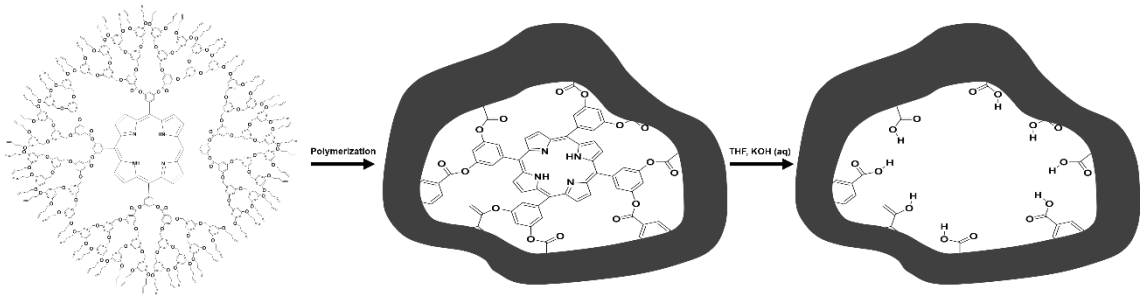

Figure I-4. Schematic design of mixed covalent-noncovalent imprinting approach based on the Fréchet-type phenyl-benzyl ether-based dendrimers and tetraphenylporphyrins.

Takeda and co-workers developed a novel molecularly imprinted polymer *via* mixed covalent-noncovalent imprinting.[16] Two allyl(4-carboxyphenyl)disulfides made a covalent conjugation with the target molecule (bisphenol A) through ester bonds (Figure I-5a). After the reductive cleavage of the disulfide bonds, remaining two thiol residues were further reacted with 4,4'-dithiodibenzoic acid to yield the imprinted cavities bearing two carboxylic acid residues for binding with bisphenol A (Figure I-5b-d).

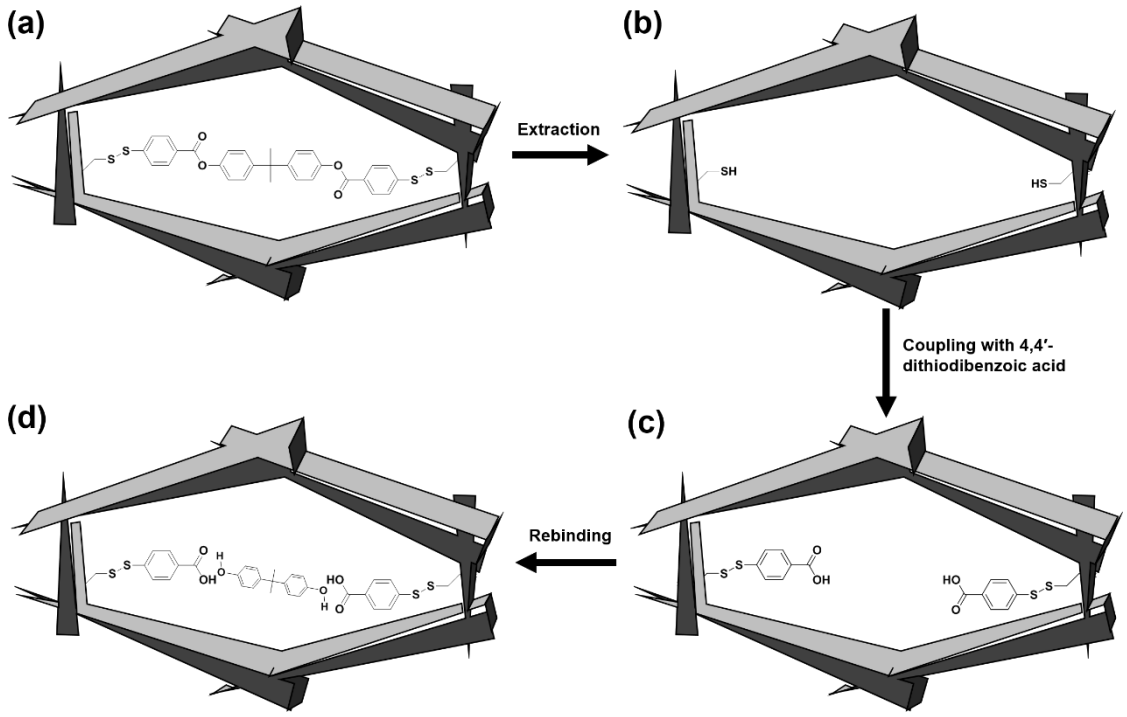

Figure I-5. Schematic designs of mixed covalent-noncovalent imprinting approach based on the construction of prosthetic group-coupled tunable binding cavities.

Metal ion coordination was also investigated for molecular imprinting in order to provide a better elaborate conformation of the stable monomer-template complex. Li group designed a molecularly imprinted polymer which used zinc(II)-protoporphyrin (ZnPP) as a fluorescent functional monomer for the recognition of histamine (template).[17] As shown in Figure I-6, a co-functional monomer, methacrylic acid (MAA),

could interact with histamine through the hydrogen bonding and ZnPP could make a coordination with histamine simultaneously, which formed a stable complex of histamine with ZnPP and MAA. Liu *et al.* introduced a new functional monomer containing amidine group and triamine functionality for the preparation of a molecularly imprinted polymer (Figure I-7).[18] Amidine group formed hydrogen bonds with the phosphate group of the template. Copper ion (Cu^{2+}) was coordinated by the triamine part of a functional monomer, which was further coordinated with the pyridine nitrogen of the template, thus providing more stable conformation of the complex.

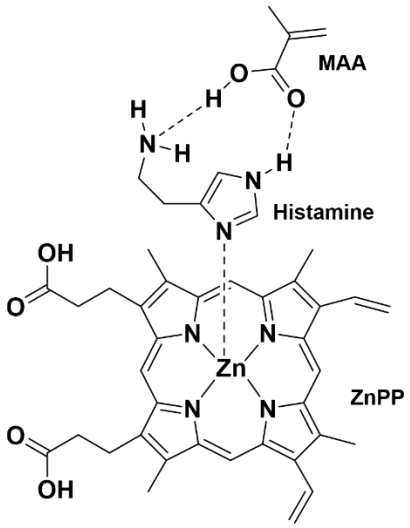

Figure I-6. Schematic description for the assembly of histamine with ZnPP and MAA.

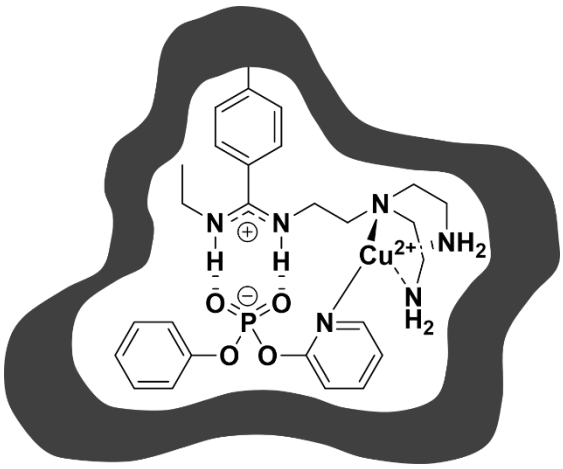

Figure I-7. Schematic design of a cross-linked functional monomer-template complex having amidine and triamine moieties for the preparation of a MIP.

Introducing a *sacrificial spacer (sacrificial covalent bond)* was a more sophisticated semi-covalent molecular imprinting approach.[19] The breakable chemical bonds such as carbonate or urea bonds were required to be used to form a linkage with the template molecule. Ye group prepared MIP microspheres based on a cholesterol-linked template monomer, cholesteryl (4-vinyl)phenyl carbonate (Figure I-8a).[20] This carbonate ester bond was easily hydrolyzed to produce imprinted sites in the polymer. The two-point binding site *via* the urea functionality was suggested by Lübke *et al.* (Figure I-8b).[21] The reductive cleavage of a carbonyl spacer produced aromatic amines which formed hydrogen bonds to the model target during the rebinding process.

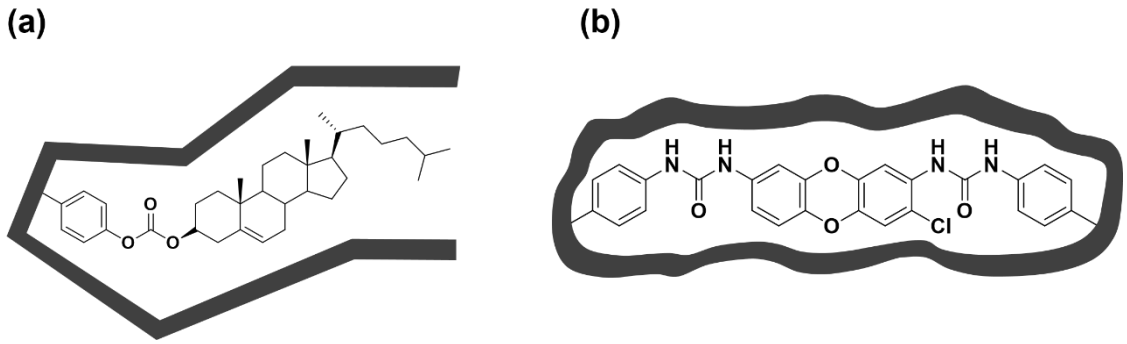

Figure I-8. Schematic design for a MIP based on the covalent conjugation of (a) a cholesterol *via* a carbonate ester bond and (b) 2,3,7,8-tetrachlorodibenzodioxin *via* a urea bond.

The thermally reversible urethane bond, the phenyl urethane bond was also widely investigated as one of sacrificial covalent bonds.[22] It can be easily cleaved to be isocyanate and phenol groups upon heating (Scheme I-1). The resulting isocyanate group

was electrophilic, so easily converted to various functionalities through the reaction with the corresponding nucleophiles.

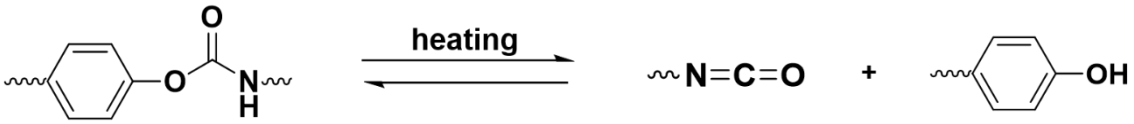

Scheme I-1. Cleavage of thermally reversible urethane bond.

Several studies have focused on the template-monomer complexation *via* thermo-reversible urethane bonds. Lee and coworkers suggested the template-monomer complex where two polymerziable maleimides having an isocyanate group reacted with the template *via* thermally reversible urethane bond (Figure I-9a).[23] Jung *et al.* introduced a molecular imprinting into the mesoporous silica matrix.[24] An isocyanate group containing two reactive silyl groups reacted with the template to give the template-monomer complex where two thermally reversible urethane bridges were designed to act as sacrificial spacers (Figure I-9b).

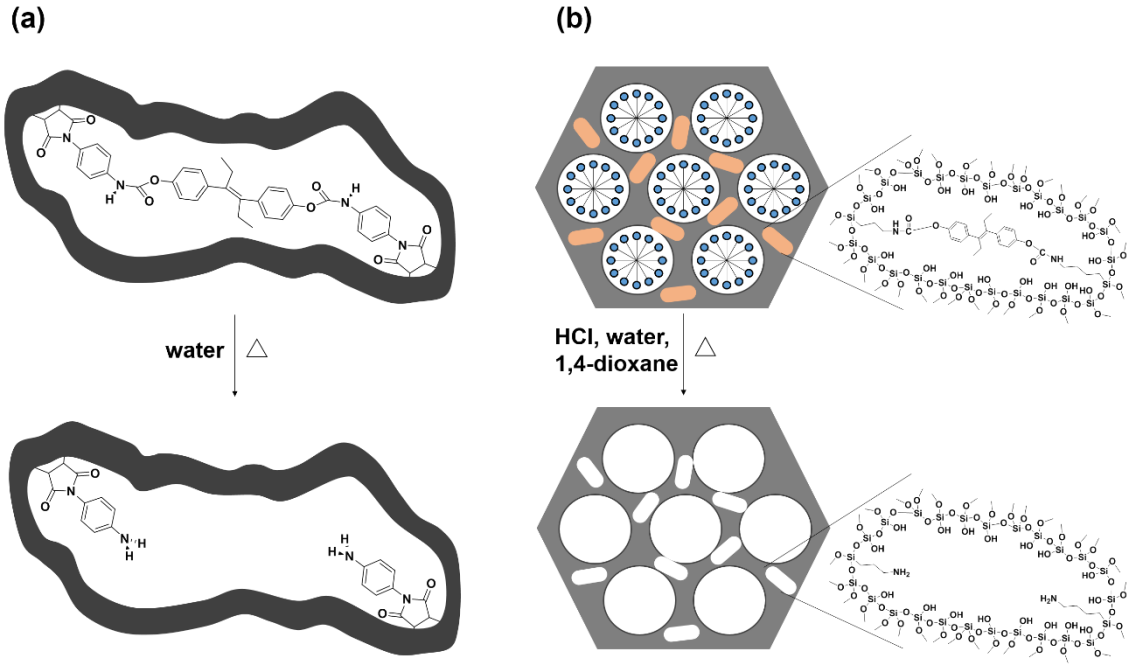

Figure I-9. Schematic designs for thermo-reversible urethane bond assisted MIP systems imprinted by diethylstilbestrol.

I-1-2. Application of Molecularly Imprinted Nanomaterials for Fluorescent Sensor

Conventional detection methods, including liquid and gas chromatography, mass spectrometry and enzyme-linked immunosorbent assay required a tedious isolation, long operation time and laborious sample preparation procedures. MIPs have been used for the direct sensing of the target in combination with quartz crystal microbalance, surface plasmon resonance and optical or electrochemical methods. Among these, the fluorescence-based optical methods may be valuable since they have simple procedures, non-destructive and fast response time, which opened the applications to various physiological samples.

A variety of fluorescent materials have been used for MIPs-based fluorescent sensor.

The lanthanide(III) ions showed unique photophysical properties resulting from intraconfigurational f-f transition in sensor applications based on MIPs.[25,26] Kim *et al.* reported a molecularly imprinted matrix fabricated by radical polymerization with the loading of europium(III) ions (MIP-Eu) (Figure I-10).[27] The europium(III) ion can coordinate with three β-diketones and one picloram (template) to form a defined complex for the MIP synthesis. The luminescence of europium(III) ions incorporated in the binding cavities of the imprinted polymer was strongly intensified by the addition of picloram. The increase in the luminescence was originated from the formation of a stable coordination where an alternative and indirect excitation of the europium(III) ions can be allowed *via* an organic-based antenna. A europium(III) ion coordinated with three β-diketones further coordinated with one picloram, which resulted in the formation of a

luminescent europium(III) complex.

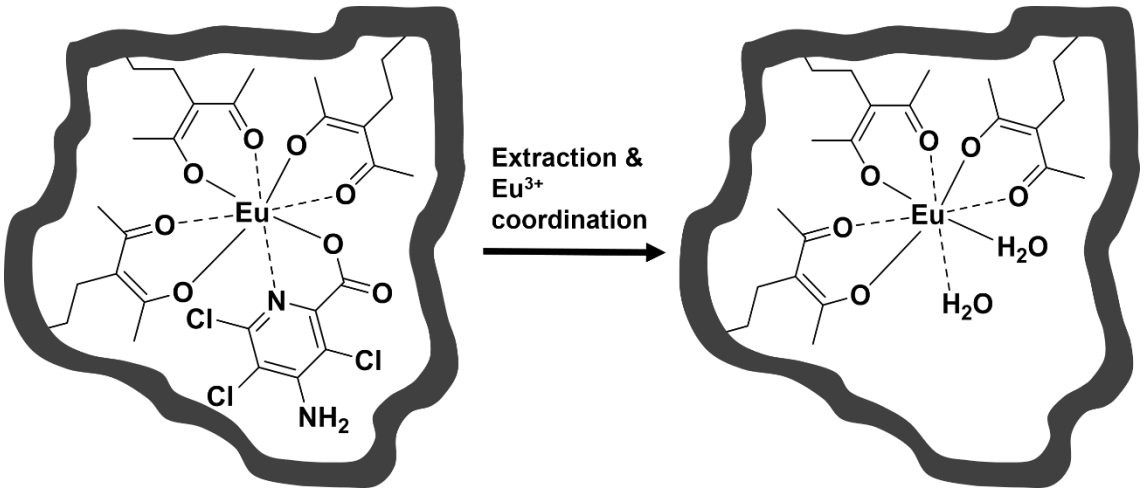

Figure I-10. Schematic design of a MIP system based on the europium(III) ion coordination.

Organic fluorescent moieties were also incorporated into MIPs. A nitrobenzoxadiazole (NBD) type of functional monomer was constructed by Wan and coworkers.[28] It had a polymerizable methacrylate group with both a urea group (4-position) and a short ethylene spacer which can allow the Y-shaped hydrogen bond with the target molecule carrying the carboxylate unit (*N*-carbobenzyloxy-L-phenylalanine, Z-L-Phe) (Figure I-11). The fluorescence of NBD monomer turned to increase upon the subsequent binding of Z-L-Phe arising from an intramolecular charge transfer (ICT) process.

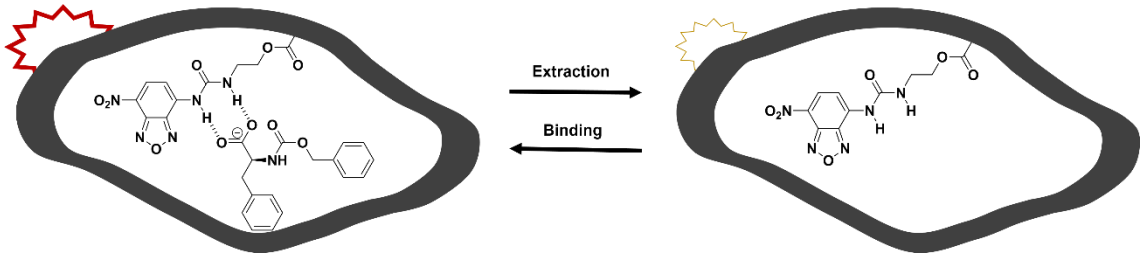

Figure I-11. Schematic design of a highly fluorescent MIP system based on a NBD type

of fluorescent monomer.

Murase *et al.* reported core-shell type MIP particles by two-step emulsifier-free emulsion polymerizations.[29] As described in Figure I-12, the model template (cortisol) was connected to methacryl group. After the polymerization in shell layers, the cortisol was removed to form a specific binding cavity. The performance of the cortisol recognition was confirmed by rebinding the cortisol labeled with a fluorophore, the dansyl group (Dansyl-Cortisol). Specific binding ability of target analytes with core-shell type cortisol-imprinted polymer was evaluated by fluorescence measurements.

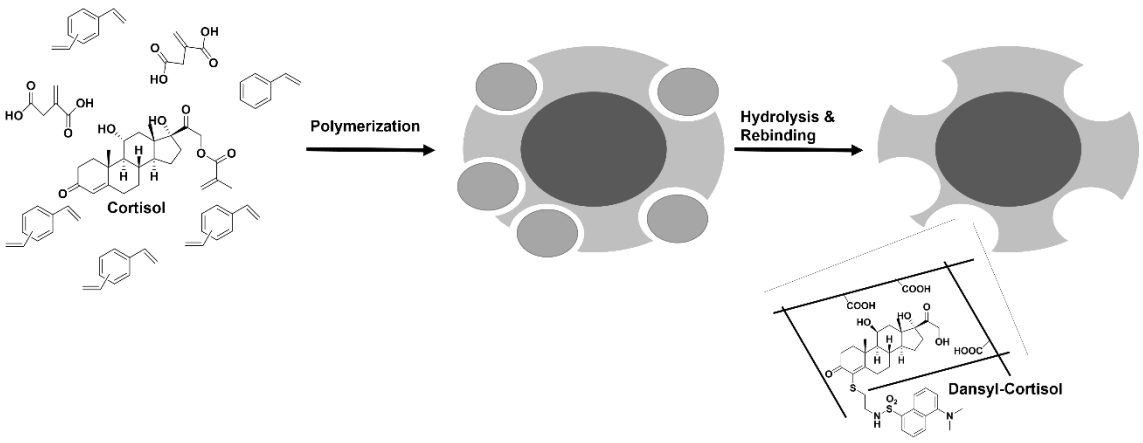

Figure I-12. Schematic design of the core-shell type MIP nanoparticles based on the rebinding of a dansyl-labeled cortisol.

Quantum dots (QDs) with unique size-dependent optical properties have attracted much attention as a signal transducer. Recently, Xu *et al.* reported a molecularly imprinted polymer coated QD (MIP@QD) sensor as a ratiometric fluorescence probe for the detection of 2,4,6-trinitrotoluene (TNT).[30] The incorporation of two differently sized CdTe QDs emitting red and green fluorescence into core-shell structured matrix was conducted: the red-emitting QD in silica nanoparticles as the core and the green-emitting

one in imprinted mesoporous silica as the shell (Figure I-13). The red QD-encapsulated silica nanoparticles as the core was prepared using the reverse micro-emulsion method. The green QD-embedded silica shell having imprinted sites was fabricated on the surface of the core by the surface imprinting technique introducing dummy template (trinitrophenol), functional monomer (3-aminopropyl triethoxysilane) and cross-linker (tetraethyl orthosilicate) in the presence of green QDs. In addition, using cetyltrimethylammonium bromide allowed the shell to form the mesoporous structure. When TNT rebound to the imprinted cavity the fluorescence of QDs can be quenched by the charge-transfer induced resonance energy transfer.

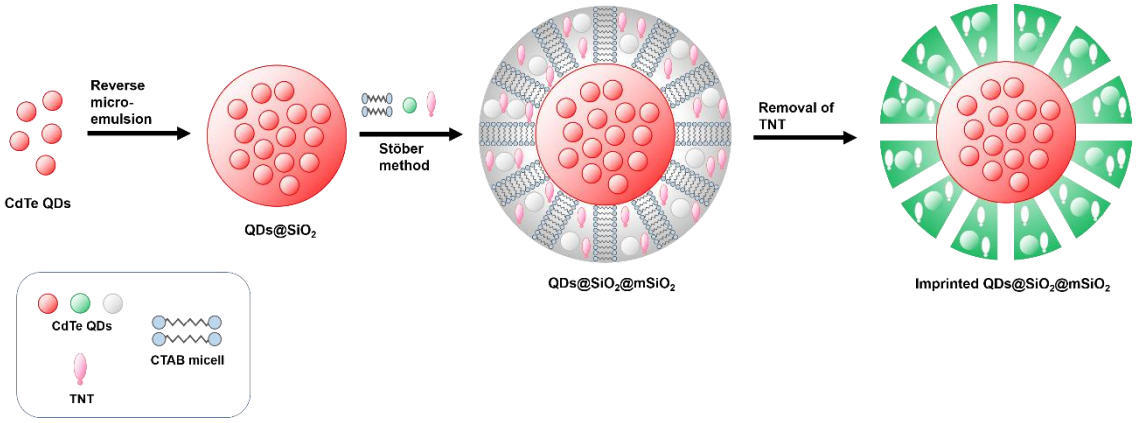

Figure I-13. Schematic design of mesoporous silica based MIP@QD ratiometric fluorescence probe.

I-2. Mesoporous Silica

I-2-1. Sol-Gel Reaction

The sol-gel reaction is a representative chemical wet process used for the preparation of glassy and ceramic materials. During the reaction, the sol state underwent gradual changes towards the growth of a gel-like network bearing both a liquid phase and a solid phase. The solid phase exhibited a broad range of structure or morphology from discrete colloidal particles to continuous chain-like polymer networks.

The mesoporous silica which is a form of silica having well-defined mesopore structure can be fabricated by this sol-gel reaction with the aid of self-organization of the templates (surfactant). Even though Japanese researchers firstly synthesized mesoporous silica nanoparticles, Mobil Corporation laboratories also prepared the same materials and classified them as Mobil Crystalline of Materials (MCM). MCM-41 has a hexagonal arrangement of mesopores with space group *p*6*mm*.[31] MCM-48 has a cubic arrangement of mesopores with space group *Ia*3*d*.[32] MCM-50 has a laminar structure with space group *p*2.[33]

A material comprised of both organic and inorganic building blocks can attract a great attention due to the capability to integrate an extensive functional modification of organic chemistry with advantages of highly stable inorganic substrate. The range of this hybrid materials can be broaden by the surface functionalization. The general methods regarding the development of the porous hybrid materials based on organosilica units were the following[33]: 1) the functional modification of the pore surface of a pure inorganic silica material (grafting), 2) the condensation of an inorganic silica with organosilica precursors (co-condensation) and 3) the introduction of organic moieties as bridging units into the

pore wall using bissilylated organosilica precursors (periodic mesoporous organosilica).

I-2-2. Post Synthetic Functionalization of Mesoporous Silica (Grafting)

Grafting of as-synthesized mesoporous support involved the post functionalization of the inner surface of mesopores by the attachment of organic functional groups.[34-44] The sol-gel reaction of organosilane containing an organic residue, R [$(R'O)_3SiR$] with a single ($\equiv$Si-OH) and the geminal ($=Si(OH)_2$) silanol group of the pore surface can form corresponding organic residues inside the pore (Figure I-14). This organic residue can be various organic functional moieties by the postsynthetic modification. The grafting method usually maintained the original mesostructure of the pure silica phase, whereas the silica wall lining led to the reduction in the porosity of the material. During the initial stage of the reaction, the process in which the reaction of organosilane occurred concurrently with the opening of a pore caused the disturbance of additional diffusion of molecules into the center of pores. As a result, the pores can be closed by the nonhomogeneous distribution of organic groups.

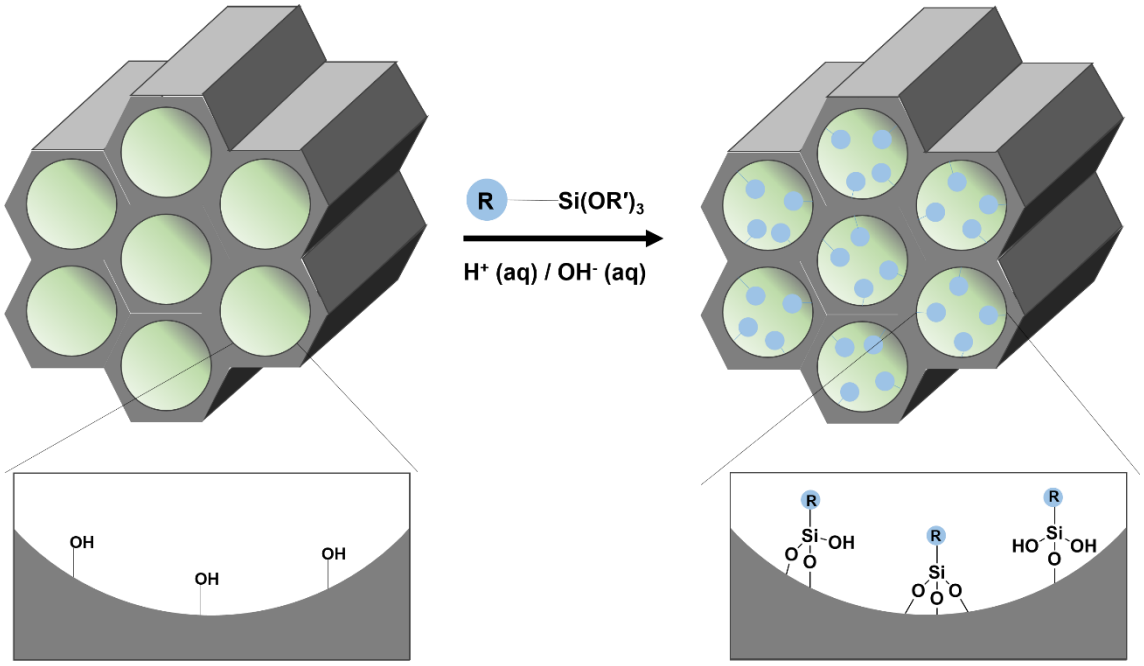

Figure I-14. Schematic route for an organic functional group modification of mesoporous silica phases having terminal organosilanes *via* grafting method (R = organic functional group).

I-2-3. Direct Synthesis (Co-Condensation)

Direct synthesis method which also refers to co-condensation method was another approach to synthesize functionalized mesoporous silica.[45-62] The co-condensation of tetraalkoxysilanes [$(RO)_4Si$] with terminal trialkoxyorganosilane [$(R'O)_3SiR$] in the presence of structure-directing agents can produce mesoporous silica where pore walls are anchored covalently with organic functional groups (Figure I-15). Compared to the grafting method, the blocking of a pore can be prevented since functionalized organic residues are direct components of the silica matrix. In addition, much more homogeneous distribution of organic functionalities was expected to occur. However, the concentration of terminal trialkoxyorganosilane precursors was very sensitive to the degree of mesoscopic order of the material. Different silica precursors can exhibit different

hydrolysis and condensation reaction rates, which may cause the homocondensation reaction. It was a major drawback of co-condensation process because different organic units cannot be guaranteed to be distributed homogeneously. To retain the organic functionality, only extraction can be used during the removal of the structure-directing agent.

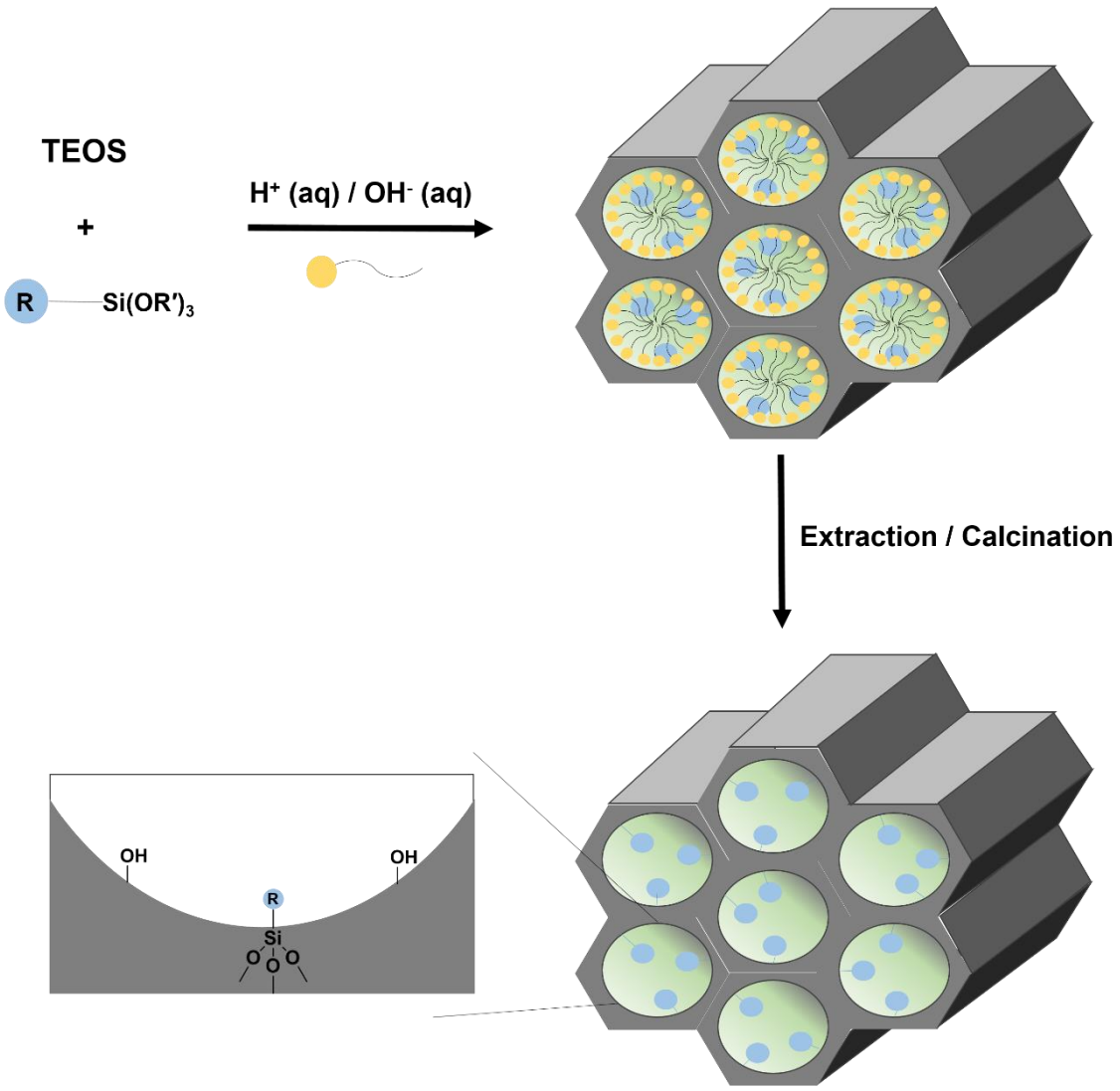

Figure I-15. Schematic route for an organic functional group modification of mesoporous silica phases having terminal organosilanes *via* co-condensation method (R = organic functional group).

I-2-4. Periodic Mesoporous Organosilica (PMO)

It has been well known that organic-inorganic hybrid silica can be obtained by sol-gel reaction of bridged organosilane precursors of the type $(R'O)_3Si\text{-}R\text{-}Si(OR')_3$.[63,64] It has a large surface area of up to 1800 m^2g^{-1} as well as high thermal stability, but the pore system was disordered with a wide pore size distribution. The periodic mesoporous organosilica (PMO) can be prepared by sol-gel reaction of bissilylated organosilica precursors with the template which was used for the synthesis of pure mesoporous silica. The organic bridge can act as an integral component of the silica network for PMO (Figure I-16).[65-75] Organic bridge units present in PMO were introduced in the three-dimensional network of silica matrix *via* two covalent bonds, and thus followed the homogeneous distribution in pore walls. The pore system was periodically ordered with a narrow pore size distribution. The stoichiometric functionalization of organic units also facilitated a high degree of organic functional groups. PMO is emerging as a promising material for a series of technical applications in sensing, delivery, separation and catalysis.[76]

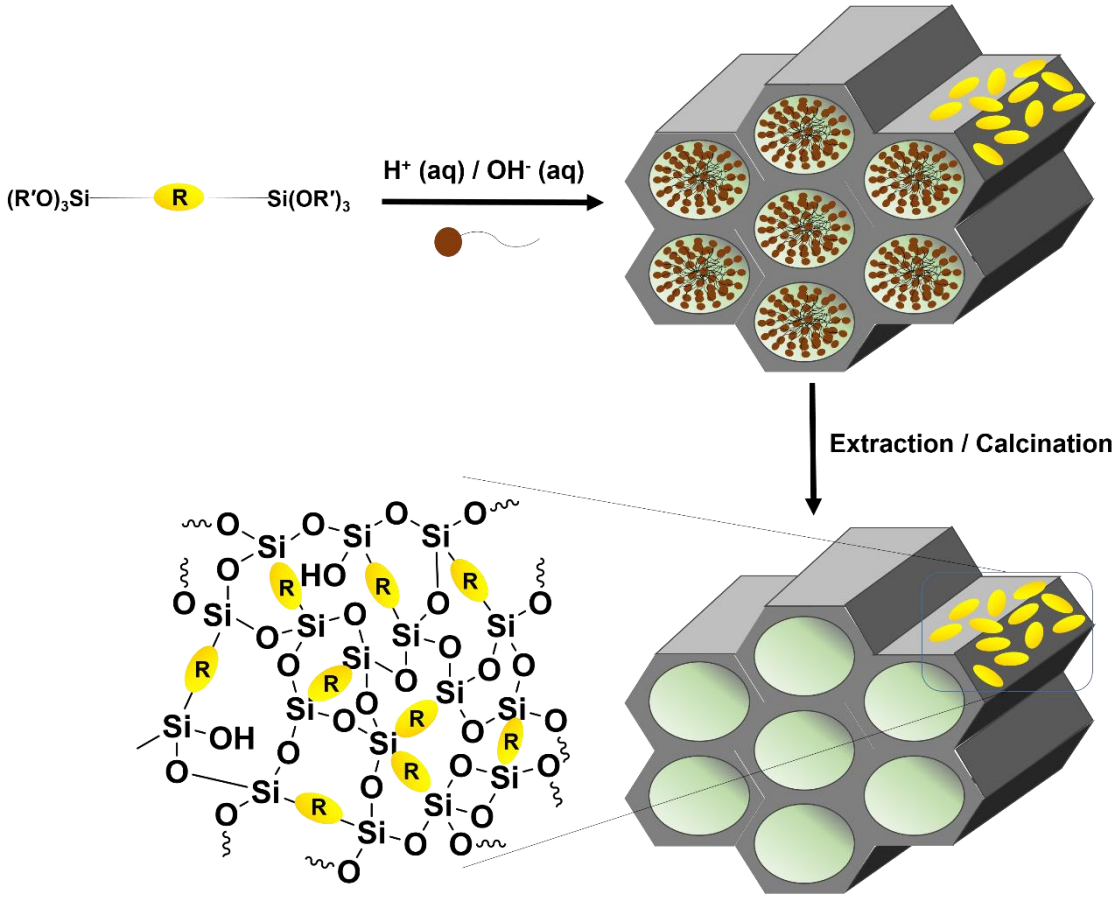

Figure I-16. Schematic synthetic pathway of PMOs using bissilylated organic bridging units (R = organic bridge).

I-3. Organogel

I-3-1. Definition of Organogel

There has been a considerable increase of interest during the last many years in the properties and structure of gels. The terminology of a "gel" has been used since prehistoric times but the definition of a gel was a matter of discussion.[77-79] Even though there are still many different definitions of a gel, a substance can be defined as a gel in general if (i) the material shows a continuous morphology on a microscopic scale with macroscopic dimensions that is unchanged on the time scale of an analytical experiment and (ii) its rheological behavior exhibits a solid-like material and yet it is composed predominately of a liquid at microscopic level.[80]

Depending on the interchain interaction in the three-dimensional network structure, this gel can be classified into two groups: chemical and physical gel. Chemical gels usually involved the formation of covalently cross-linked networks swollen with a liquid (solvent) and are thermally irreversible.[81] The formation of physical gels where the interchain attractions were attributed to non-covalent interactions, including electrostatic, hydrogen bonding and π-π stacking was thermally reversible and the gel stability highly depended on the temperature, pH, and the nature of the liquid.[82]

An organogel, a viscoelastic system, can be defined as a semi-solid formulation which has an immobilized external solvent. It was also described as thermoreversible physical gels. The apolar phase was immobilized within the three-dimensional network structure formed owing to the physical interactions among the self-assembling structures of compounds regarded as organogelators. Especially the organic molecules of a molar mass less than 3000 Da are classified as low molecular-mass organogelators (LMOGs).[83]

They can be self-assembled to form a three-dimensional fibrillar network structure, which can be reversibly disassembled (sol) upon heating and reassembled (gel) upon cooling. The gelation process depended not only on the organogelator molecules but also on the solvent, which made the organogels difficult to obtain.

I-3-2. Driving Force of Fibrous Networks in Organogel

The organic gelator molecules self-assembled *via* strong intermolcular interactions, allowing preferential one-dimensional growth, generally to form fibers, strands, or crystals.[84] Figure I-17 described the formation of a three-dimensional gel network. An organogel was usually prepared by heating a organogelator in an organic solvent until the gelator molecules were fully dissolved, and then cooling the solution to the temperature below which the flow no longer was recognizable over long periods. The structure of linear aggregates in the gel was determined by the direction and strength of the intermolecular forces. Because of the directional anisotropy in these forces, the self-assembly of gelator molecules can be preferred in one-dimensional growth and resulted in the formation of thin fibers. Several thin fibers created bundles which can minimize the interfacial free energy of a single fiber. The growth and entanglement of these bundles led to the formation of a three-dimensional gelator organization that was discernable at macroscopic scale.

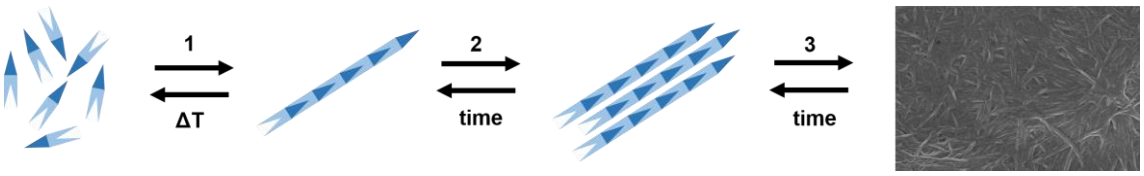

Figure I-17. Schematic illustration of the mechanism of gel formation of a 3D network.

Aggregation in organogels resulted from a different set of intermolecular interactions between gelator molecules such as ionic-ionic, hydrogen bonding, dipole-dipole, van der Waals and π-π stacking. Various simple geometries, for example spheres, lamellae and fibrills, result from a balance between intermolecular interactions of organogelators with organic liquids. Crystallization can also occur instead of gelation.[85]

I-3-3. Types of Organogelators

In designing the structure of a gelator, specific intermolecular interactions determined the anisotropy that was required for the gelation.[86] The inherent strength, self-complementarity and directionality were also significant factors for a gelator. In particular, the organogelators can be categorized into two groups based on their capability to form hydrogen bonding. The kinds of organogelators which do not form hydrogen bonds included anthracene, anthraquinone and steroid-based molecules, whereas the hydrogen bond-forming organogelators usually comprised amino acids, amide, hydroxy, urea moieties and carbamate. The organogel was a promising candidate for the fabrication of functional materials due to its nanoscale morphology with macroscopic length. It can, however, suffer from the lack of mechanical and chemical stability that limits the application.

Hydrogen bond forming organogelators

The amino acid moieties can effectively promote the physical junctions for gelation process in the organic solvent predominantly by hydrogen bonding. Certain *N*-stearoyl amino acid derivatives possessing a long hydrophobic alkyl tail with free terminal amine

groups formed the stable gels with long thin fibers of several micrometers in organic solvents such as toluene or acetonitrile (Figure I-18).[87] A long-chain aminoamide derivative was modified by replacing the iminodiacetic acid core with various forms of a chiral and natural L-amino acid, including L-glycine, L-alanine, L-phenylalanine, L-glutamic acid and L-serine.

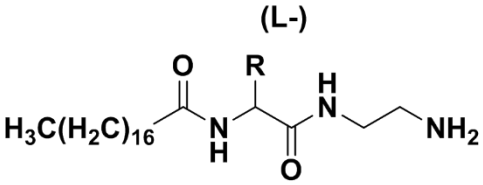

1: R = H
2: R = CH_3
3: R = Bn
4: R = $CH_2CH_2CONHCH_2CH_2NH_2$
5: R = CH_2OH

Figure I-18. Molecular description of *N*-(2-aminoethyl)-α-[(1-oxoheptadecyl)amino]acetamide derivative organogelators.

The simple types of a LMOG formed from a cyclic β-aminoalcohol was synthesized as shown in Figure I-19.[88] 1,2,3,4-Tetrahydroisoquinoline derivative was capable of forming reversible gels in common polar and apolar solvents through hydrogen bonding between amine and hydroxyl group as the driving force. During the process of gelation the one-dimensional linear aggregates could grow into a two-dimensional bilayer structure by the hierarchical self-assembly. The subsequent stacking of bilayers resulted in a lamellar structure which further yielded entangled fibers.

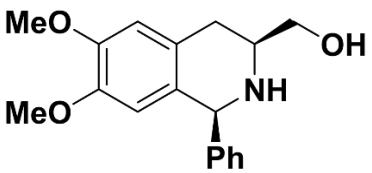

Figure I-19. Molecular design of a derivative of 1,2,3,4-tetrahydroisoquinoline organogelator.

Several carbamate and urea-based organogelators were prepared and compared in aspects of the strength of the intermolecular binding.[89] As presented in Figure I-20, the urea groups have the extra hydrogen-donor compared to carbamate ones. Each C=O group on urea-based organogelator can interact through hydrogen bonding with both N-H groups of the adjacent molecule, leading to a three centers-two bonds interaction. As a result, the urea-based organogelator showed an increase in thermal stability with a low critical gelation concentration.

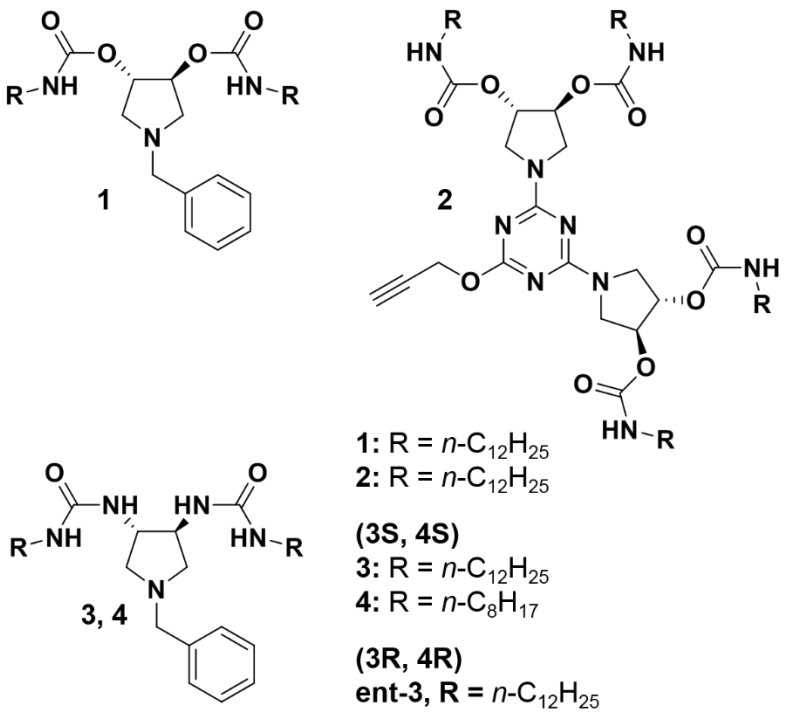

Figure I-20. Molecular descriptions of the carbamate (1 and 2) and the urea (3, 4 and ent-3) based organogelators.

π-π interactions-based organogelators

The increasing interest in π-conjugated materials has aroused the study for supramolecular organization in the bulk state.[90-94] Accordingly, besides hydrogen bonding, weak non-covalent interactions such as π-π interactions[95], electrostatic[96], dipole-dipole[97] and van der Waals forces[98] can also control the preferential formation of the supramolecular organization in the molecular structure. A novel peripherally dimethyl isophthalate (DMIP) functionalized poly(benzyl ether) dendron-based organogelator with photoresponsive azobenzene moieties self-assembled into the stable organogels in various apolar and polar organic solvents with a low critical gelation concentration (Figure I-21).[99] The dendritic organogels showed multistimuli-responsive behavior upon reversible gel-solution phase transition. The main driving force of the formation of the dense three-dimensional fibrillar networks was attributed to the strong intermolecular multiple π-π stacking of the peripheral DMIP motifs along with the dendritic architecture.

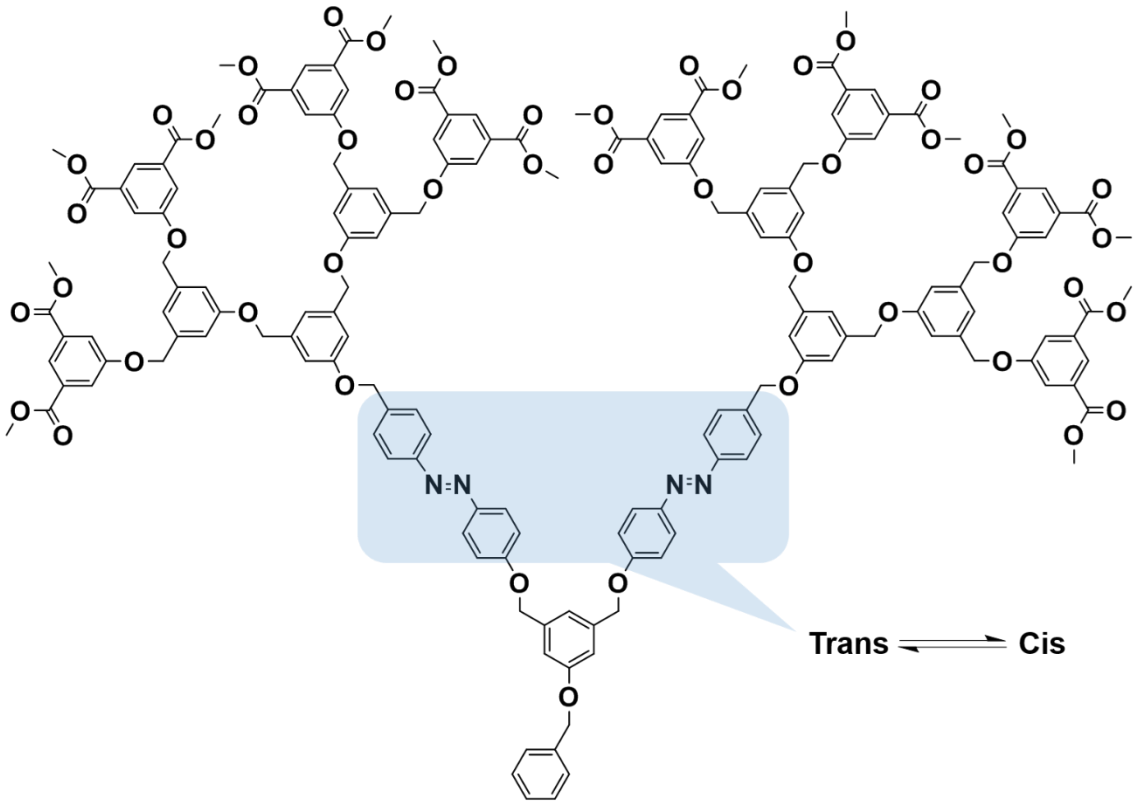

Figure I-21. Molecular description of poly(benzyl ether) dendritic organogelator containing azobenzene.

LMOG system composed of an anthracene, a uracil, and long alkyl chains exhibited excellent gelation ability toward organic aromatic solvents, cyclohexane, DMSO, ethanol, and ethyl acetate (Figure I-22).[100] Both the aromatic anthracene unit and long alkyl chains contributed to the enhancement of π-π interactions in aromatic solvents. The additional uracil group which possesses the amidic N-H achieved the cooperation of hydrogen bonding to form a large three-dimensional fibrous gel network.

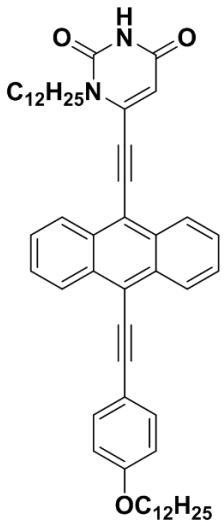

Figure I-22. Molecular description of an anthracene organogelator based on uracil.

The molecules containing modified steroid units also showed gelation behavior.[101] The cholesterol-linked organogelator having both azobenzene and diacetylenic units formed the helical fiber in the gel network (Figure I-23). The self-assembly of cholesteryl moieties were known to be achieved *via* weak van der Waals interactions. The azobenzene group can undergo photo-induced isomerization. When the rate and degree of isomerization reached a specific point, the molecular helical packing in the gel network can be formed. The rigid diacetylene unit can be topo-polymerized, which dramatically enhanced the stability of the designed helical gel phases.

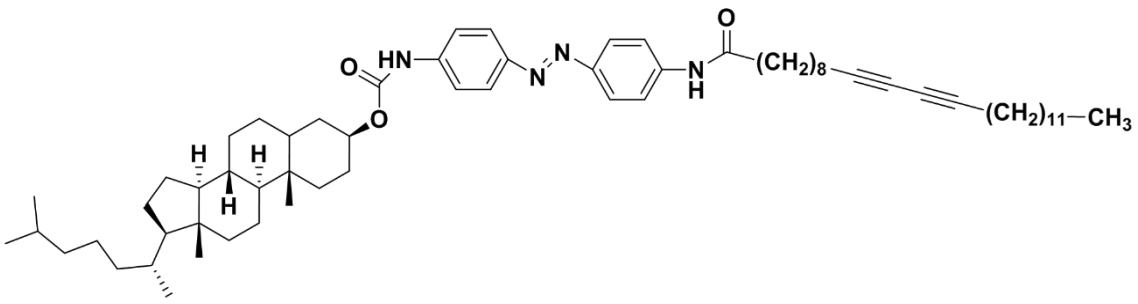

Figure I-23. Molecular description of a cholesterol derivative organogelator containing both azobenzene and diacetylenic moieties.

Polymerizable organogelators

The organogelators bearing the polymerizable groups, including vinyl, methacrylate, acrylate, or diacetylene units have been reported. The bis(amido)cyclohexane and bis(ureido)cyclohexane derivatives 1 and 2 which contain two methacrylate groups formed a stable gel from the solution state (Figure I-24).[102] The subsequent photopolymerization resulted in a highly cross-linked well-ordered gel structure.

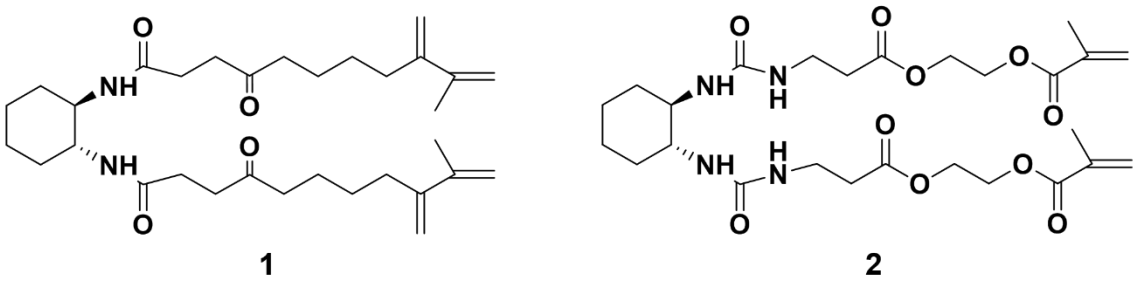

Figure I-24. Molecular descriptions of polymerizable organogelators based on bis(amido)cyclohexane and bis(ureido)cyclohexane derivatives 1 and 2.

A series of ureido substituted organogelators having diacetylenic moieties were designed as shown in Figure I-25.[103] To obtain the high solubility, the triethoxysilane function that can provide the steric hindrance and the lipophilicity was introduced, resulting in the formation of a stable translucent organogel. The short alkylene spacer length hindered the photopolymerization due to the rigidity of urea unit. Increasing the length of the alkylene spacer minimized the influence of the rigidity of two hydrogen bonded urea moiety close to the polymerizable group, and thereby the urea function was kept way from the polymerizable function.

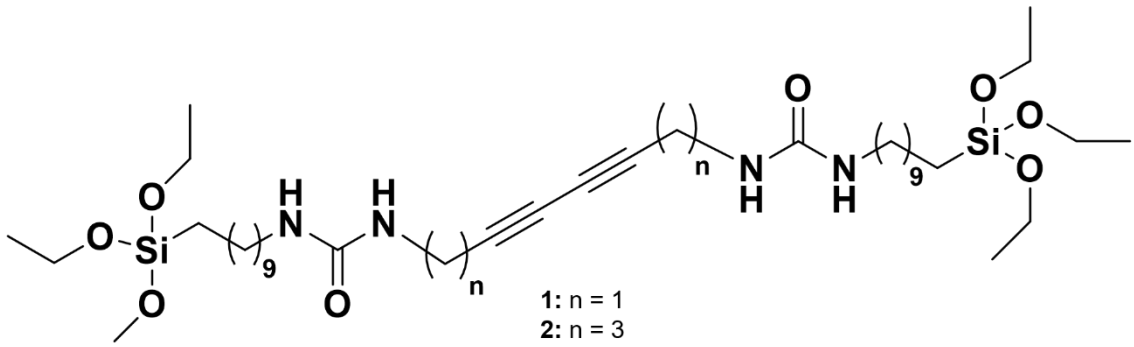

Figure I-25. Molecular description of ureido substituted diacetylenic organogelators.

To pursue a unique structural feature where the nano-scale thin fibers formed by the self-assembly of the organogelators were embedded in a polymer matrix, a novel hetero-bifunctional organogelator was designed (Figure I-26).[104] It consisted of two different polymerizable groups, acryl and diacetylene functions and exhibited the gelation ability in common organic solvents at room temperature. Both of polymerizable groups participated in the gel state polymerization of an organogel by UV irradiation. The polymerization of acryl groups could produce a polymer matrix while simultaneously maintaining the gel network. At the same time, the resulting polydiacetylene chains allowed the formation of more distinct nanofibrillar structure.

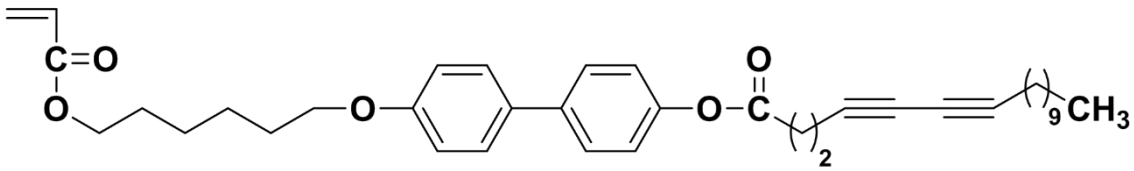

Figure I-26. Molecular description of a hetero-bifunctional organogelator based on two different polymerizable fragments.

I-4. References

1. Ramamurhy, V.; Eaton, D. F. *Chem. Mater.* **1994**, 6, 1128-1136.

2. Wang, H.-J.; Zhou, W.-H.; Yin, X.-F.; Zhuang, Z.-X.; Yang, H.-H.; Wang, X.-R. *J. Am. Chem. Soc.* **2006**, 128, 15954-15955.

3. Hu, X.; Li, G.; Huang, J.; Zhang, D.; Qiu, Y. *Adv. Mater.* **2007**, 19, 4327-4332.

4. Emgenbroich, M.; Wulff, G. *Chem. Eur. J.* **2003**, 9, 4106-4117.

5. Nemoto, K.; Kubo, T.; Nomachi, M.; Sano, T.; Matsumoto, T.; Hosoya, K.; Hattori, T.; Kaya, K. *J. Am. Chem. Soc.* **2007**, 129, 13626-13632.

6. Markowitz, M. A.; Kust, P. R.; Deng, G.; Schoen, P. E.; Dordick, J. S.; Clark, D. S.; Gaber, B. P. *Langmuir* **2000**, 16, 1759-1765.

7. Carter, S. R.; Rimmer, S. *Adv. Funct. Mater.* **2004**, 14, 553-561.

8. Katz, A.; Davis, M. E. *Nature* **2000**, 403, 286-289.

9. Wulff, G.; Vesper, W.; Grobe-Einsler, R.; Sarhan, A. *Makromol. Chem.* **1977**, 178, 2799-2816.

10. Wulff, G.; Heide, B.; Helfmeier, G. *J. Am. Chem. Soc.* **1986**, 108, 1089-1091.

11. Shea, K. J.; Dougherty, T. K. *J. Am. Chem. Soc.* **1986**, 108, 1091-1093.

12. Mosbach, K. *Trends Biochem. Sci.* **1998**, 19, 9-14.

13. Haupt, K.; Mosbach, K. *Trends Biotechnol.* **1998**, 16, 468-475.

14. Sasaki, D. Y.; Alam, T. M. *Chem. Mater.* **2000**, 12, 1400-1407.

15. Zimmerman, S. C.; Zharov, I.; Wendland, M. S.; Rakow, N. A.; Suslick, K. S. *J. Am. Chem. Soc.* **2003**, 125, 13504-13518.

16. Takeda, K.; Kuwahara, A.; Ohmori, K.; Takeuchi, T. *J. Am. Chem. Soc.* **2009**, 131, 8833-8838.

17. Tong, A.; Dong, H.; Li, L. *Anal. Chim. Acta* **2002**, 466, 31-37.

18. Liu, J.-q.; Wulff, G. *J. Am. Chem. Soc.* **2004**, 126, 7452-7453.

19. Whitcombe, M. J.; Vulfson, E. N. *Adv. Mater.* **2001**, 13, 467-478.

20. Boonpangrak, S.; Prachayasittikul, V.; Bülow, L.; Ye, L. *J. Appl. Polym. Sci.* **2006**, 99, 1390-1398.

21. Lübke, M.; Whitcombe, M. J.; Vulfson, E. N. *J. Am. Chem. Soc.* **1998**, 120, 13342-13348.

22. Ki, C. D.; Oh, C.; Oh, S.-G.; Chang, J. Y. *J. Am. Chem. Soc.* **2002**, 124, 14838-14839.

23. Lee, K.; Ki, C. D.; Kim, H.; Chang, J. Y. *Macromolecules* **2004**, 37, 5544-5549.

24. Jung, B. M.; Kim, M. S.; Kim, W. J.; Chang, J. Y. *Chem. Commun.* **2010**, 46, 3699-3701.

25. Southard, G. E.; Van Houten, K. A.; Murray, G. M. *Macromolecules* **2007**, 40, 1395-1400.

26. Liu, C.; Song, Z.; Pan, J.; Wei, X.; Gao, L.; Yan, Y.; Li, L.; Wang, J.; Chen, R.; Dai, J.; Yu, P. *J. Phys. Chem. C* **2013**, 117, 10445-10453.

27. Kim, H.; Kim, Y.; Chang, J. Y. *J. Polym. Sci. A Polym. Chem.* **2012**, 50, 4990-4994.

28. Wan, W.; Biyikal, M.; Wagner, R.; Sellergren, B.; Rurack, K. *Angew. Chem. Int. Ed.* **2013**, 52, 7023-7027.

29. Murase, N.; Taniguchi, S.-I.; Takano, E.; Kitayama, Y.; Takeuchi, T. *Macromol. Chem. Phys.* **2015**, 216, 1396-1404.

30. Xu, S.; Lu, H. *Chem. Commun.* **2015**, 51, 3200-3203.

31. Liang, Y.; Hanzlik, M.; Anwander, R. *J. Mater. Chem.* **2006**, 16, 1238-1253.

32. Zhao, W.; Li, Q. *Chem. Mater.* **2003**, 15, 4160-4162.

33. Hoffmann, F.; Cornelius, M.; Morell, J.; Fröba, M. *Angew. Chem. Int. Ed.* **2006**, 45, 3216-3251.

34. Yokoi, T.; Yoshitake, H.; Tatsumi, T. *J. Mater. Chem.* **2004**, 14, 951-957.

35. Zhang, C.; Zhou, W.; Liu, S. *J. Phys. Chem. B* **2005**, 109, 24319-24325.

36. Luechinger, M.; Prins, R.; Pirngruber, G. D. *Micropor. Mesopor. Mater.* **2005**, 85, 111-118.

37. Yoshitake, H.; Koiso, E.; Horie, H.; Yoshimura, H. *Micropo. Mesopor. Mater.* **2005**, 85, 183-194.

38. Angloher, S.; Kecht, J.; Bein, T. *Chem. Mater.* **2007**, 19, 5797-5802.

39. Miyajima, T.; Abry, S.; Zhou, W.; Albela, B.; Bonneviot, L.; Oumi, Y.; Sano, T.; Yoshitake, H. *J. Mater. Chem.* **2007**, 17, 3901-3909.

40. Angloher, S.; Kecht, J.; Bein, T. *Chem. Mater.* **2007**, 19, 3568-3574.

41. Salmio, H.; Brühwiler, D. *J. Phys. Chem. C* **2007**, 111, 923-929.

42. Xie, Y.; Quinlivan, S.; Asefa, T. *J. Phys. Chem. C* **2008**, 112, 9996-10003.

43. Puanngam, M.; Unob, F. *J. Hazard. Mater.* **2008**, 154, 578-587.

44. Baca, M.; de la Rochefoucauld, E.; Ambroise, E.; Krafft, J.-M.; Hajjar, R.; Man, P. P.; Carrier, X.; Blanchard, J. *Micropor. Mesopor. Mater.* **2008**, 110, 232-241.

45. Wang, X.; Lin, K. S. K.; Chan, J. C.C.; Cheng, S. *Chem. Commun.* **2004**, 2762-2763.

46. Wang, X.; Tseng, Y.-H.; Chan, J. C.C.; Cheng, S. *Micropor. Mesopor. Mater.* **2005**, 85, 241-251.

47. Wahab, M. A.; Imae, I.; Kawakami, Y.; Ha, C.-S. *Chem. Mater.* **2005**, 17, 2165-2174.

48. Wahab, M. A.; Imae, I.; Kawakami, Y.; Kim, I.; Ha, C.-S. *Micropo. Mesopor. Mater.* **2006**, 92, 201-211.

49. Yan, Z.; Tao, S.; Yin, J.; Li, G. *J. Mater. Chem.* **2006**, 16, 2347-2353.

50. Wang, X.; Chan, J. C.C.; Tseng, Y.-H.; Cheng, S. *Micropor. Mesopor. Mater.* **2006**, 95, 57-65.

51. Yan, Z.; Li, G.; Mu, L.; Tao, S. *J. Mater. Chem.* **2006**, 16, 1717-1725.

52. Ji, X.; Hu, Q.; Hampsey, E.; Qiu, X.; Gao, L.; He, J.; Lu, Y. *Chem. Mater.* **2006**, 18, 2265-2274.

53. Sun, L.-N.; Zhang, H.-J.; Peng, C.-Y.; Yu, J.-B.; Meng, Q.-G.; Fu, L.-S.; Liu, F.-Y.; Guo, X.-M. *J. Phys. Chem. B* **2006**, 110, 7249-7258.

54. Yokoi, T.; Yoshitake, H.; Yamada, T.; Kubota, Y.; Tatsumi, T. *J. Mater. Chem.* **2006**, 16, 1125-1135.

55. Wang, X.; Cheng, S.; Chan, J. C.C.; Chao, J. C.H. *Micropo. Mesopor. Mater.* **2006**, 96, 321-330.

56. Alauzun, J.; Mehdi, A.; Reyé, C.; Corriu, R. *New J. Chem.* **2007**, 31, 911-915.

57. Gao, C.; Sakamoto, Y.; Terasaki, O.; Sakamoto, K.; Che, S. *J. Mater. Chem.* **2007**, 17, 3591-3602.

58. Yokoi, T.; Yamataka, Y.; Ara, Y.; Sato, S.; Kubota, Y.; Tatsumi, T. *Micropor. Mesopor. Mater.* **2007**, 103, 20-28.

59. Sun, L.-N.; Yu, J.-B.; Zhang, H.-J.; Meng, Q.-G.; Ma, E.; Peng, C.-Y.; Yang, K.-Y. *Micropor. Mesopor. Mater.* **2007**, 98, 156-165.

60. Liu, X.; Du, Y.; Guo, Z.; Gunasekaran, S.; Ching, C.-B.; Chen, Y.; Leong, S. S. J.; Yang, Y. *Micropor. Mesopor. Mater.* **2009**, 122, 114-120.

61. Jeong, E.-Y.; Burri, A.; Lee, S.-Y.; Park, S.-E. *J. Mater. Chem.* **2010**, 20, 10869-10875.

62. Borah, P.; Ma, X.; Nguyen, K. T.; Zhao, Y. *Angew. Chem. Int. Ed.* **2012**, 51, 7756-7761.

63. Loy, D. A.; Shea, K. J. *Chem. Rev.* **1995**, 95, 1431-1442.

64. Shea, K. J.; Loy, D. A. *Chem. Mater.* **2001**, 13, 3306-3319.

65. Inagaki, S.; Guan, S.; Fukushima, Y.; Ohsuna, T.; Terasaki, O. *J. Am. Chem. Soc.* **1999**, 121, 9611-9614.

66. Melde, B. J.; Holland, B. T.; Blanford, C. F.; Stein, A. *Chem. Mater.* **1999**, 11, 3302-

3308.

67. Asefa, T.; MacLachlan, M. J.; Coombs, N.; Ozin, G. A. *Nature* **1999**, 402, 867-871.

68. Nakajima, K.; Lu, D.; Kondo, J. N.; Tomita, I.; Inagaki, S.; Hara, M.; Hayashi, S.; Domen, K. *Chem. Lett.* **2003**, 32, 950-951.

69. Guan, S.; Inagaki, S.; Ohsuna, T.; Terasaki, O. *J. Am. Chem. Soc.* **2000**, 122, 5660-5661.

70. Sayari, A.; Hamoudi, S.; Yang, Y.; Moudrakovski, I. L.; Ripmeester, J. R. *Chem. Mater.* **2000**, 12, 3857-3863.

71. Hamoudi, S.; Yang, Y.; Moudrakovski, I. L.; Lang, S.; Sayari, A. *J. Phys. Chem. B* **2001**, 105, 9118-9123.

72. Asefa, T.; MacLachlan, M. J.; Grondey, H.; Coombs, N.; Ozin, G. A. *Angew. Chem. Int. Ed.* **2000**, 39, 1808-1811.

73. Ren, T.; Zhang, X.; Suo, J. *Micropor. Mesopor. Mater.* **2002**, 54, 139-144.

74. Yoshina-Ishii, C.; Asefa, T.; Coombs, N.; MacLachlan, M. J.; Ozin, G. A. *Chem. Commun.* **1999**, 2539-2540.

75. Temtsin, G.; Asefa, T.; Bittner, S.; Ozin, G. A. *J. Mater. Chem.* **2001**, 11, 3202-3206.

76. Wang, W.; Lofgreen, J. E.; Ozin, G. A. *Small* **2010**, 6, 2634-2642.

77. Dean, R. B. *Modern Colloids*, D. Van Nostrand Co., New York, **1948**.

78. Ferry, J. D. *Viscoelastic Properties of Polymers*, Wiley, New York, **1961**.

79. Flory, P. *J. Discuss Faraday Soc.* **1974**, 57, 7-18.

80. Weiss, R. G.; Terech, P. *Molecular gels: materials with self-assembled fibrillar networks*, Springer, Dordrecht, **2006**.

81. Gesser, H. D.; Goswami, P. C. *Chem. Rev.* **1989**, 89, 765-788.

82. Najeh, M.; Munch, J.-P.; Guenet, J.-M. *Macromolecules* **1992**, 25, 7018-7023.

83. Abdallah, D. J.; Weiss, R. G. *Adv. Mater.* **2000**, 12, 1237-1247.

84. Cai, M.; Liang, Y.; Zhou, F.; Liu, W. *J. Mater. Chem.* **2011**, 21, 13399-13405.

85. Brotin, T.; Utermöhlen, R.; Fages, F.; Bouas-Laurent, H.; Devergne, J.-P. *J. Chem. Soc. Chem. Commun.* **1991**, 416-418.

86. Llusar, M.; Sanchez, C. *Chem. Mater.* **2008**, 20, 782-820.

87. Delbecq, F.; Tsujimoto, K.; Ogue, Y.; Endo, H.; Kawai, T. *J. Colloid Interface Sci.* **2013**, 390, 17-24.

88. Kang, C.; Bian, Z.; He, Y.; Han, F.; Qiu, X.; Gao, L. *Chem. Commun.* **2011**, 47, 10746-10748.

89. Lascialfari, L.; Pescitelli, G.; Brandi, A.; Mannini, M.; Berti, D.; Cicchi, S. *Soft Matter* **2015**, 11, 8333-8341.

90. Hoeben, F. J. M.; Jonkheijm, P.; Meijer, E. W.; Schenning, A. P. H. J. *Chem. Rev.* **2005**, 105, 1491-1546.

91. Varghese, S.; Das, S. *J. Phys. Chem. Lett.* **2011**, 2, 863-873.

92. Moulin, E.; Cid, J.-J.; Giuseppone, N. *Adv. Mater.* **2013**, 25, 477-487.

93. Babu, S. S.; Hollamby, M. J.; Aimi, J.; Ozawa, H.; Saeki, A.; Seki, S.; Kobayashi, K.; Hagiwara, K.; Yoshizawa, M.; Möhwald, H.; Nakanishi, T. *Nat. Commun.* **2013**, 4, 1-8.

94. Babu, S. S.; Praveen, V. K.; Ajayaghosh, A. *Chem. Rev.* **2014**, 114, 1973-2129.

95. Shao, H.; Parquette, J. R. *Chem. Commun.* **2010**, 46, 4285-4287.

96. Taguchi, S.; Matsumoto, T.; Ichikawa, T.; Katob, T.; Ohno, H. *Chem. Commun.* **2011**, 47, 11342-11344.

97. Mamiya, J.; Kanie, K.; Hiyama, T.; Ikeda, T.; Kato, T. *Chem. Commun.* **2002**, 1870-1871.

98. Kramb, R. C.; Zukoski, C. F. *Langmuir* **2008**, 24, 7565-7572.

99. Liu, Z.-X.; Feng, Y.; Yan, Z.-C.; He, Y.-M.; Liu, C.-Y.; Fan, Q.-H. *Chem. Mater.* **2012**, 24, 3751-3757.

100. Xing, L.-B.; Yang, B.; Wang, X.-J.; Wang, J.-J.; Chen, B.; Wu, Q.; Peng, H.-X.; Zhang, L.-P.; Tung, C.-H.; Wu, L.-Z. *Langmuir* **2013**, 29, 2843-2848.

101. Wang, J.; Yang, G.; Jiang, H.; Zou, G.; Zhang, Q. *Soft Matter* **2013**, 9, 9785-9791.

102. de Loos, M.; van Esch, J.; Stokroos, I.; Kellogg, R. M.; Feringa, B. L. *J. Am. Chem. Soc.* **1997**, 119, 12675-12676.

103. Dautel, O. J.; Robitzer, M.; Lère-Porte, J.-P.; Serein-Spirau, F.; Moreau, J. J. E. *J. Am. Chem. Soc.* **2006**, 128, 16213-16223.

104. Kang, S. H.; Jung, B. M.; Chang, J. Y. *Adv. Mater.* **2007**, 19, 2780-2784.

Chapter II.

Preparation of CdSe Quantum Dot-Encapsulated Molecularly Imprinted Mesoporous Silica Nanoparticles for Fluorescent Sensing of Bisphenol A

II-1. Introduction

Molecular imprinting is a promising methodology to fabricate materials that function as synthetic receptors with predetermined recognition sites.[1] Molecular imprinted materials have several merits such as mechanical and chemical stability, ease of preparation and wide range of applications as compared to biological receptors,[2-4] but often suffer from poor site accessibility and low selectivity. Some of these shortcomings have been overcome by adopting various nanofabrication techniques,[5-8] but it is still demanding to prepare imprinted materials with high sensitivity and selectivity. The challenge is also on a way to convert binding events into quantitative measurements.[9-13] In recent years, there has been a keen interest in simultaneous detection and removal of highly toxic organic pollutants.

Herein, a novel molecularly imprinted fluorescent sensor is developed. A CdSe quantum dot (QD) and mesoporous silica nanoparticle are used as a signal transducer and an imprinting material, respectively. QDs are monodispersed colloidal semiconductor nanocrystals. Owing to its discrete size-dependent characteristic optical properties,

flexible chemical processability and great photostability, the application of QDs towards sensing and recognizing elements is of a considerable interest.[14-16] A mesoporous silica nanoparticle has a highly crosslinked rigid structure, which is suitable for the generation of a delicate binding site by a molecular imprinting technique. The formation of recognition sites near the surface that offers high accessibility for a target molecule is guaranteed due to its high pore volume and nano-sized wall thickness.[17,18] Moreover, a variety of functional groups can be introduced into the mesoporous silica by co-condensation and grafting methods. Selectively functionalized mesoporous silica particles have been widely studied for wide applications in sensing, delivery, separation and catalysis.[19-23] The recent development of sol-gel chemistry allowed controllable fabrication of a highly sensitive and selective fluorescent sensor and selective functionalization of mesoporous silica nanoparticles is used to mitigate the drawbacks of conventional bulk imprinted materials.

II-2. Experimental Section

Materials. 3-(Triethoxysilyl)propyl isocyanate, allyltriethoxysilane and 1,10-decanedithiol were obtained from Tokyo Chemical Industry. Lumidot^{TM} CdSe (capping agent: hexyldecylamine), dibutyltin dilaurate (DBDU), tetraethyl orthosilicate (TEOS), cetyltrimethylammonium bromide (CTAB), bisphenol A, 4,4'-biphenol, diethylstilbestrol and hydroquinone were purchased from Aldrich. All chemicals were used without any purification.

Instruments. ^{1}H NMR and ^{13}C NMR spectra were recorded on a Bruker Avance DPX-300 (300 MHz) and a Jeol JNM-LA400 (100 MHz) spectrometer, respectively. Solid-state ^{13}C CP/MAS NMR spectra were obtained on a Bruker Avance DSX-400 (100 MHz) spectrometer equipped with the CP/MAS probe. Samples were spun in air at approximately 7 kHz. Powder X-ray diffractograms were obtained with the use of a Bruker Nanostar Small Angle X-Ray Scattering system (Cu Kα radiation, = 1.54 Å). Scanning electron microscopy (SEM) images were obtained by using a JEOL JSM-6330F microscope. Transmission electron microscopy (TEM) images were obtained by a Carl Zeiss LIBRA 120 operating at 120 kV. TEM samples were dispersed in methanol and a drop of the mixture was placed on a carbon-coated copper TEM grid. N_2 adsorption-desorption measurements were carried out using Belsorp-Max (BEL Japan, Inc.) and the pore size distribution was calculated using the Barrett-Joyner-Halenda (BJH) model on the adsorption branch. Fluorescence measurements were performed using a Shimadzu RF-5301PC spectrofluorometer. UV-vis spectra were measured with the use of a SCINCO

S-3150.

Synthesis of Triethoxysilane-template (bisphenol A) complex (TES-BPA). This compound was synthesized according to the reported procedure.[18]

Synthesis of 10-(3-(Triethoxysilyl)propylthio)decane-1-thiol (TES-SH). 1,10-Decanedithiol (0.43 mL, 2.0 mmol) was added to a solution of allyltriethoxysilane (0.45 mL, 2.0 mmol) in methanol (2.0 mL) in a quartz flask. The reaction mixture was stirred under UV radiation (254 nm) for 24 h at room temperature. After evaporation of the solvent, the product was isolated by column chromatography on the silica gel (ethyl acetate : *n*-hexane = 1 : 8 v/v) as a colorless oil. Yield: 80 %. ^{1}H NMR (300 MHz, $CDCl_3$, ppm): δ 3.85 (q, OCH_2, 6H), 2.47-2.56 (SCH_2, 6H), 1.51-1.79 ($SCCH_2$, 6H), 1.19-1.42 (CH_2, 12H), 1.21 (t, CH_3, 9H), 0.74 ($SiCH_2$, 2H). ^{13}C NMR (100 MHz, $CDCl_3$, ppm): δ 58.2, 35.1, 33.9, 31.9, 29.6, 29.3, 28.9, 28.8, 28.2, 24.5, 23.1, 18.2, 9.8. Anal. Calcd for $C_{19}H_{42}O_3S_2Si$: C, 55.56; H, 10.31; S, 15.61. Found: C, 55.48; H, 10.24; S, 15.33.

Preparation of BPA embedded mesoporous silica (BPA-MS) particles. An aq. NaOH solution (2.0 M, 3.5 mL) was added to a solution of CTAB (0.94 g, 2.6 mmol) in distilled water (480 mL). A solution of TES-SH (0.059 g, 0.15 mmol) in THF (2.0 mL) was added slowly to the solution and then a solution of TEOS (5.12 g, 24.5 mmol) and TES-BPA (0.22 g, 0.30 mmol) in THF (20 mL) was added dropwise. The reaction mixture was stirred at 70 ^{0}C for 3 h. The precipitated product was filtered, washed with distilled

water, methanol, chloroform and acetone, and dried in a vacuum oven at 25 ^{0}C for 3 days.

Preparation of BPA imprinted mesoporous silica (SH-MIMS) particles. BPA-MS (1.0 g) was stirred in a mixture of HCl (35 wt%, 10 g), distilled water (50 g) and 1,4-dioxane (150 g) at 110 ^{0}C for 24 h. The product was filtered, washed with 1,4-dioxane, methanol and acetone, and dried in a vacuum oven at 25 ^{0}C for 3 days.

Preparation of CdSe QD encapsulated, molecularly imprinted mesoporous silica (QD-MIMS) particles. To a suspension of SH-MIMS (0.1 g) in toluene (10 mL), a toluene solution (1.0 mL) of CdSe quantum dots (Lumidot^{TM} CdSe) (5 mg mL^{-1}) was added. The mixture was stirred at room temperature for 1 h and the product was isolated by filtration, washed with toluene and dried in a vacuum oven at 25 ^{0}C for 3 days.

Preparation of non-imprinted mesoporous silica (SH-NIMS) and CdSe QD encapsulated NIMS (QD-NIMS) particles. SH-NIMS and QD-NIMS were prepared by using the same procedure as for SH-MIMS and QD-MIMS except that no TES-BPA was added.

Kinetic binding test. QD-MIMS (2.0 mg) was dispersed in a solution of BPA (450 ng mL^{-1}) in methanol (20 mL) and the fluorescence spectrum was recorded every 10 min.

Rebinding test. In each vial, QD-MIMS or QD-NIMS (2.0 mg) was dispersed in a solution of different concentrations of BPA (100 - 900 ng mL^{-1}) in methanol (20 mL). After stirring for 1 min, the fluorescence spectrum of each solution was obtained.

Selectivity test. 4,4'-Biphenol, diethylstilbestrol and hydroquinone were used as analogs of BPA. In each vial, QD-MIMS or QD-NIMS (2.0 mg) was dispersed in solutions of different concentrations of these analogs (100 - 600 ng mL^{-1}) in methanol (20 mL). After stirring for 1 min, the fluorescence spectrum of each solution was obtained.

II-3. Results and Discussion

II-3-1. Synthesis and Structural Characterization

The approach to the fabrication of the molecularly imprinted mesoporous silica nanoparticles with thiol functional groups on the pore wall is described in Scheme II-1. Bisphenol A was chosen as a model template, which is known as an endocrine disruptor that can cause harmful effects on humans and wildlife *via* interactions with the endocrine system. Given that the awareness of the risks involved with endocrine disrupting compounds is growing, the determination of these contaminants of concern at ng mL^{-1} levels is of great importance.[24-27] A triethoxysilane-template complex (TES-BPA) was prepared by the reaction between 3-(triethoxysilyl)propyl isocyanate and BPA.[18] To functionalize the pore wall selectively, A thiol-functionalized amphiphilic silica precursor (TES-SH) was synthesized through the radical reaction of allyltriethoxysilane and 1,10-decanedithiol. The thiol groups were used later for QD encapsulation.

The thiol-functionalized, BPA embedded mesoporous silica (BPA-MS) particles were prepared by co-condensation of TES-BPA, TES-SH and tetraethyl orthosilicate (TEOS) in the presence of cetyltrimethylammonium bromide (CTAB) under basic conditions. Both amphiphiles, CTAB and TES-SH, formed a micellar structure in an aqueous solution where hydrophobic portions of the amphiphiles were located inside the pore. The silica precursors, TEOS, TES-BPA and TES-SH, were allowed to react in this aqueous solution to form silica particles.

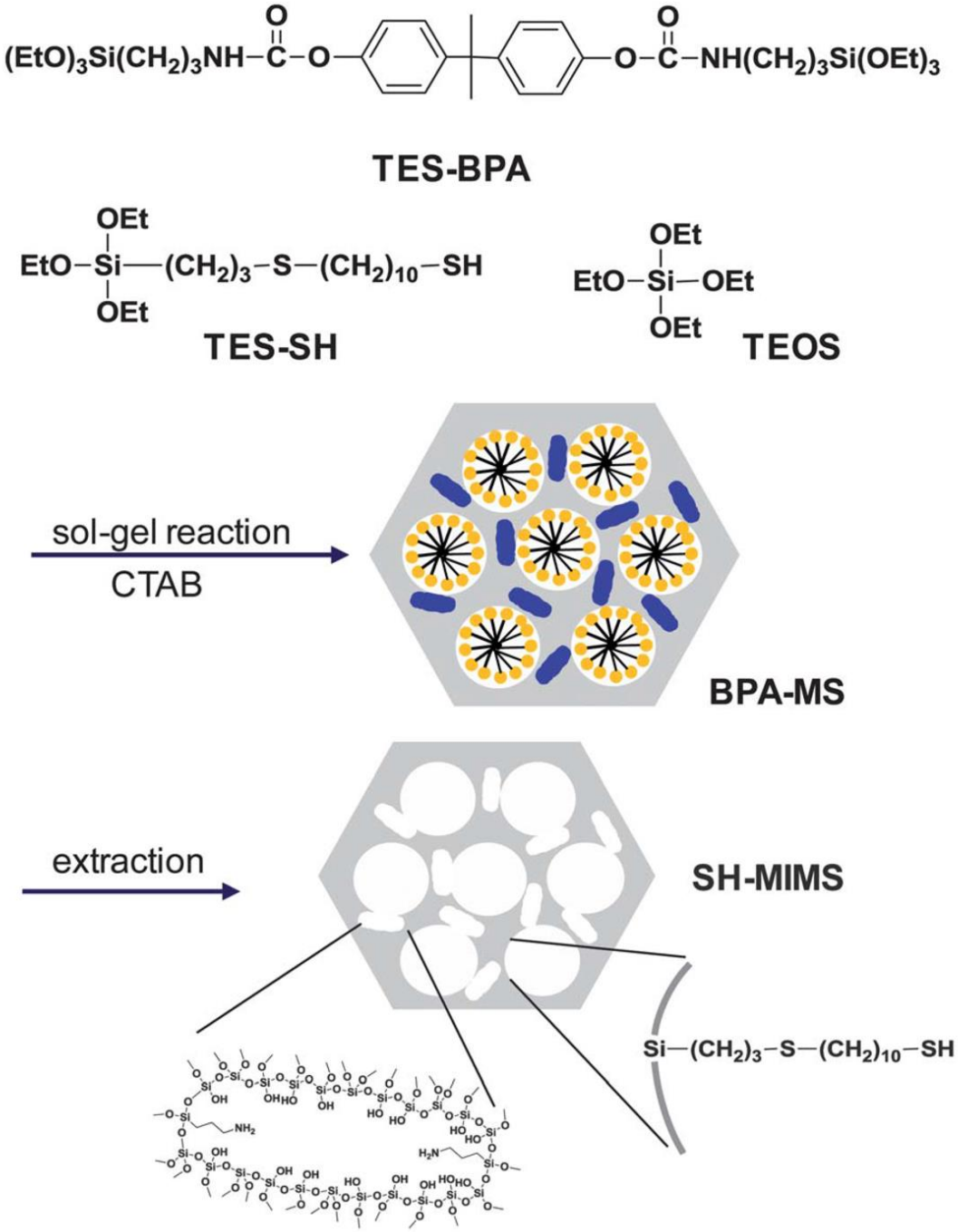

Scheme II-1. Synthetic procedure of thiol-functionalized, BPA imprinted mesoporous silica particles (SH-MIMS).

The surfactant molecules in the pores could be removed by a reflux in a mixture of 1,4-dioxane, HCl and deionized water. However, the thiol-functionalized hydrophobic

groups in the pores remained since they were covalently tethered to the pore wall by the sol-gel reaction. By the reflux, the template molecules were also removed as a result of dissociation of thermally reversible urethane bonds between the template and the silica matrix. The dissociated isocyanate groups were reacted with water to yield amino groups. The successful extraction of CTAB was confirmed by the decrease in the characteristic FT-IR absorptions of CTAB in the 3000-2800 cm^{-1} region (Figure II-1).

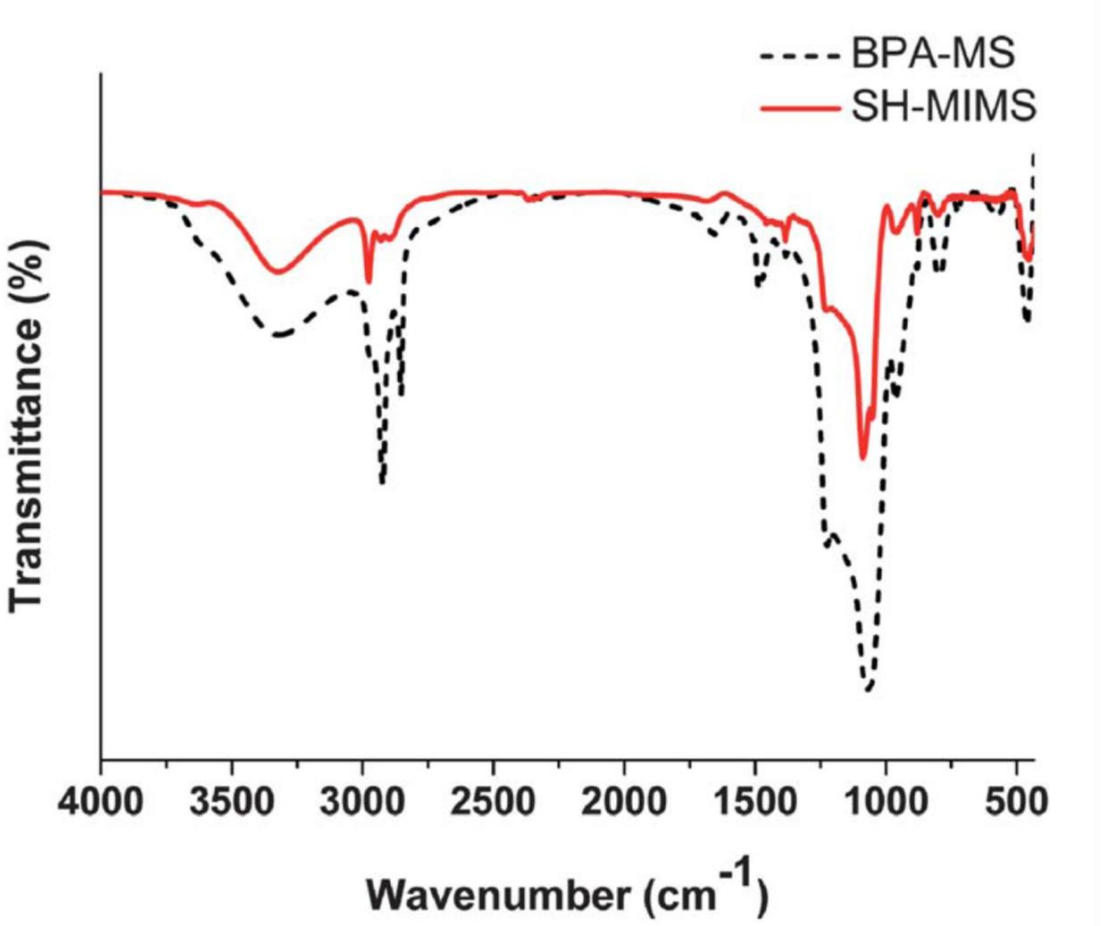

Figure II-1. FT-IR spectra of BPA-MS and SH-MIMS.

The structures of BPA-MS and the thiol-functionalized, BPA imprinted mesoporous silica (SH-MIMS) particles were investigated by solid-state ^{13}C CP/MAS NMR spectroscopy. BPA-MS showed the signals for the aromatic carbons of BPA at around 165

ppm.[18] In the spectrum of SH-MIMS, however, these signals disappeared, indicating that most of the template molecules were removed. The peak for the aminomethylene carbon on the silica framework appeared at 42 ppm. The strong signal at 29 ppm was assigned to methylene carbons of the thiol-functionalized hydrophobic groups (Figure II-2).[28]

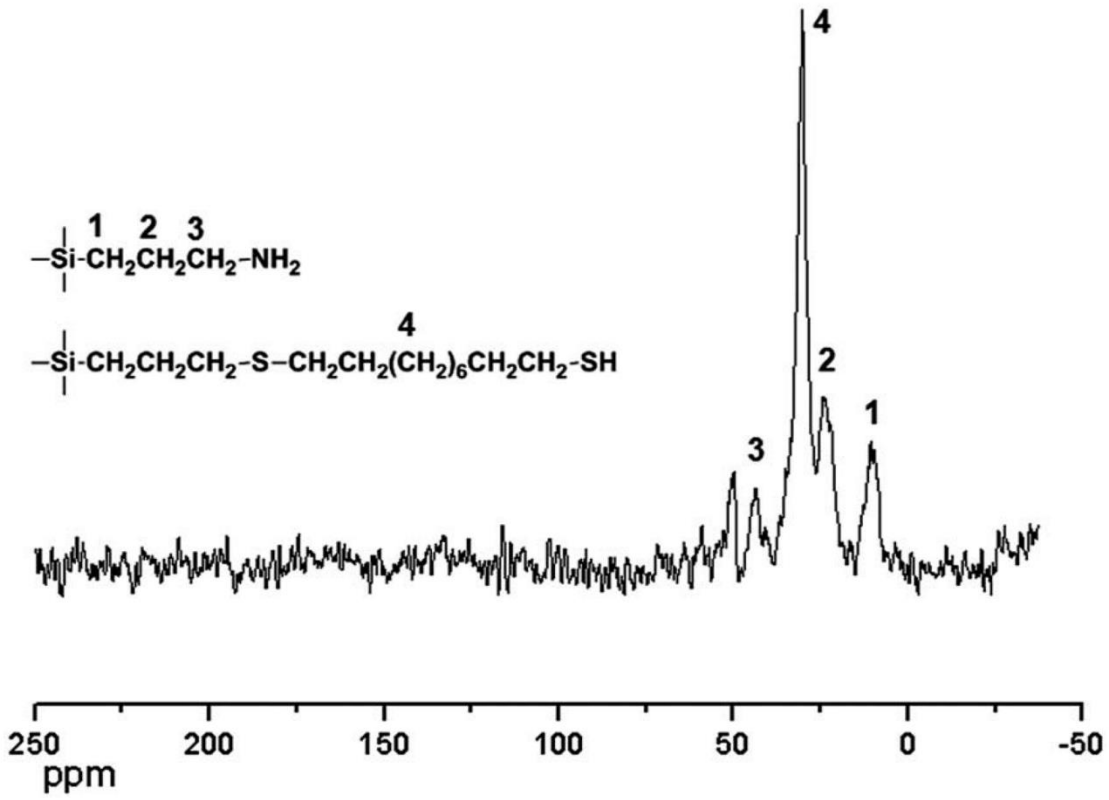

Figure II-2. Solid-state ^{13}C CP/MAS NMR spectrum of SH-MIMS.

The small angle X-ray diffractogram of SH-MIMS showed three resolved peaks with *d*-spacings of 42.5, 24.5 and 21.4 Å, corresponding to (100), (110) and (200) reflections of a hexagonal structure with a lattice parameter of a = 49.1 Å, respectively (Figure II-3a). Nitrogen adsorption-desorption isotherms were of type IV, indicating that the pore sizes were in the mesopore range (Figure II-3b). The average pore size estimated by the Barrett-Joyner-Halenda (BJH) pore size distribution was 3 nm and the Brunauer-Emmett-

Teller (BET) surface area was 1157 m^2g^{-1}. The overall morphology of SH-MIMS was characterized by SEM and TEM measurements. Figure II-3c exhibited particles with an average size of 90 nm. Figure II-3d showed the hexagonal array of the mesopores as proposed by the X-ray analysis.

CdSe quantum dots were encapsulated into the pores of SH-MIMS by ligand exchange. Hexyldecylamine (HDA)-capped Lumidot^{TM} CdSe QDs with a size of about 2.1 nm were mixed with SH-MIMS in toluene. The TEM image of the QD-encapsulated, molecularly imprinted mesoporous silica (QD-MIMS) particles demonstrated the successful ligation of CdSe QDs (Figure II-3e). QDs were entrapped in the pores by the displacement of HDA with the thiol group on the pore walls. QD-MIMS had two point binding sites formed between the pores and CdSe QDs encapsulated in the pores. Once BPA was captured in the binding site, the fluorescence of the QDs was expected to be quenched possibly by charge transfer between QD and BPA.[29-31]

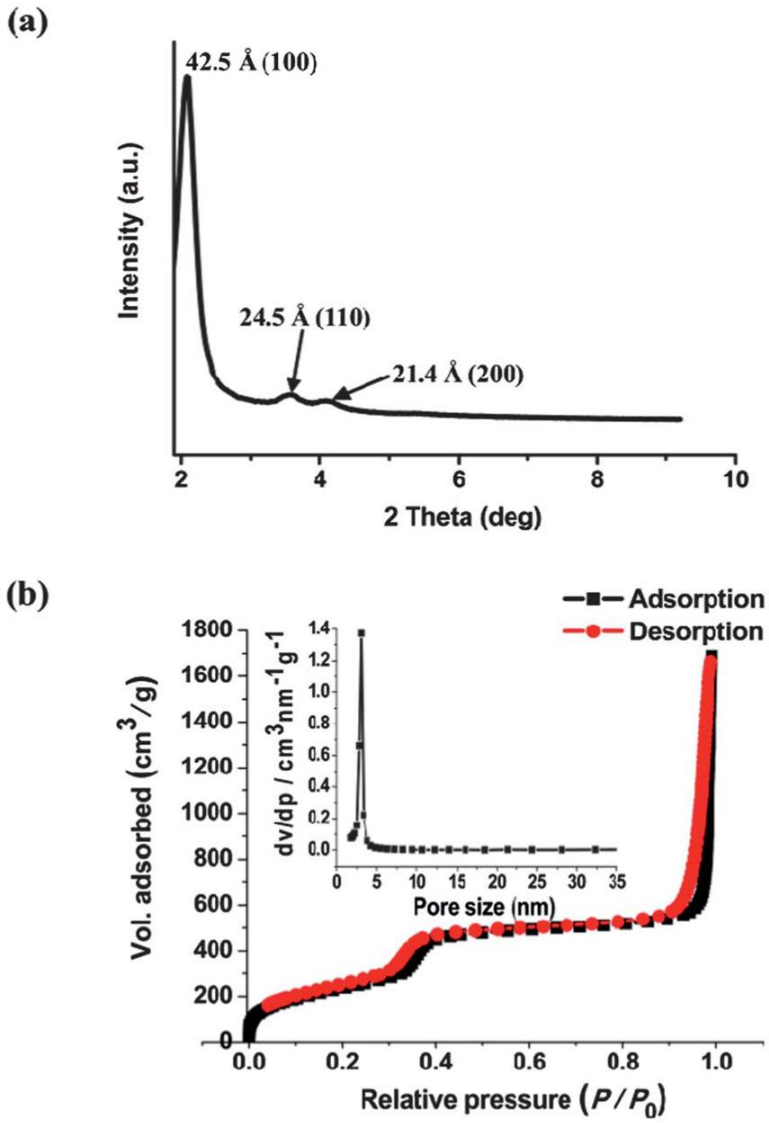
(a)
42.5 Å (100)
24.5 Å (110)
21.4 Å (200)
Intensity (a.u.)
2 Theta (deg)
(b)
Adsorption
Desorption
Vol. adsorbed (cm3/g)
dv/dp / cm3nm-1g-1
Pore size (nm)
Relative pressure (P/P0)
(c)
100 nm
(d)
50 nm
(e)
50 nm

Figure II-3. (a) Small angle X-ray diffractogram and (b) nitrogen adsorption-desorption isotherms of SH-MIMS (inset: pore size distribution plot). (c) SEM and (d) TEM images of SH-MIMS. (e) TEM image of QD-encapsulated, BPA imprinted MS (QD-MIMS).

II-3-2. Photophysical and Kinetic Binding Properties of QD-MIMS

As shown in Figure II-4a, the characteristic absorption of BPA occurred around 270 nm. Given the wide range of absorption wavelength of the QD-MIMS (Figure II-4b), the emission spectrum of QD-MIMS dispersed in methanol was obtained by excitation at 290 nm, which fit in the absorption range of BPA. QD-MIMS showed a strong fluorescence emission peak at 545 nm (Figure II-4c) in addition to the Rayleigh scattering peaks at 290 and 580 nm. In the presence of BPA, the fluorescence intensity of QD-MIMS decreased with increasing BPA concentration and incubation time.

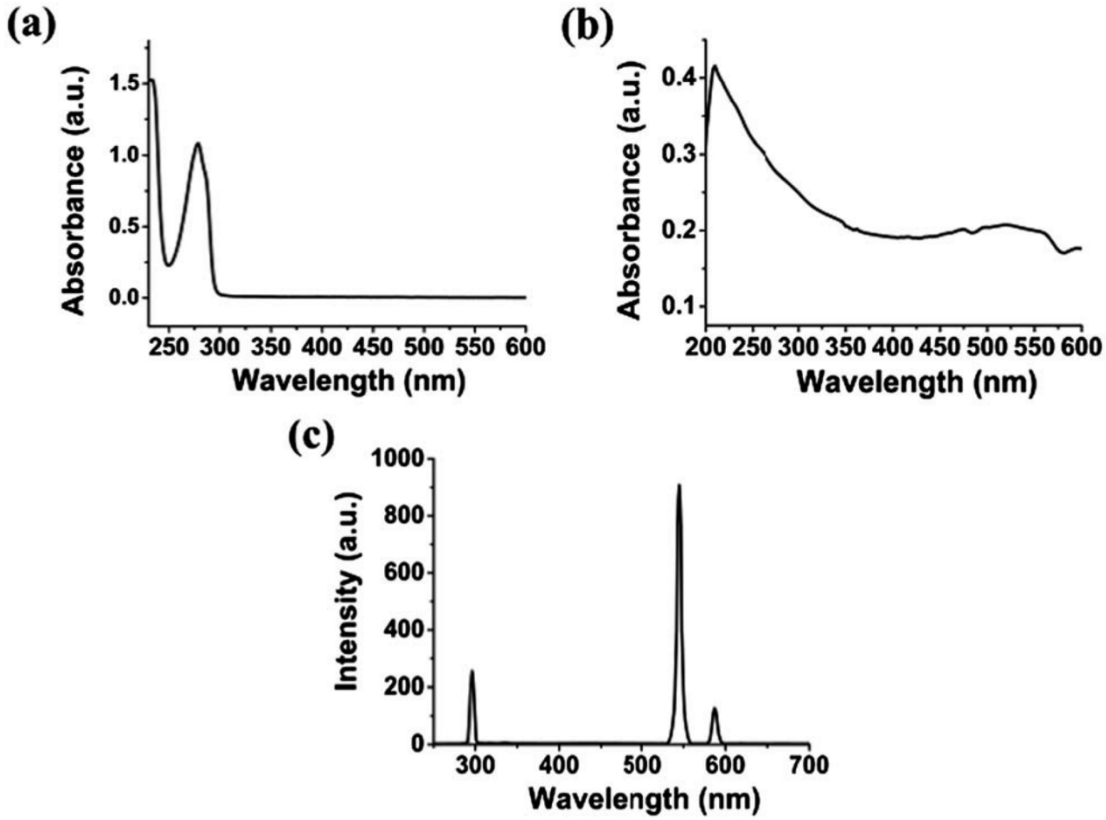

Figure II-4. (a) UV-vis absorption spectrum of bisphenol A. (b) UV-vis absorption and (c) emission spectra of QD-MIMS dispersed in methanol (λ_{ex} = 290 nm).

To study the kinetic binding behavior of QD-MIMS for BPA, QD-MIMS (2 mg) were dispersed in a solution of BPA (450 ng mL^{-1}) in methanol (20 mL) with stirring and the fluorescence spectrum was measured at 20 min intervals. The fluorescence intensity rapidly decreased up to 20 min and thereafter slowly decreased (Figure II-5).

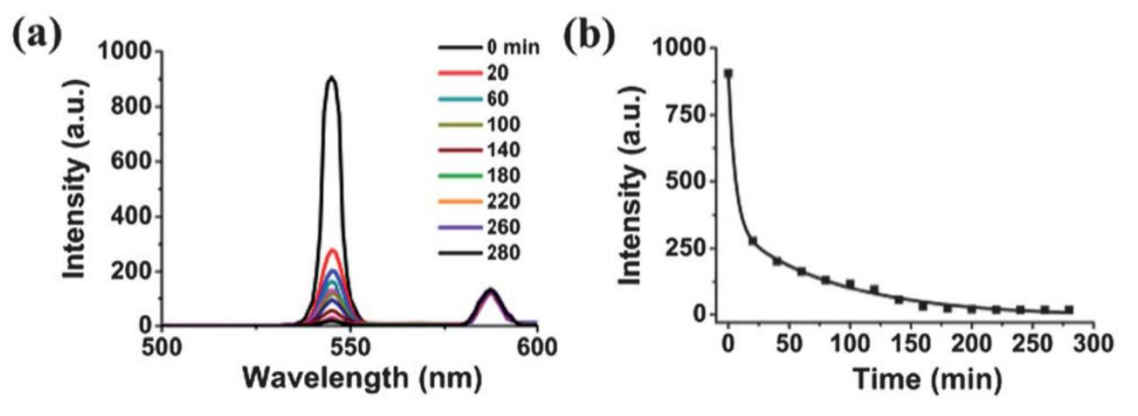

Figure II-5. (a) Evolution of fluorescence spectra of QD-MIMS (100 μg mL^{-1}) in the presence of bisphenol A (450 ng mL^{-1}) obtained after incubating for different periods of time in methanol (λ_{ex} = 290 nm). (b) Plot of the maximum fluorescence intensity *vs.* incubation time.

II-3-3. Sensitivity and Selectivity Study of QD-MIMS

Although the maximum quenching reached after 3 h, a rapid detection of BPA after 1 min incubation was explored. QD-MIMS was mixed in a solution of BPA in methanol at varied concentrations with stirring for 1 min and the fluorescence spectrum of each solution was measured. The fluorescence intensity was very sensitive to the concentration of BPA. Figure II-6a depicts the change of the fluorescence intensity of the QD as the concentration of BPA increases in methanol. The fluorescence intensity of the QD was gradually decreased with an increase of the BPA concentration. This result could be attributed to the fact that BPA bound to the selective imprinted site and the charge transfer between the QD and BPA was followed.

QD-MIMS also showed high selectivity for BPA (Figure II-6b). Several structural analogs including 4,4'-biphenol, diethylstilbestrol (DES) and hydroquinone (HQ) were chosen for conducting the selectivity test. They are also highly toxic and possible

endocrine disruptors.[32-34] The binding the detection experiments were carried out in the same manner as described above. Compared with BPA, much less decrease in the fluorescence intensity of the QD was observed for the analogs (Figure II-6c-e), implying that it was challenging for those structural analogs to bind to the imprinted sites. Figure II-6f shows the fluorescence spectra of QD-encapsulated non-imprinted mesoporous silica (QD-NIMS) particles obtained with increasing BPA concentration. QD-NIMS was prepared in the same manner as QD-MIMS except that BPA was omitted. As shown in the result, a decrease in the fluorescence intensity of QD-NIMS was much smaller than that of QD-MIMS at the same concentration. This finding also corroborated that BPA-selective binding sites were developed successfully. A non-specific binding of the template molecule could not satisfy the proximity requirement for efficient fluorescence quenching.

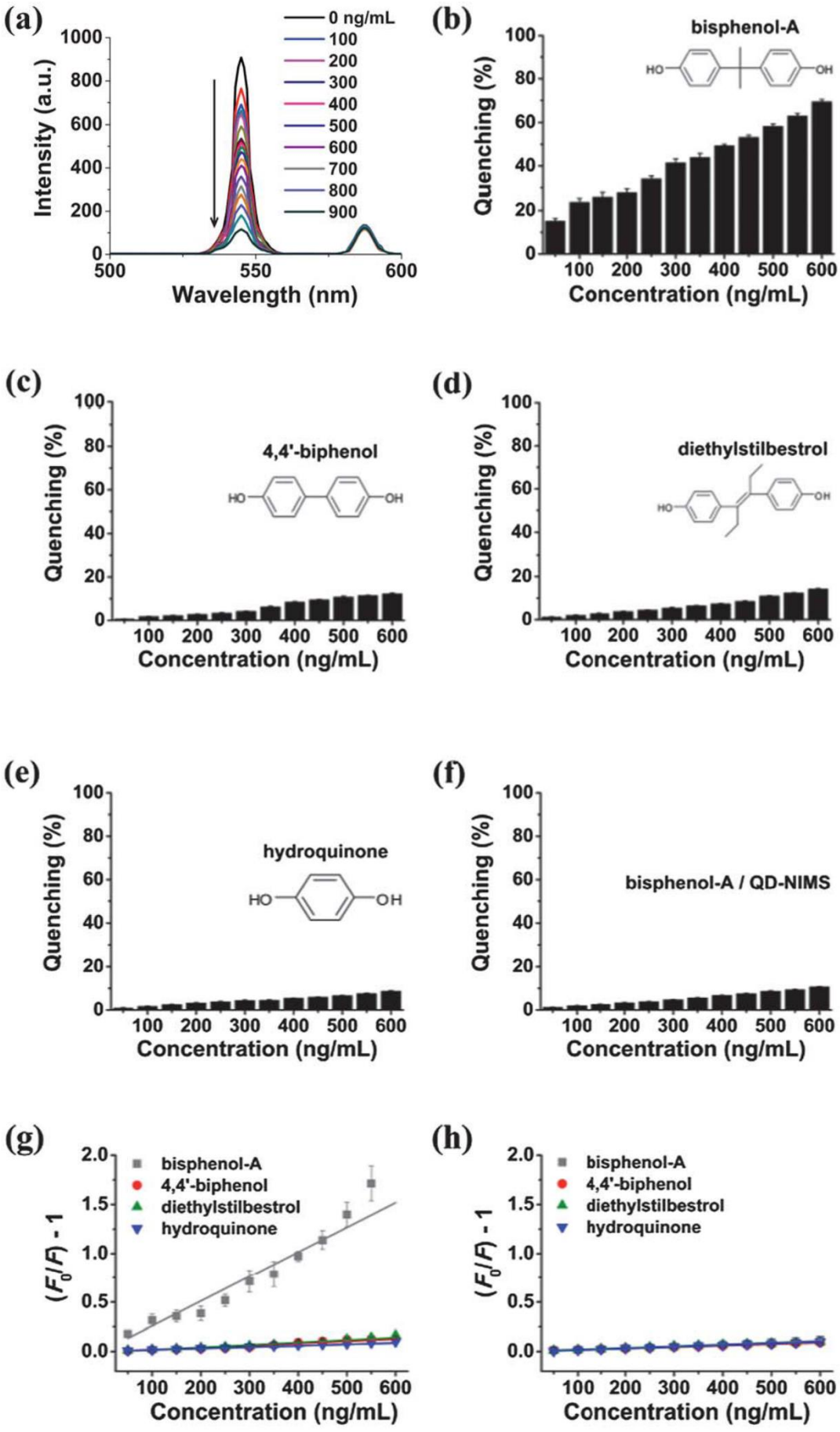
(a)
0 ng/mL
100
200
300
400
500
600
700
800
900
Intensity (a.u.)
Wavelength (nm)
(b)
bisphenol-A
Quenching (%)
Concentration (ng/mL)
(c)
4,4'-biphenol
(d)
diethylstilbestrol
(e)
hydroquinone
(f)
bisphenol-A / QD-NIMS
(g)
bisphenol-A
4,4'-biphenol
diethylstilbestrol
hydroquinone
(F0/F) - 1
(h)

Figure II-6. (a) Fluorescence spectra of QD-MIMS (100 μg mL^{-1}) obtained after 1 min incubation with the increasing concentration of BPA in methanol. Fluorescence quenching % [= (1 - F/F_0)100] of QD-MIMS (100 μg mL^{-1}) measured after 1 min incubation with the increasing concentration of (b) BPA, (c) 4,4′-biphenol, (d) DES and (e) HQ in methanol. (f) Fluorescence quenching % of QD-NIMS (100 μg mL^{-1}) obtained after 1 min incubation with the increasing concentration of BPA in methanol. (g) Stern-Volmer plots from QD-MIMS. (h) Stern-Volmer plots from QD-NIMS.

Quenching of fluorescence can be described by the following Stern-Volmer equation[35]

$$F_0/F = 1 + K_{SV}[C]$$

where F and F_0 are the fluorescence intensities of QD-MIMS in the presence and absence of an analyte, respectively. K_{SV} is the Stern-Volmer quenching constant and [C] is the analyte concentration. This equation can be used to evaluate the selectivity toward the imprinted molecule quantitatively. Both QD-MIMS (Figure II-6g) and QD-NIMS (Figure II-6f) showed a linear Stern-Volmer relationship for BPA and its analogs. Quenching constants were determined from the slopes of the Stern-Volmer plots. The much larger quenching constant of QD-MIMS for BPA (by more than ten times) than those for BPA analogs clearly demonstrated the high selectivity of QD-MIMS (Figure II-7). The imprinting factor (IF), defined as the ratio of the quenching constant of QD-MIMS for BPA to that of QD-NIMS, was 13.6.

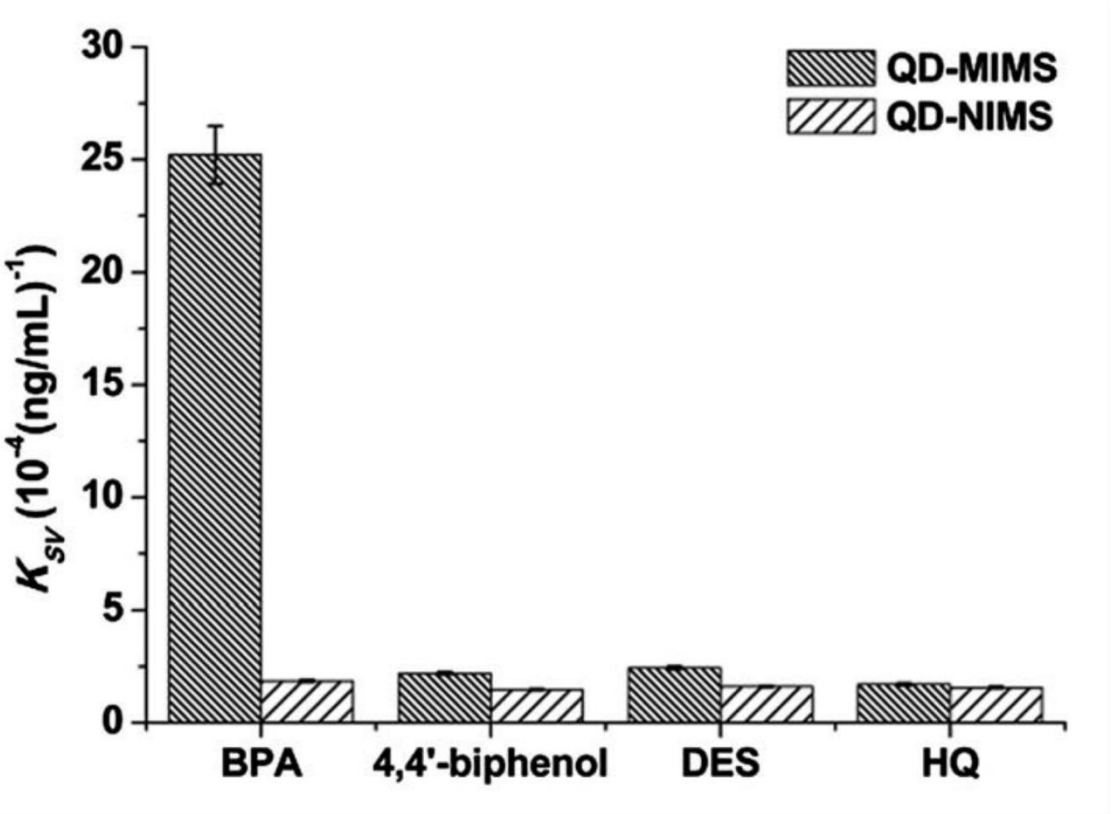

Figure II-7. Stern-Volmer quenching constants of QD-MIMS and QD-NIMS toward different target molecules. For all the experiments, the excitation wavelength was 290 nm.

II-4. Conclusions

A CdSe QD-encapsulated molecularly imprinted mesoporous silica nanoparticle (QD-MIMS) was prepared as a fluorescent sensor. Selective binding sites between the pores could be introduced and CdSe QDs were successfully encapsulated into the pores of the mesoporous silica. QD-MIMS exhibited excellent molecular recognition properties in terms of both sensitivity and selectivity. Due to the proximity of the binding cavities to the QDs, a significant, concentration-sensitive fluorescence quenching was observed in the presence of the template molecule, BPA.

II-5. References

1. Haupt, K.; Mosbach, K. *Chem. Rev.* **2000**, 100, 2495-2504.

2. Wulff, G. *Chem. Rev.* **2002**, 102, 1-27.

3. Whitcombe, M. J.; Vulfson, E. N. *Adv. Mater.* **2001**, 13, 467-478.

4. Ye, L.; Mosbach, K. *Chem. Mater.* **2008**, 20, 859-868.

5. Li, Z.; Ding, J.; Day, M.; Tao, Y. *Macromolecules* **2006**, 39, 2629-2636.

6. Ki, C. D.; Chang, J. Y. *Macromolecules* **2006**, 39, 3415-3419.

7. Yang, H.-H.; Zhang, S.-Q.; Tan, F.; Zhuang, Z.-X.; Wang, X.-R. *J. Am. Chem. Soc.* **2005**, 127, 1378-1379.

8. Kim, W. J.; Jung, B. M.; Kang, S. H.; Chang, J. Y. *Soft Matter* **2011**, 7, 4160-4162.

9. Liu, J.; Chen, H.; Lin, Z.; Lin, J. M. *Anal. Chem.* **2010**, 82, 7380-7386.

10. Zhang, W.; He, X. W.; Chen, Y.; Li, W. Y.; Zhang, Y. K. *Biosens. Bioelectron.* **2011**, 26, 2553-2558.

11. Tong, A.; Dong, H.; Li, L. *Anal. Chim. Acta* **2002**, 466, 31-37.

12. Malosse, L.; Buvat, P.; Adès, D.; Siove, A. *Analyst* **2008**, 133, 588-595.

13. Li, J.; Kendig, C. E.; Nesterov, E. E. *J. Am. Chem. Soc.* **2007**, 129, 15911-15918.

14. Medintz, I. L.; Stewart, M. H.; Trammell, S. A.; Susumu, K.; Delehanty, J. B.; Mei, B. C.; Melinger, J. S.; Blanco-Canosa, J. B.; Dawson, P. E.; Mattoussi, H. *Nat. Mater.* **2010**, 9, 676-684.

15. Feng, Q.; Dong, L.; Huang, J.; Li, Q.; Fan, Y.; Xiong, J.; Xiong, C. *Angew. Chem. Int. Ed.* **2010**, 49, 9943-9946.

16. Zhao, Y.; Ma, Y.; Li, H.; Wang, L. *Anal. Chem.* **2012**, 84, 386-395.

17. Jung, B. M.; Kim, M. S.; Kim, W. J.; Chang, J. Y. *Chem. Commun.* **2010**, 46, 3699-

3701.

18. Lofgreen, J. E.; Moudrakovski, I. L.; Ozin, G. A. *ACS Nano* **2011**, 5, 2277-2287.

19. Du, J.; Cipot-Wechsler, J.; Lobez, J. M.; Loock, H. P.; Crudden, C. M. *Small* **2010**, 6, 1168-1172.

20. Kim, M. S.; Chang, J. Y. *J. Mater. Chem.* **2011**, 21, 8766-8771.

21. Zhao, Y.-L.; Li, Z.; Kabehie, S.; Botros, Y. Y.; Stoddart, J. F.; Zink, J. I. *J. Am. Chem. Soc.* **2010**, 132, 13016-13025.

22. Lu, S.; Wang, D.; Jiang, S. P.; Xiang, Y.; Lu, J.; Zeng, J. *Adv. Mater.* **2010**, 22, 971-976.

23. Shylesh, S.; Wagener, A.; Seifert, A.; Ernst, S.; Thiel, W. R. *Angew. Chem. Int. Ed.* **2010**, 49, 184-187.

24. Ye, X.; Kuklenyik, Z.; Needham, L. L.; Calafat, A. M. *Anal. Chem.* **2005**, 77, 5407-5413.

25. Lu, C.; Li, J.; Yang, Y.; Lin, J.-M. *Talanta* **2010**, 82, 1576-1580.

26. Zhong, S.; Tan, S. N.; Ge, L.; Wang, W.; Chen, J. *Talanta* **2011**, 85, 488-492.

27. Feng, Y.; Ning, B.; Su, P.; Wang, H.; Wang, C.; Chen, F.; Gao, Z. *Talanta* **2009**, 80, 803-808.

28. Ki, C. D.; Emrick, T.; Chang, J. Y. *Adv. Mater.* **2005**, 17, 230-233.

29. Freeman, R.; Finder, T.; Bahshi, L.; Willner, I. *Nano Lett.* **2009**, 9, 2073-2076.

30. Santhosh, K.; Patra, S.; Soumya, S.; Khara, D. C.; Samanta, A. *ChemPhysChem* **2011**, 12, 2735-2741.

31. Huang, J.; Huang, Z.; Jin, S.; Lian, T. *J. Phys. Chem. C* **2008**, 112, 19734-19738.

32. Paris, F.; Balaguer, P.; Térouanne, B.; Servant, N.; Lacoste, C.; Cravedi, J.-P.; Nicolas, J.-C.; Sultan, C. *Mol. Cell. Endocrinol.* **2002**, 193, 43-49.

33. Kitamura, T.; Nishimura, S.; Sasahara, K.; Yoshida, M.; Ando, J.; Takahashi, M.;

Shirai, T.; Maekawa, A. *Cancer Lett.* **1999**, 141, 219-228.

34. Peters, M. M.; Jones, T. W.; Monks, T. J.; Lau, S. S. *Carcinogenesis* **1997**, 18, 2393-2401.

35. Wang, H.-F.; He, Y.; Ji, T.-R.; Yan, X.-P. *Anal. Chem.* **2009**, 81, 1615-1621.

Chapter III.

Preparation of a Fluorescent Sensor by Organogelation: CdSe/ZnS Quantum Dots Embedded Molecularly Imprinted Organogel Nanofibers

III-1. Introduction

The molecular imprinting technique provides a platform for the fabrication of selective synthetic receptors.[1] In the molecular imprinting process, a complex of a functional monomer with a template is polymerized in the presence of a cross-linking agent and the template is subsequently removed to form a binding cavity in a cross-linked polymer matrix. Molecularly imprinted polymers (MIPs) as versatile synthetic receptors have several potential advantages such as ease of preparation, high physiochemical stability and broad range of working conditions compared to natural receptors.[2-4] Although poor binding site accessibility and low selectivity have been considered as the drawbacks of MIPs, recent studies showed that these shortcomings are less severe by using nanosized imprinting matrices such as nanoparticles[5-7] or nanofibers,[8-12] where recognition sites are generated at the surface or in the proximity of the surface.

An organogel is a viscoelastic material consisting of a large number of solvent molecules and a nanofiber network produced by the self-assembly process of low mass gelator molecules.[13] The supramolecular nanofibers are stable when equilibrating with

solvent molecules in an organogel, but are easily disrupted by thermal and mechanical stimuli. Some organogels have shown gel to sol or gel to gel transitions in the presence of chemicals such as anions with accompanying fluorescent emission changes. Fluorescent sensors based on organogels have been developed by utilizing their chemical stimuli-responsive properties.[14-17] The efficiency of these sensing systems relies on fast phase transitions through specific interactions of an analyte with a gelator molecule, which is often difficult to achieve.

A novel MIP-based fluorescent sensor fabricated through an organogelation process is investigated in this chapter. Molecularly imprinted nanofibers were prepared by the gel-state polymerization of an organogelator bearing two different polymerizable groups.[10] In the development of MIP-based sensors, transformation of binding events into measurable signals is a major concern.[18-28] A fluorescent CdSe/ZnS quantum dot (QD) is used as a signal transducer. QDs are finding increasing utility in sensing applications due to their discrete size-dependent optical properties and good photostability.[29-35] The QDs capped with ligands having long alkyl chains were incorporated into organogel nanofibers through interactions between the ligands and the gelator molecules.[36] Histamine was chosen as a model template. Histamine is a representative biogenic amine which is formed by decarboxylation of an amino acid. The reliable determination of histamine at low concentrations is of great importance in clinical chemistry and food science. Histamine is a neurotransmitter and involved in various physiological functions. It is released during allergic reactions, which causes irritation and inflammation.[37,38] A high level of histamine is also found in spoiled foods. The detection of histamine in conjunction with different analytical approaches such as high performance liquid chromatography, enzyme-linked immunosorbent assay, and capillary electrophoresis has been attempted.[39-41]

III-2. Experimental Section

Materials. 10,12-Tricosadiynoic acid (96%) was purchased from Alfa Aesar. Divinylbenzene (DVB) and *N*,*N*-(dimethylamino)pyridine (DMAP, 99%) were purchased from Aldrich. Histamine (97%) and serotonin hydrochloride (98%) were purchased from Acros Organics. Allopurinol (98%), dopamine hydrochloride (98%), 6-bromo-1-hexanol (95%), 4'-hydroxy-4-biphenyl-carboxylic acid (98%), 2,6-di-tert-butylphenol (98%), *N*,*N*-diethylaniline (99%), acryloyl chloride (95%), 4,4'-biphenol (99%), and *N*,*N*-dicyclohexylcarbodiimide (DCC, 98%) were purchased from Tokyo Chemical Industry. CdSe/ZnS quantum dot (particle size: ~3.4 nm, capping agent: trioctylphosphine oxide) was obtained from Nanosquare Inc. 2,2,-Dimethoxy-2-phenylacetophenone (DMPA) was obtained from Ciba Specialty. All chemicals and reagents were used as received. Tetrahydrofuran (THF) was dried over sodium metal and distilled.

Measurements. ^{1}H and ^{13}C NMR spectra were recorded on a Bruker Avance DPX-300 (300 MHz for ^{1}H NMR) spectrometer and a Bruker Avance 600 (150 MHz for ^{13}C NMR) spectrometer. Fourier transform infrared (FT-IR) spectra were measured on a Nicolet 6700 FT-IR spectrophotometer (Thermo Scientific, USA) using KBr pellets. Scanning electron microscopy (SEM) images were measured by a Carl Zeiss SUPRA 55VP. High resolution transmission electron microscopy (HRTEM) images were obtained by a FEI Tecnai F20 operating at 200 kV. UV-vis spectrum was obtained with the use of a SCINCO S-3150 instrument. Fluorescence measurements were performed using a Shimadzu RF-5301PC spectrofluorometer.

Synthesis of 4-[4-(6-acryloyloxyhexyloxy)phenyl]benzoic acid (FM). This compound was prepared as a functional monomer according to our previous report.[42]

Synthesis of 4-hydroxy-4'-[6-(acryloyl)hexyloxy]biphenyl. This compound was synthesized according to our previous report.[43]

Synthesis of 4'-(6-(acryloyloxy)hexyloxy)biphenyl-4-yl tricosa-10,12-diynoate (PG). DCC (0.76 g, 3.7 mmol) and DMAP (0.080 g, 0.74 mmol) were added to a solution of 4-hydroxy-4'-[6-(acryloyl)hexyloxy]biphenyl (1.04 g, 3.06 mmol) and 10,12-tricosadiynoic acid (0.600 g, 3.06 mmol) in methylene chloride (50 mL), and the mixture was stirred for 12 h at room temperature. Insoluble solids were removed by filtration. After evaporation of the solvent, the crude products were purified by column chromatography on the silica gel using THF and *n*-hexane (1:5) as eluents to give white solids. Yield: 68.9%. ^{1}H NMR (300 MHz, $CDCl_3$, ppm): δ 7.44 (dd, overlap, Ar, 4H), 7.12 (d, J = 8.4 Hz, COOAr, 2H), 6.94 (d, J = 8.4 Hz, -OAr, 2H), 6.43 (d, J = 17.4 Hz, =CH, 1H), 6.12 (dd, J = 10.5, 10.5 Hz, =CH, 1H), 5.82 (d, J = 10.2 Hz, =CH, 1H), 4.18 (t, J = 6.6 Hz, $-OCH_2$, 2H), 4.00 (t, J = 6.6 Hz, $-ArOCH_2-$, 2H), 2.57 (t, J = 7.2 Hz, $-OCOCH_2-$, 2H), 2.25 (t, J = 5.1 Hz, $\equiv CCH_2-$, 2H), 1.85-1.72 (overlap, $\equiv CCCH_2-$, 2H, $-ArOCCH_2-$, 2H, $-COOCCH_2-$, 2H, $-OCOCCH_2-$, 2H), 1.54-1.26 (m, $-CH_2-$, 26H), 0.88 (t, J = 6.5 Hz, $-CH_3$, 3H). ^{13}C NMR (150 MHz, $CDCl_3$, ppm): δ 169.1, 165.1, 157.8, 151.7, 134.0, 130.4, 128.7, 128.3, 128.0, 127.7, 121.6, 115.0, 75.7, 72.3, 66.7, 62.9, 33.9, 31.9,

29.6, 29.3, 29.1, 28.9, 28.8, 28.2, 27.2, 26.5, 26.3, 25.2, 23.1, 18.2, 15.9 ppm. IR (KBr, cm^{-1}): 2921, 2852, 2242, 2145, 1745, 1721, 1639, 1607, 1499, 1470, 1410, 1388, 1324, 1290, 1272, 1249, 1216, 1196, 1170, 1153, 1035, 996, 925, 892, 823, 718. Anal. Calcd for $C_{44}H_{60}O_5$: C, 79.00; H, 9.04; O, 11.96. Found: C, 79.08; H, 9.09; O, 11.72.

Preparation of CdSe/ZnS QD-incorporated, histamine imprinted organogel nanofibers (QD-HIOGNF). Histamine (2.0 mg, 0.018 mmol), FM (13 mg, 0.036 mmol) and DMPA (30 mg) were dissolved in *n*-decane (0.37 g). To a solution, PG (38 mg) and DVB (3.7 mg) were added and the mixture was heated at 65 ^{0}C until a clear solution was obtained. After the subsequent addition of CdSe/ZnS quantum dots (0.5 mL, 5 mg mL^{-1} in *n*-decane), the solution was cooled to room temperature to form a stable organogel. The photopolymerization of the organogel was performed by UV irradiation (a high-pressure mercury arc lamp, 3 mW cm^{-2}) for 3 h at room temperature. Histamine was extracted by stirring the reaction mixture in methanol/acetic acid (20 mL, 9:1 v/v) for 24 h and Soxhlet extraction with methanol for 48 h. The resulting histamine imprinted nanofibers were isolated by filtration and dried in vacuo. CdSe/ZnS QD-incorporated, non-imprinted organogel nanofibers (QD-NIOGNF) were prepared using the same procedure as that used for the preparation of QD-HIOGNF, except that no histamine was added.

Kinetic binding test. QD-HIOGNF (3 mg) was dispersed in a solution of histamine (500 ng mL^{-1}) in methanol (20 mL) and the fluorescence spectrum was measured every 10 min.

Rebinding test. In each vial, QD-HIOGNF or QD-NIOGNF (3 mg) was immersed in different concentrations of histamine solutions (100 – 700 ng mL^{-1}) in methanol (20 mL). After stirring for 10 min, the fluorescence spectrum of each solution was measured.

Selectivity test. Allopurinol, serotonin, and dopamine were used as analogs of histamine. QD-HIOGNF or QD-NIOGNF (3 mg) was dispersed in solutions of different concentrations of these analogs (100 – 700 ng mL^{-1}) in methanol (20 mL). After stirring for 10 min, the fluorescence spectrum of each solution was obtained.

Recyclability. QD-HIOGNF (3 mg) was added to a solution of histamine (100 ng mL^{-1}) in methanol (20 mL) and the fluorescence spectrum of the mixture was measured after stirring for 30 min. After evaporation of methanol, the solid residue was stirred in methanol/acetic acid (20 mL, 9:1 v/v) for 12 h and Soxhlet-extracted with methanol for 12 h. QD-HIOGNF was isolated by filtration, dried and reused for the binding test.

III-3. Results and Discussion

III-3-1. Preparation of Organogel Nanofibers

The approach used in this study to fabricate a fluorescent sensor by organogelation is described in Scheme III-1. The sensor fabrication was carried out in three steps: 1) organogelation of a polymerizable gelator (PG) in the presence of the QD and the template, 2) gel-state polymerization and 3) extraction of the template.

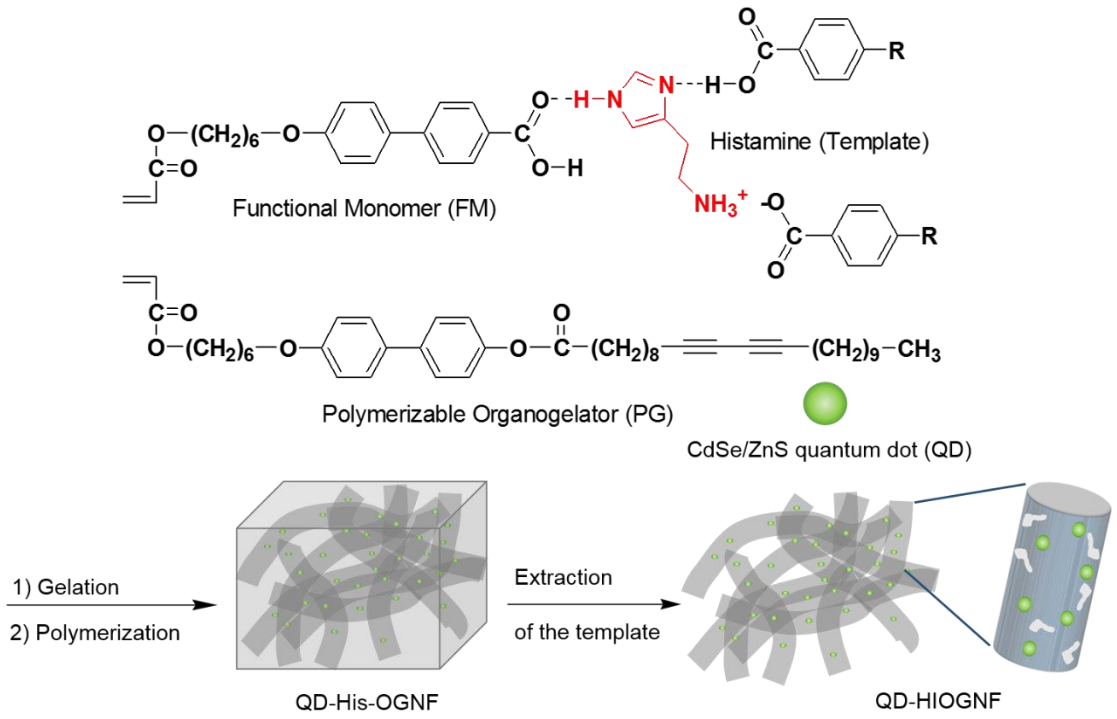

Scheme III-1. Schematic route of the preparation of QD-incorporated, histamine imprinted organogel nanofibers (QD-HIOGNF).

A heterobifunctional organogelator (PG) bearing two different polymerizable groups was prepared by an esterification reaction of an acrylate having a phenolic group with a diacetylene-containing carboxylic acid (Scheme III-2). PG showed an ability to gelate *n*-

decane, methanol and ethanol. The critical gelation concentration was 1.5 wt% in *n*-decane.

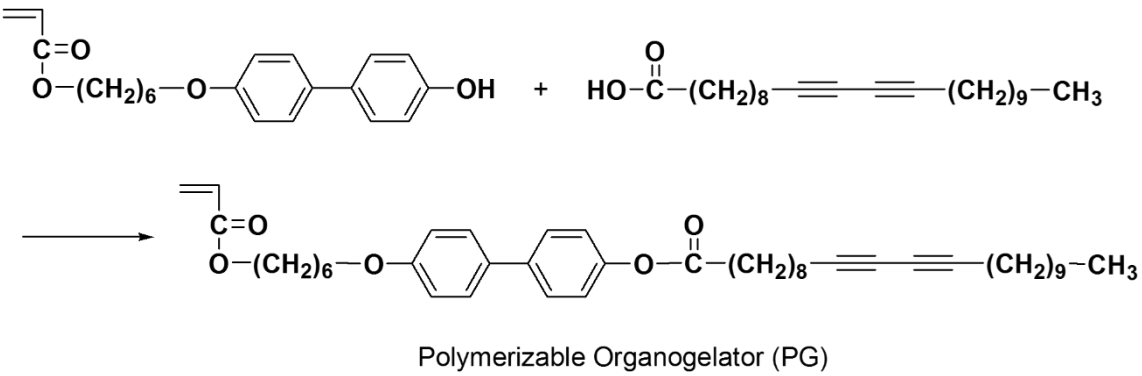

Scheme III-2. Synthesis of the polymerziable organogelator (PG).

As a functional monomer for complexation with the template, an acrylate having a carboxyl group was synthesized. Histamine (template) is an aminoalkylated imidazole which could form ionic and hydrogen bondings with a carboxyl group. Since both the functional monomer (FM) and the organogelator (PG) had a similar acrylate structure bearing a hexyloxybiphenyl group, they were expected to be co-assembled into nanofibers during organogelation.

The template-monomer complex was prepared by dissolving histamine (2.0 mg) and functional monomer FM (13 mg) together with a photoinitiator (DMPA) (30 mg) in *n*-decane (0.5 mL). After the addition of organogelator PG (38 mg) and cross-linker DVB (3.7 mg), the mixture was heated at 65 ^{0}C until a clear solution was obtained. After the addition of trioctylphosphine oxide capped CdSe/ZnS quantum dots (0.5 mL, 5 mg mL^{-1} in *n*-decane), the solution was cooled to room temperature to form a stable organogel. The organogel of PG alone formed in *n*-decane was milky white in color. The QD-containing organogel appeared yellowish green and emitted a bright green luminescence under UV light irradiation (Figure III-1). CdSe/ZnS quantum dots could be successfully

incorporated into the organogel nanofibers through interactions between long alkyl chains of the QD capping agent and the organogelator.

The QD-containing organogel was UV irradiated for 3 h at room temperature. In this process, acrylate and diacetylene groups and DVB were polymerized to produce highly cross-linked, CdSe/ZnS QD-incorporated, histamine embedded organogel nanofibers (QD-His-OGNF). The template molecules embedded in QD-His-OGNF were removed by washing with methanol/acetic acid (9:1, v/v) and Soxhlet extraction with methanol, resulting in the formation of the QD-incorporated, histamine imprinted organogel nanofibers (QD-HIOGNF).

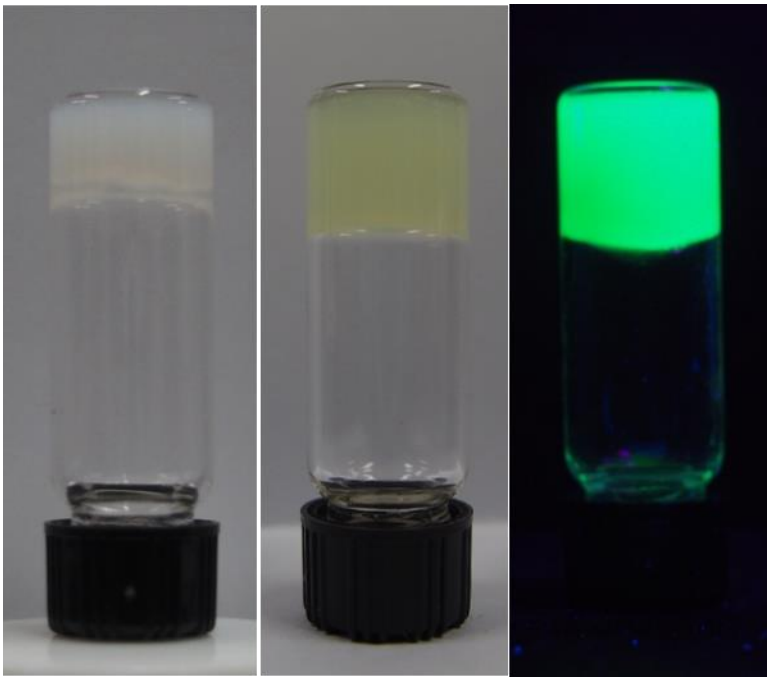

Figure III-1. Photographs of the organogel of PG alone under day light, the organogel containing QDs under day light and UV light (from left to right).

III-3-2. Structural and Morphological Analysis of Organogel Nanofibers

The structures of the organogel, QD-His-OGNF and QD-HIOGNF were characterized

by FT-IR spectroscopy (Figure III-2). The two absorptions at 2242 and 2145 cm^{-1} corresponding to the diacetylene groups were observed in the dried organogel,[44] but disappeared after polymerization, indicating that the polymerization proceeded *via* 1,4-addition reaction. The peak for the newly formed C≡C bonds was hardly noticeable, probably due to their symmetric structure. The successful removal of histamine from the nanofiber was confirmed from the FT-IR spectra of QD-His-OGNF and QD-HIOGNF. QD-His-OGNF showed the asymmetric and symmetric stretching vibration band for ammonium group of histamine at 3165 and 3065 cm^{-1}, respectively.[45] After the extraction process, they disappeared.

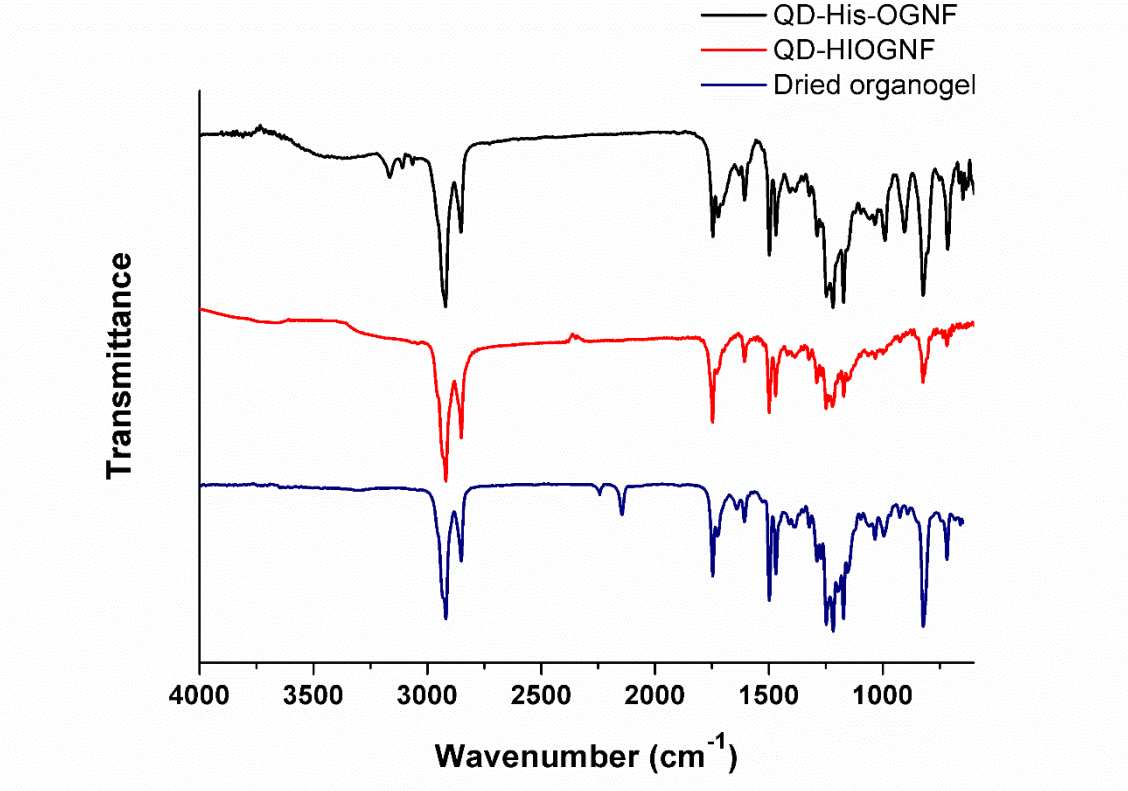

Figure III-2. FT-IR spectra of dried organogel, QD-His-OGNF, and QD-HIOGNF.

The morphological features of organogel nanofibers were investigated by SEM and

high resolution TEM (HRTEM) measurements. Figure III-3a and 3b show representative SEM images of the organogel nanofibers obtained by drying the organogel of PG alone formed in *n*-decane and the QD-incorporated imprinted nanofibers (QD-HIOGNF), respectively. The SEM image of the dried organogel exhibited entangled fibers with an average diameter of 50 nm. QD-HIOGNF showed more distinct fibrillar structures with the same diameters compared to the dried organogel, implying that the polymerization occurred within the organogel nanofibers. The QDs incorporated in the histamine imprinted organogel nanofibers were clearly observed in the HRTEM analysis (Figure III-3c). They were well dispersed in the fiber, which would be essential for them to act as a signal transducer. The QDs would interact preferentially with the analytes which were bound to the recognition sites in the fiber. As a result, a change in the fluorescence intensity of the QDs would ensue possibly *via* the charge transfer mechanism.

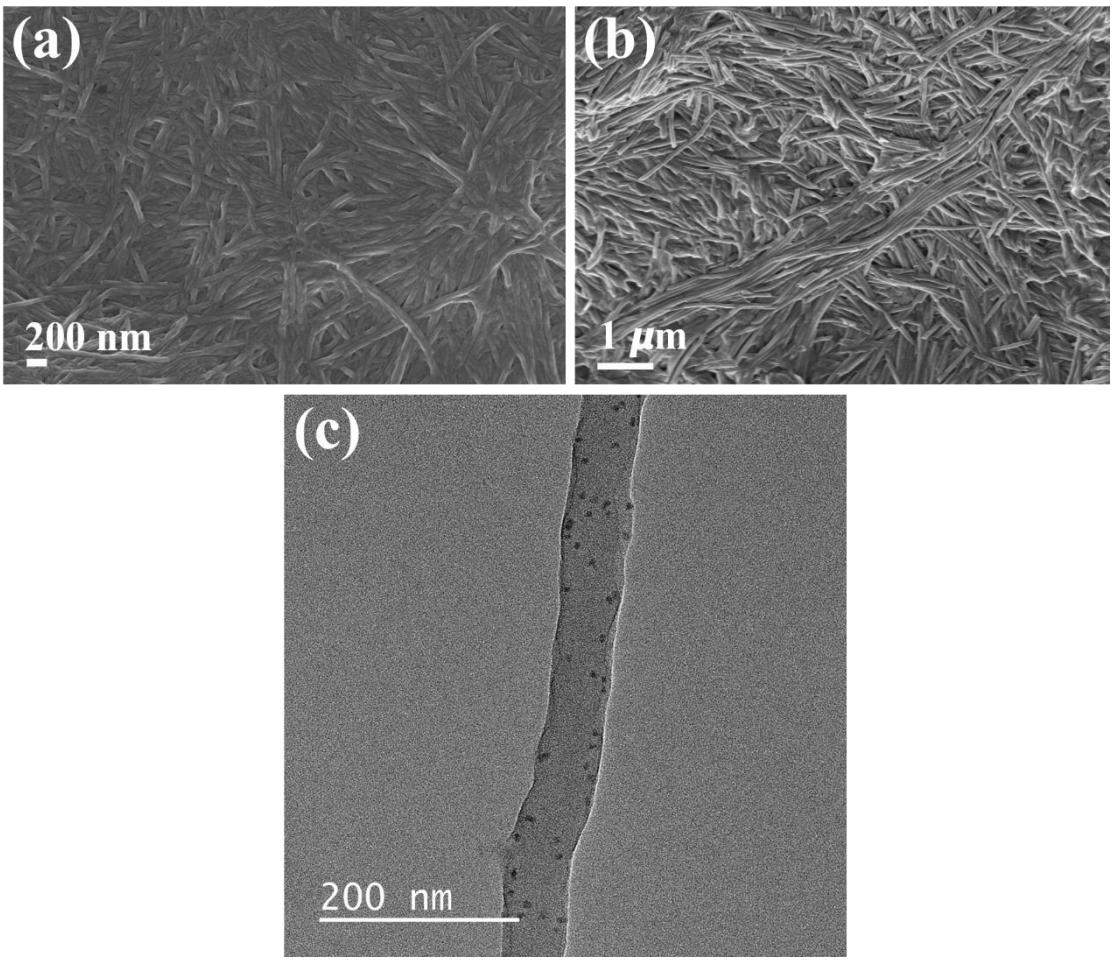

Figure III-3. (a) SEM image of the dried organogel of PG alone. (b) SEM image of QD-HIOGNF. (c) HRTEM image of QD-HIOGNF.

III-3-3. Rebinding Performance and Sensitivity of QD-HIOGNF

QD-HIOGNF exhibited a strong fluorescence peak at 550 nm in addition to the Rayleigh scattering peaks at 330 and 660 nm when excited at 330 nm (Figure III-4). A weak fluorescence around 370 – 500 nm was ascribed to the emission of polydiacetylene chain having a short conjugation length.

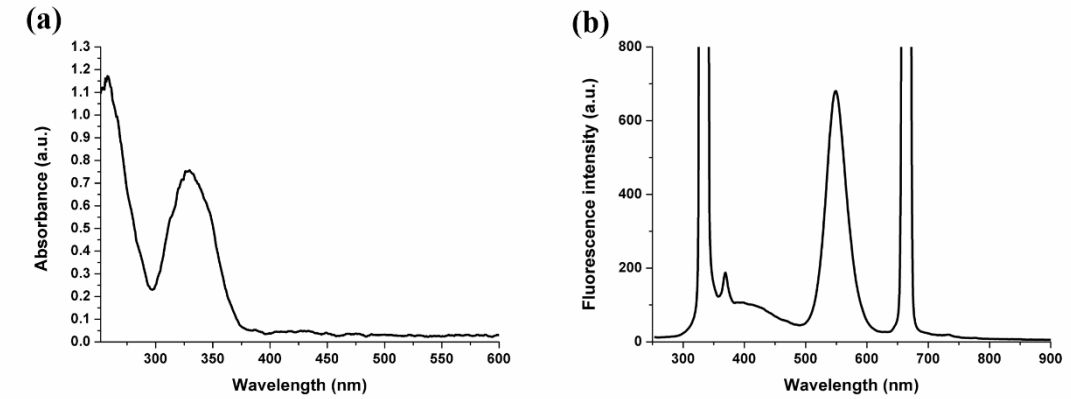

Figure III-4. (a) UV-vis absorption spectrum of QD-HIOGNF. (b) emission spectrum of QD-HIOGNF dispersed in methanol (λ_{ex}= 330 nm).

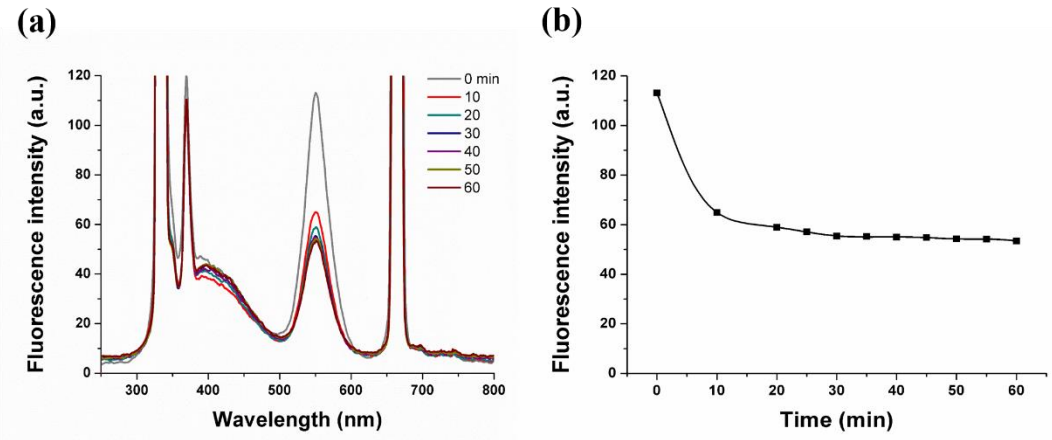

Figure III-5. (a) Kinetic profile of fluorescence emission spectra of QD-HIOGNF (150 μg mL^{-1}) in the presence of histamine (500 ng mL^{-1}) measured after incubating for certain periods of time in methanol (λ_{ex}= 330 nm). (b) Plot of the maximum fluorescence intensity in relation to incubation time.

To investigate the kinetic binding profile of QD-HIOGNF for histamine, the QD-HIOGNF (3 mg) were dispersed in a solution of histamine (500 ng mL^{-1}) in methanol (20 mL) with stirring and the fluorescence intensity was measured at 10 min intervals (Figure III-5). The fluorescence intensity decreased rapidly with time in the first 10 min. The

maximum quenching occurred within 30 min, demonstrating that the binding cavities had a high sensitivity toward the template.

The sensitivity of QD-HIOGNF to the concentration of histamine was also examined. The fluorescence of QD-HIOGNF was measured 10 min after mixing QD-HIOGNF with a solution of histamine in methanol. As depicted in Figure III-6a-b, the fluorescence intensity of QD-HIOGNF decreased as the concentration of histamine increased in the range between 100 and 700 ng mL^{-1}. Below the histamine concentration of 100 ng mL^{-1}, a fluorescence quenching was hardly observed. On the other hand, the QD-incorporated, non-imprinted organogel nanofibers (QD-NIOGNF) showed much smaller changes in their fluorescence than QD-HIOGNF with increasing concentration of histamine (Figure III-6f). QD-NIOGNF were prepared using the same procedure as that used for the preparation of QD-HIOGNF, except that no histamine was added.

III-3-4. Selectivity of QD-HIOGNF

The selectivity of QD-HIOGNF was investigated by testing its fluorescence quenching response in the presence of potential structural analogs of histamine, including allopurinol, serotonin and dopamine. Allopurinol is an isomer of hypoxanthine, which can cause injury in intestinal, renal, heart and brain tissue owing to the inhibitory effect of xanthine oxidase.[46] Serotonin and dopamine are biogenic amine neurotransmitters in biological systems, playing an important role in renal, hormonal and emotional functioning.[47,48] The selectivity experiments were conducted in the same manner as mentioned above. A diminutive change in fluorescence intensity of QD-HIOGNF was observed in the case of all analogs (Figure III-6c-6e), indicating that these structural analogs had poor binding ability to the imprinted sites.

The behavior of fluorescence quenching can be described by the Stern-Volmer equation[49]

$$F_0/F = 1 + K_{SV}[C]$$

Where F and F_0 are the fluorescence intensities of QD-HIOGNF in the presence and absence of an analyte, respectively. $[C]$ is the concentration of an analyte and K_{SV} is the Stern-Volmer quenching constant. This equation can be utilized to quantify the selectivity toward the sensing molecule. Both QD-HIOGNF and QD-NIOGNF exhibited a linear Stern-Volmer relationship as regards histamine and its structural analogs (Figure III-6g and 6h). The selectivity of QD-HIOGNF was evaluated using the Stern-Volmer quenching constant (K_{SV}) estimated from the slopes of the Stern-Volmer plots of QD-HIOGNF. A quenching constant of QD-HIOGNF for histamine was more than ten times higher than that for histamine analogs (Figure III-7). The imprinting factor calculated from the ratio of the quenching constant of QD-HIOGNF for histamine to that of QD-NIOGNF was 16.8.

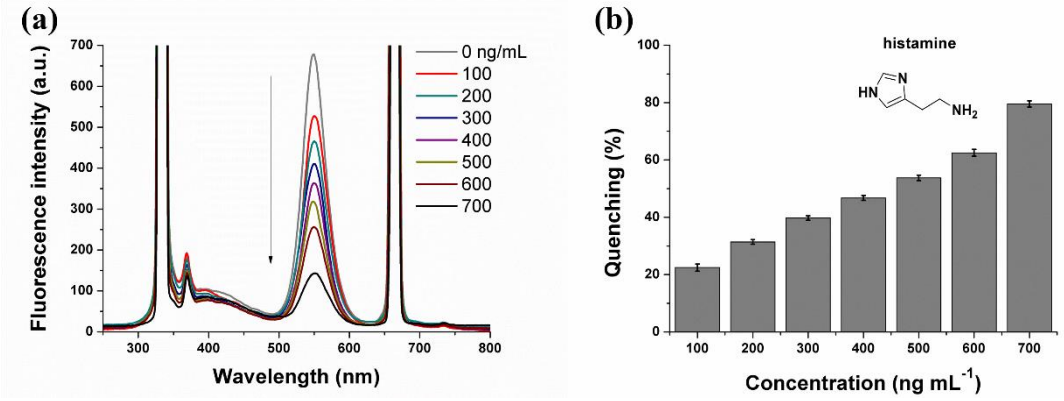

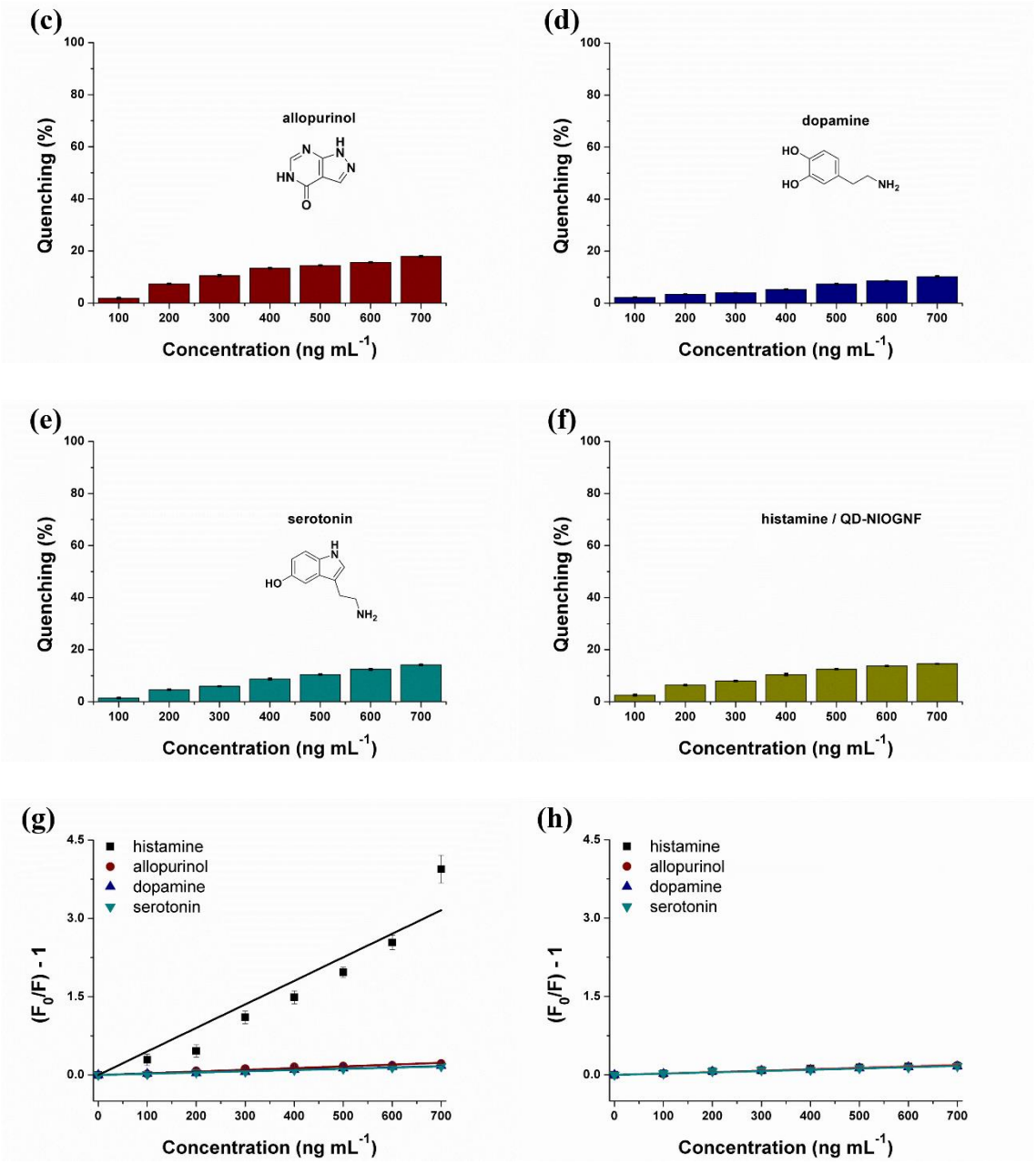

Figure III-6. (a) Fluorescence emission spectra of QD-HIOGNF (150 μg mL^{-1}) taken after 10 min stirring with an increase on histamine concentration in methanol. Amount of fluorescence quenching (%) [= (1 - F/F_0)100] of QD-HIOGNF (150 μg mL^{-1}) obtained after 10 min stirring with an increasing concentration of (b) histamine, (c) allopurinol, (d) dopamine and (e) serotonin in methanol. (f) Fluorescence quenching (%) of QD-NIOGNF (150 μg mL^{-1}) measured after 10 min stirring with an increasing concentration of histamine in methanol. (g) Estimated Stern-Volmer plots of QD-HIOGNF. (h) Estimated

Stern-Volmer plots of QD-NIOGNF.

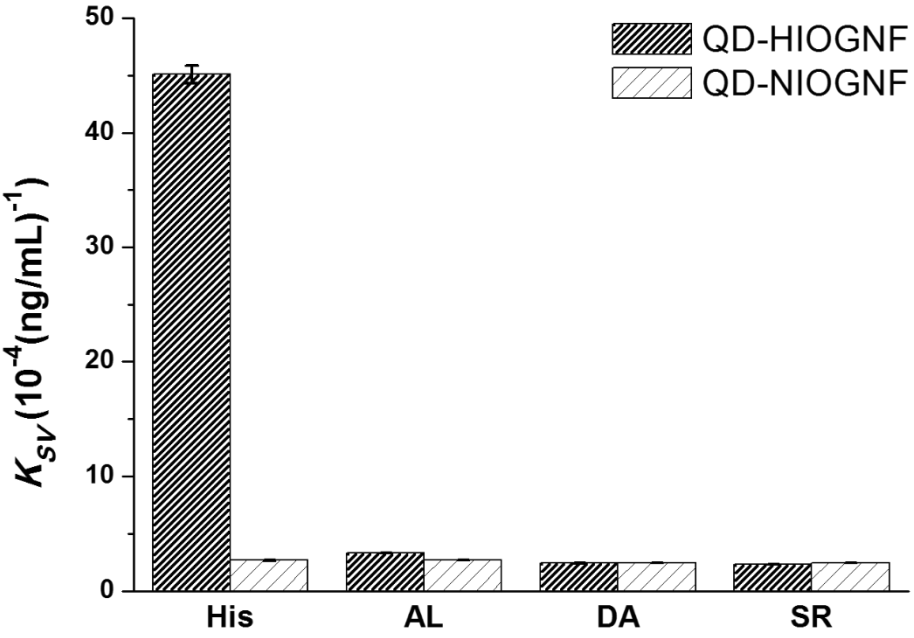

Figure III-7. Stern-Volmer constants (K_{SV}) of QD-HIOGNF and QD-NIOGNF toward different target analytes. For all experiments, the excitation wavelength was 330 nm.

III-3-5. Recyclability Test

The recyclability of QD-HIOGNF was evaluated by successive binding, extraction and rebinding experiments. QD-HIOGNF (3 mg) was incubated in a solution of histamine (100 ng mL^{-1}) in methanol (20 mL) for 30 min, allowing most binding cavities to be occupied by the template, and the bound template was then removed following the evaporation of solvent and the extraction procedure mentioned above. QD-HIOGNF recovered its initial fluorescence intensity after extraction. While repeating the binding-extraction cycles seven times, the fluorescence intensity of QD-HIOGNF decreased by

only 10% compared to that of as-prepared QD-HIOGNF (Figure III-8).

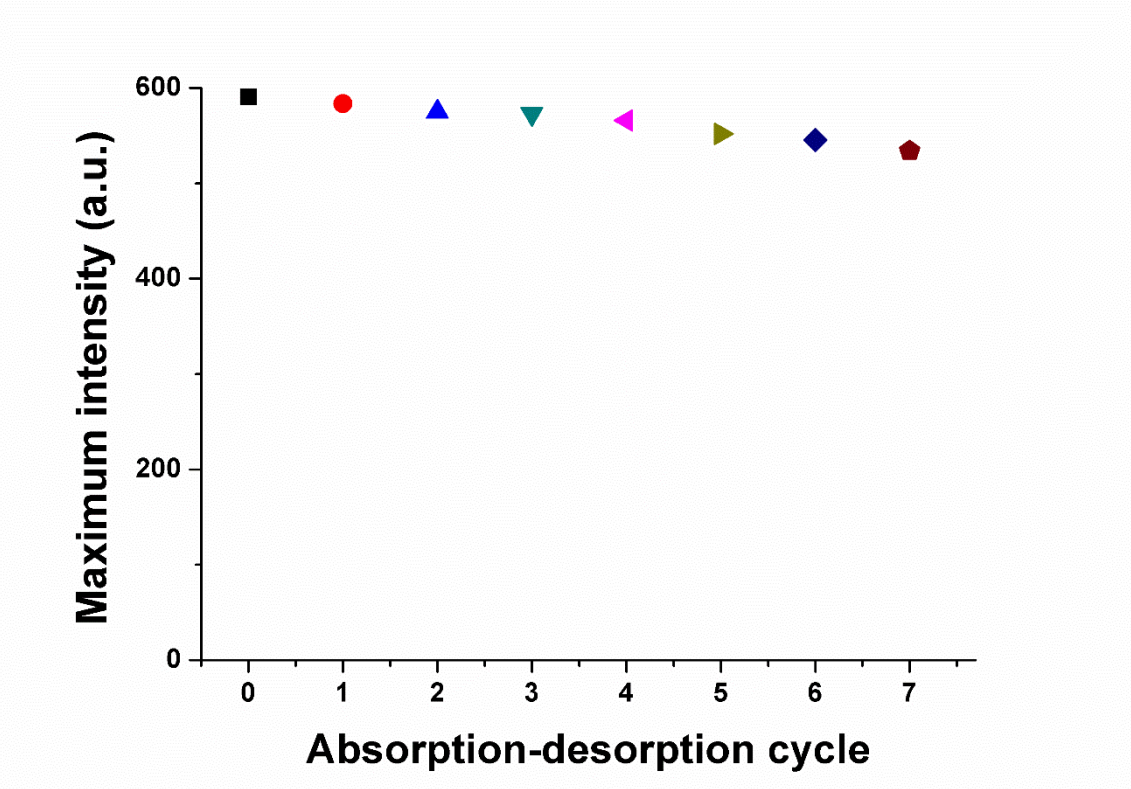

Figure III-8. Reusability of QD-HIOGNF under seven absorption-regeneration cycles.

III-4. Conslusions

A novel approach to fabricate a fluorescent histamine sensor is demonstrated. A CdSe/ZnS QD and histamine embedded organogel nanofiber was prepared by organogelation. Subsequent in-situ polymerization followed by extraction of histamine produced a polymerized nanofiber bearing QDs and binding cavities as a signal transducer and a receptor, respectively. QD-HIOGNF showed high molecular recognition properties toward histamine in terms of both sensitivity and selectivity. Because of the adequate proximity of the recognition sites to the QDs, a notable, concentration-sensitive fluorescence quenching was observed.

III-5. References

1. Haupt, K.; Mosbach, K. *Chem. Rev.* **2000**, 100, 2495-2504.

2. Wulff, G. *Chem. Rev.* **2002**, 102, 1-27.

3. Whitcombe, M. J.; Vulfson, E. N. *Adv. Mater.* **2001**, 13, 467-478.

4. Ye, L.; Mosbach, K. *Chem. Mater.* **2008**, 20, 859-868.

5. Ambrosini, S.; Beyazit, S.; Haupt, K.; Tse Sum Bui, B. *Chem. Commun.* **2013**, 49, 6746-6748.

6. Wan, W.; Han, Q.; Zhang, X.; Xie, Y.; Sun, J.; Ding, M. *Chem. Commun.* **2015**, 51, 3541-3544.

7. Sykora, S.; Cumbo, A.; Belliot, G.; Pothier, P.; Arnal, C.; Dudal, Y.; Corvini, P. F.-X.; Shahgaldian, P. *Chem. Commun.* **2015**, 51, 2256-2258.

8. Chronakis, I. S.; Milosevic, B.; Frenot, A.; Ye, L. *Macromolecules* **2006**, 39, 357-361.

9. Yoshimatsu, K.; Ye, L.; Stenlund, P.; Chronakis, I. S. *Chem. Commun.* **2008**, 2022-2024.

10. Kim, W. J.; Jung, B. M.; Kang, S. H.; Chang, J. Y. *Soft Matter* **2011**, 7, 4160-4162.

11. Kim, W. J.; Chang, J. Y. *Mater. Lett.* **2011**, 65, 1388-1391.

12. Li, Y.; Bin, Q.; Lin, Z.; Chen, Y.; Yang, H.; Cai, Z.; Chen, G. *Chem. Commun.* **2015**, 51, 202-205.

13. Wadhavane, P. D.; Galian, R. E.; Izquierdo, M. A.; Aguilera-Sigalat, J.; Galindo, F.; Schmidt, L.; Burguete, M. I.; Pérez-Prieto, J.; Luis, S. V. *J. Am. Chem. Soc.* **2012**, 134, 20554-20563.

14. Dey, N.; Samanta, S. K.; Bhattacharya, S. *ACS Appl. Mater. Interfaces* **2013**, 5, 8394-8400.

15. Huang, C.-B.; Chen, L.-J.; Huang, J.; Xu, L. *RSC Adv.* **2014**, 4, 19538-19549.

16. Lin, Q.; Zhu, X.; Fu, Y.-P.; Zhang, Y.-M.; Fang, R.; Yang, L.-Z.; Wei, T.-B. *Soft Matter* **2014**, 10, 5715-5723.

17. Rajamalli, P.; Prasad, E. *Org. Lett.* **2011**, 13, 3714-3717.

18. Li, J.; Kendig, C. E.; Nesterov, E. E. *J. Am. Chem. Soc.* **2007**, 129, 15911-15918.

19. Li, S.; Gong, S. *Adv. Funct. Mater.* **2009**, 19, 2601-2606.

20. Menaker, A.; Syritski, V.; Reut, J.; Ö pik, A.; Horváth, V.; Gyurcányi, R. E. *Adv. Mater.* **2009**, 21, 2271-2275.

21. Zhao, Y.-J.; Zhao, X.-W.; Hu, J.; Li, J.; Xu, W.-Y.; Gu, Z.-Z. *Angew. Chem. Int. Ed.* **2009**, 48, 7350-7352.

22. Cai, D.; Ren, L.; Zhao, H.; Xu, C.; Zhang, L.; Yu, Y.; Wang, H.; Lan, Y.; Roberts, M. F.; Chuang, J. H.; Naughton, M. J.; Ren, Z.; Chiles, T. C. *Nat. Nanotechnol.* **2010**, 5, 597-601.

23. Liang, R.-N.; Song, D.-A.; Zhang, R.-M.; Qin, W. *Angew. Chem. Int. Ed.* **2010**, 49, 2556-2559.

24. Li, S.; Ge, Y.; Turner, A. P. F. *Adv. Funct. Mater.* **2011**, 21, 1194-1200.

25. Kim, H.; Kim. Y.; Chang, J. Y. *J. Polym. Sci. A Polym. Chem.* **2012**, 50, 4990-4994.

26. Wan, W.; Biyikal, M.; Wagner, R.; Sellergren, B.; Rurack, K. *Angew. Chem. Int. Ed.* **2013**, 52, 7023-7027.

27. Awino, J. K.; Zhao, Y. *Chem. Commun.* **2014**, 50, 5752-5755.

28. Kim, H.; Kim, Y.; Chang, J. Y. *Macromol. Chem. Phys.* **2014**, 215, 1274-1285.

29. Jin, T.; Yoshioka, Y.; Fujii, F.; Komai, Y.; Seki, J.; Seiyama, A. *Chem. Commun.* **2008**, 5764-5766.

30. Freeman, R.; Finder, T.; Bahshi, L.; Willner, I. *Nano Lett.* **2009**, 9, 2073-2076.

31. Medintz, I. L.; Stewart, M. H.; Trammell, S. A.; Susumu, K.; Delehanty, J. B.; Mei,

B. C.; Melinger, J. S.; Blanco-Canosa, J. B.; Dawson, P. E.; Mattoussi, H. *Nat. Mater.* **2010**, 9, 676-684.

32. Ruedas-Rama, M. J.; Orte, A.; Hall, E. A. H.; Alvarez-Pez, J. M.; Talavera, E. M. *Chem. Commun.* **2011**, 47, 2898-2900.

33. Zhu, G.; Yang, K.; Zhang, C.-y. *Chem. Commun.* **2015**, 51, 6808-6811.

34. Chen, C.; Zhang, P.; Zhang, L.; Gao, D.; Gao, G.; Yang, Y.; Li, W.; Gong, P.; Cai, L. *Chem. Commun.* **2015**, 51, 11162-11165.

35. Xu, S.; Lu, H. *Chem. Commun.* **2015**, 51, 3200-3203.

36. Bardelang, D.; Badruz Zaman, M.; Moudrakovski, I. L. Pawsey, S.; Margeson, J. C.; Wang, D.; Xu, X.; Ripmeester, J. A.; Ratcliffe, C. I.; Yu, K. *Adv. Mater.* **2008**, 20, 4517-4520.

37. Naila, A.; Flint, S.; Fletcher, G.; Bremer, P.; Meerdink, G. *J. Food. Sci.* **2010**, 75, R139-R150.

38. Leng, P.-Q.; Zhao, F.-L.; Yin, B.-C.; Ye, B.-C. *Chem. Commun.* **2015**, 51, 8712-8714.

39. Yoshitake, T.; Ichinose, F.; Yoshida, H.; Todoroki, K.-i.; Kehr, J.; Inoue, O.; Nohta, H.; Yamaguchi, M. *Biomed. Chromatogr.* **2003**, 17, 509-516.

40. Luo, L.; Xu, Z.-L.; Yang, J.-Y.; Xiao, Z.-L.; Li, Y.-J.; Beier, R. C.; Sun, Y.-M.; Lei, H.-T.; Wang, H.; Shen, Y.-D. *J. Agric. Food Chem.* **2014**, 62, 12999-12308.

41. Vitali, L.; Valese, A. C.; Azevedo, M. S.; Gonzaga, L. V.; Costa, A. C. O.; Piovezan, M.; Vistuba, J. P.; Micke, G. A. *Talanta* **2013**, 106, 181-185.

42. Kang, S. H.; Jang, K. S.; Theato, P.; Zentel, R.; Chang, J. Y. *Macromolecules* **2007**, 40, 8349-8354.

43. Kang, S. H.; Jung, B. M.; Chang, J. Y. *Adv. Mater.* **2007**, 19, 2780-2784.

44. Cho, H. J.; Seo, K.; Lee, C. J.; Yun, H.; Chang, J. Y. *J. Mater. Chem.* **2003**, 13, 986-990.

45. Collado, J. A.; Ramirez, F. J. *J. Raman Spectrosc.* **1999**, 30, 391-397.

46. Raj, M. A.; John, S. A. *Electrochim. Acta* **2014**, 117, 360-366.

47. Wang, Y.; Wang, S.; Tao, L.; Min, Q.; Xiang, J.; Wang, Q.; Xie, J.; Yue, Y.; Wu, S.; Li, X.; Ding, H. *Biosens. Bioelectron.* **2015**, 65, 31-38.

48. Bagheri, H.; Afkhami, A.; Hashemi, P.; Ghanei, M. *RSC Adv.* **2015**, 5, 21659-21669.

49. Wang, H.-F.; He, Y.; Ji, T.-R.; Yan, X.-P. *Anal. Chem.* **2009**, 81, 1615-1621.

Chapter IV.

Preparation of Molecularly Imprinted Fullerene-Silica Nanocomposites for Sensitive and Selective Recognition of Diethylstilbestrol

IV-1. Introduction

Molecularly imprinted polymers (MIPs) are widely used in sensing applications as a synthetic receptor.[1] In particular, MIPs are well adapted in fluorescent sensing where a fluorophore is used as a probe. MIP-based fluorescent sensors detect changes in the emission of fluorophores upon the molecular binding process. A variety of fluorophores such as quantum dots[2], organic dyes[3], and lanthanide ion[4,5] have been used for this purpose.

Recently carbon dots have emerged as promising fluorophores because of their physiochemical stability and biocompatibility.[6] Carbon nanomaterials have advantages over cytotoxic semiconducting quantum dot in sensing applications as a fluorescent probe.[7,8] Carbon dots are prepared by breaking down carbonaceous materials or by carbonization of small organic molecules. They usually have quasi-spherical shapes with a size of less than 10 nm in diameter.

Fullerenes are another class of interesting carbon dots and have a compact size of about 1 nm. They have been a subject of a great interest owing to their potential applications in electronics/photovoltaic devices, and most recently, bioimaging and sensor system.[9-11] Fullerenes have small band gaps between the ground and excited states.[12] The photoluminescence (PL) of fullerene powders peaking around 729 nm is very weak in normal conditions.[13] However, interestingly, the PL of fullerene embedded in silica aerogel or polymer matrix becomes strong.[14,15] Jeong *et al*. have reported tetraethylene glycol-conjugated fullerene nanoparticles with color-tunable photoluminescence.[16] They also investigate fullerene-silica hybrid nanoparticles (FSNPs) showing strong photoluminescence.[17] Compared with a feeble emission of pure fullerene at 720 nm, FSNPs show bright PL at 600 nm.

In this study, molecularly imprinted fullerene-silica nanocomposites for fluorescent sensing of diethylstilbestrol (DES) is reported. DES which is a synthetic form of the hormone estrogen is the one of well-known endocrine disrupting chemicals.[18] The sol-gel chemistry allowed the introduction of fullerene into the silica network and formation of delicate imprinted sites inside of the network. A core-shell type silica particle where the shell had an imprint cavity was also prepared and its performance toward the molecular recognition was investigated.

IV-2. Experimental Section

Materials. Fullerene (C_{60}, 99.5%), tetraethyl orthosilicate (TEOS), diethylstilbestrol, bisphenol-A, hexestrol and β-estradiol were purchased from Sigma-Aldich. Cyclohexane, hexanol and Triton X-100 were purchased from Tokyo Chemical Industry. All other chemicals and reagent grade solvents were obtained from Junsei Chemical and used without any further purification.

Measurements. ^{1}H NMR spectrum was recorded on a Bruker Avance DPX-300 (300 MHz) spectrometer. Solid-state ^{13}C CP/MAS NMR spectra were obtained on a Bruker Avance DSX-400 (100 MHz) spectrometer equipped with the CP-MAS probe. Samples were spun in air at approximately 7 kHz. Fourier transform infrared spectra (4000-500 cm^{-1}) were measured on a Nicolet 6700 FT-IR spectrophotometer (Thermo Scientific, USA) using KBr pellets. Scanning electron microscopy (SEM) images were measured by a Leica TCS SP8X Gated STED. Fluorescence measurements were performed using a Shimadzu RF-5301PC spectrofluorometer. UV-vis spectra were measured with the use of a SCINCO S-3150.

Synthesis of triethoxysilane-template (diethylstilbestrol) complex (TES-DES).

TES-DES was synthesized according to the reported procedure.[19]

Preparation of DES embedded fullerene-silica nanocomposites (DES-FSNCs). FSNCs were synthesized according to the reported procedure.[17] C_{60} fullerene solution (100 mg in 20 mL toluene) was added to microemulsion solutions containing cyclohexane (50 mL), hexanol (20 mL), distilled water (5 mL), and Triton X-100 (17 mL). After the addition of ammonium hydroxide (28 wt%, 0.6 mL), the dark purple solution turned a dark brown color within 5 min and then TEOS (1 mL) and TES-DES (0.138 g) was added directly. The reaction mixture was stirred at room temperature for 24 h. The mixture was suspended in ethanol (150 mL) to stop the reaction. The precipitated product was filtered, washed with distilled water and ethanol. The resultant products were resuspended in ethanol and centrifuged at 3000 rpm. After the supernatant removal, the nanocomposites were dried in a vacuum oven at 60 ^{0}C for 24 h.

Core-shell DES embedded fullerene-silica nanoparticles (CS-DES-FSNCs). C_{60} fullerene solution (100 mg in 20 mL toluene) was added to microemulsion solutions containing cyclohexane (50 mL), hexanol (20 mL), distilled water (5 mL), and Triton X-100 (17 mL). The dark purple solution became a dark brown after the injection of ammonium hydroxide (28 wt%, 0.6 mL) within 5 min. After the core formation by adding TEOS (0.5 mL) during 24 h, the shell was formed by adding more TEOS (0.5 mL) and TES-DES (0.138 g) and the product was stirred for additional 24 h.

DES imprinted fullerene-silica nanocomposites (MIFSNCs / CS-MIFSNCs). DES-FSNCs / CS-DES-FSNCs (0.2 g) was stirred in a mixture of 1,4-dioxane and distilled water (7 : 1 v/v) at 110 ^{0}C for 24 h. The product was filtered, washed with 1,4-dioxane, distilled water and ethanol, and dried in a vacuum oven at 80 ^{0}C for 2 days.

Nonimprinted fullerene-silica nanocomposites (NIFSNCs). NIFSNCs were fabricated by using the same procedure as for DES-FSNCs except that APTES was added instead of TES-DES.

Kinetic binding study. MIFSNCs (2.0 mg) was dispersed in a solution of DES (200 ng mL^{-1}) in ethanol (20 mL) and the fluorescence spectrum was measured every 10 min.

Detection of DES by fluorescence measurement. To each different concentrations (100 - 700 ng mL^{-1}) of DES in ethanol (20 mL), MIFSNCs (2.0 mg) was added. After the samples were stirred for 5 min, the fluorescence measurement was carried out.

Selective Competitive Binding Test. Bisphenol-A, β-estradiol, and hexestrol were used as analogs of DES. MIFSNCs (2.0 mg) was added to the various concentrations of each analyte solution in ethanol ranging from 100 to 700 ng/mL, followed by stirring during 5 min. Then, the corresponding fluorescence emission was also investigated.

IV-3. Results and Discussion

IV-3-1. Preparation and Structural Characterization

Molecularly imprinted fullerene-silica nanocomposites (MIFSNCs) were synthesized by the sol-gel reaction of a triethoxysilane-template complex (TES-DES) and TEOS in the presence of C_{60} fullerene and subsequent removal of the template (Figure IV-1). It was suggested that the fullerene carbon was embedded in the silica network by forming oxide bond such as C-O-Si.[17] As-prepared MIFSNCs were well dispersed in organic solvents, including ethanol, methanol and chloroform. Core-shell type molecularly imprinted fullerene-silica nanocomposites (CS-FSNCs) were obtained by the sol-gel reaction of TEOS in the presence of C_{60} (core) followed by the reaction of additional TEOS and TES-DES (shell containing imprinted sites).

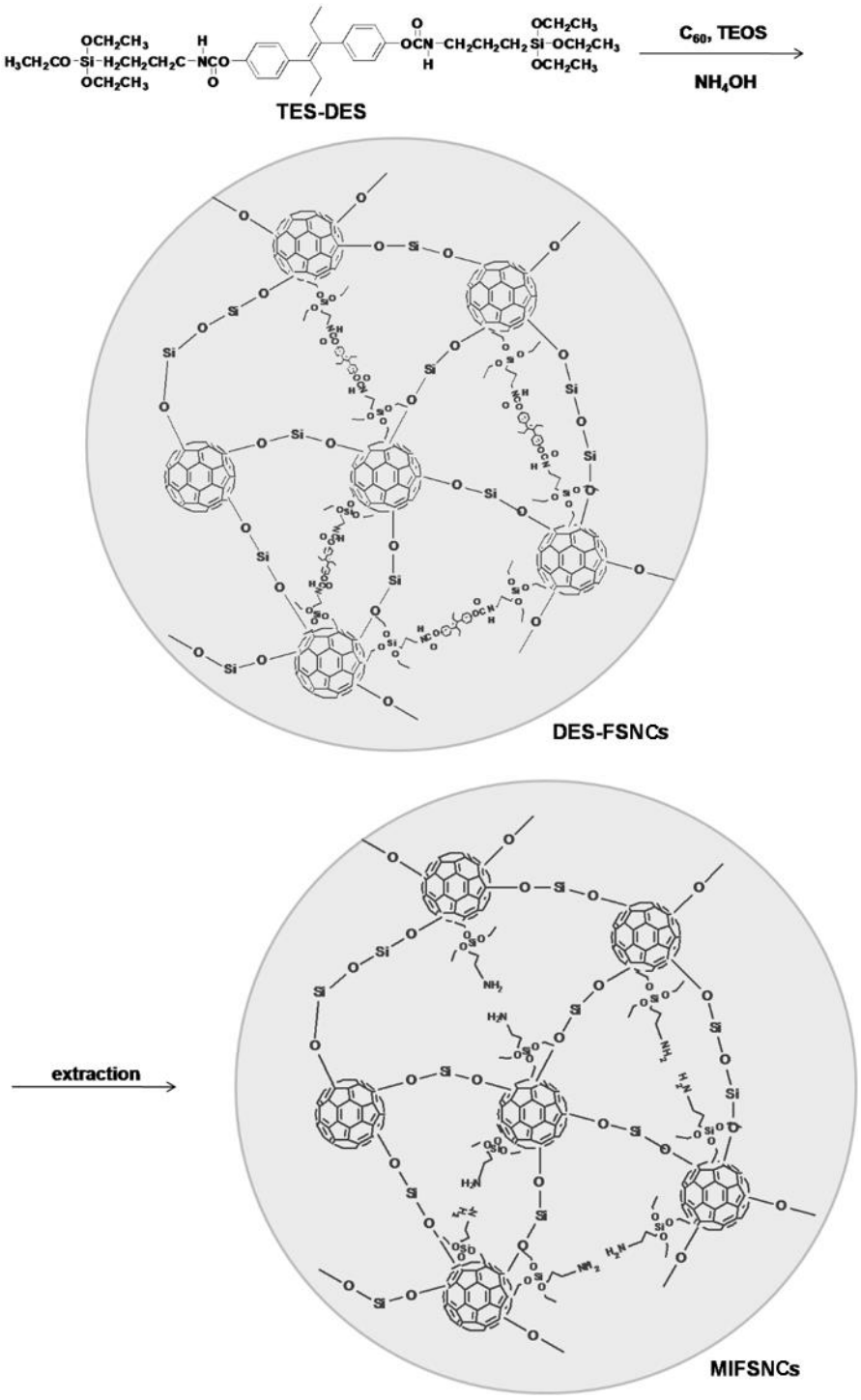

Figure IV-1. Schematic route of the preparation of molecularly imprinted fullerene-silica nanocomposites (MIFSNCs) *via* sol-gel reaction.

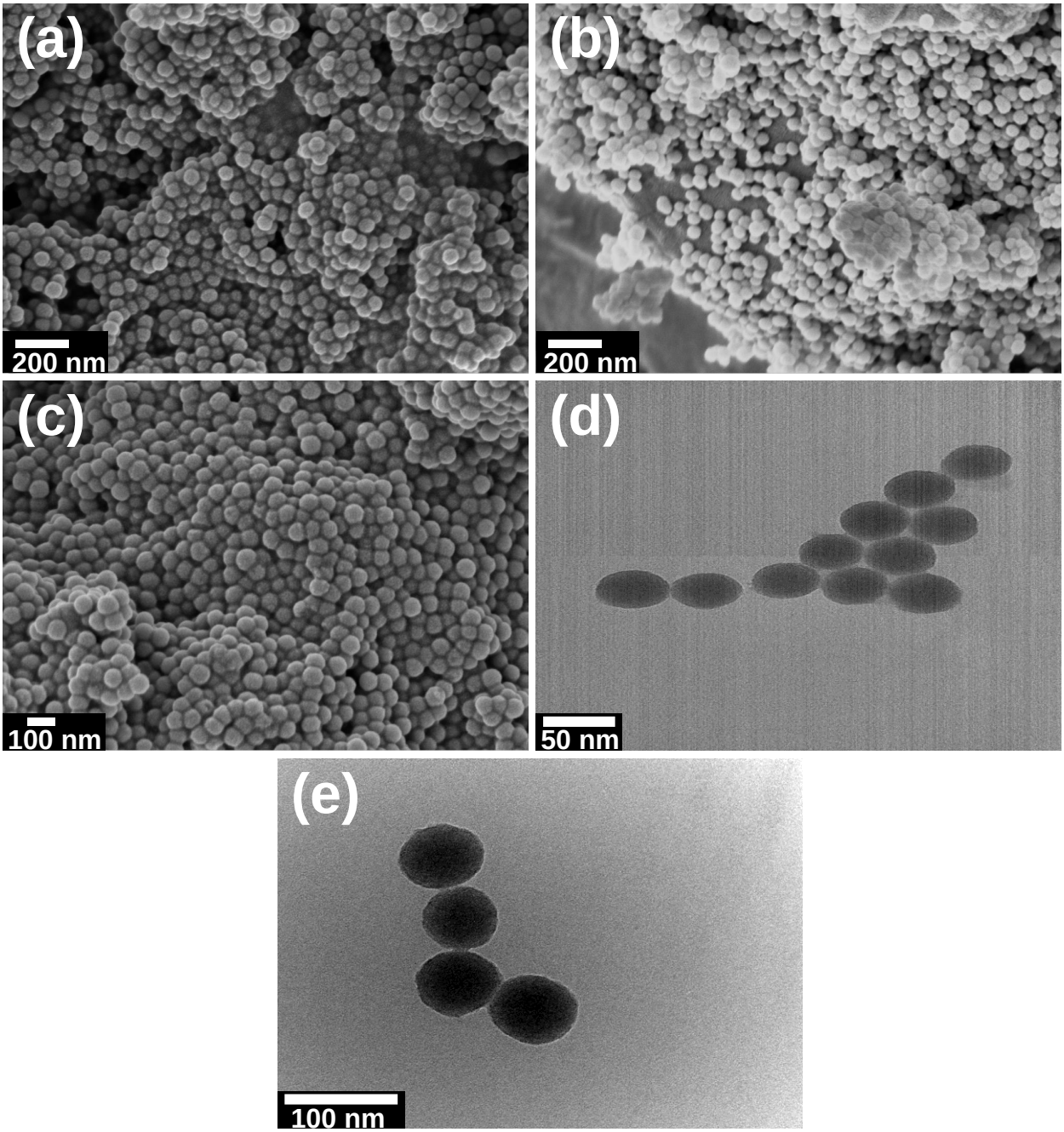

Figure IV-2. SEM images of (a) MIFSNCs, (b) NIFSNCs and (c) CS-MIFSNCs and TEM images of (d) MIFSNCs and (e) CS-MIFSNCs.

The overall morphology of prepared samples was characterized by SEM measurements (Figure IV-2). Both imprinted and non-imprinted particles exhibited the

similar morphological structures of spherical shape. As seen in Figure 2a, b, and d, the average size of FSNCs was 50 nm. The average size of core-shell FSNCs was larger owing to the additional shell thickness, determining to be 70 nm (Figure 2c, e).

In order to ensure the formation of a well-defined imprinted cavity, spectroscopic studies were performed. Firstly, the breakage of the urethane bond in DES-FSNCs was confirmed by Fourier transform infrared (FT-IR) spectroscopy (Figure IV-3). Absorption band at about 1720 cm^{-1} that corresponds to stretching of C=O from TES-DES was eliminated after the reflux, indicating that DES was removed successfully. The NH_2 bending mode that overlaps with an OH bending mode at 1640 cm^{-1} was clearly visible for MIFSNCs, showing that the carbamate group was converted to an amine during the thermal treatment in the presence of water.[18] The bands for Si-O-Si (468, 800, 1080-1200 cm^{-1}), aromatic C=C (1509 cm^{-1}) and covalent linkage between the fullerene carbon and silica network, C-O-Si (954, 1070 cm^{-1}) indicated that fullerene-silica nanocomposites were successfully formed.[17]

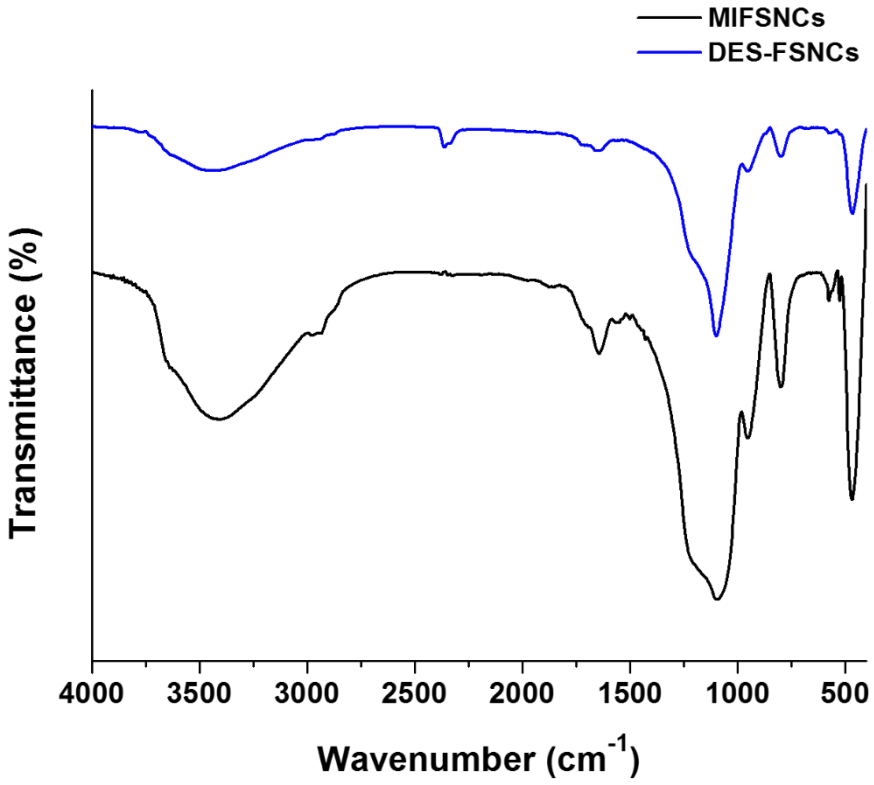

Figure IV-3. FT-IR spectra of DES-FSNCs and MIFSNCs.

For further characterization of the chemical structures of DES-FSNCs and MIFSNCs, the solid-state ^{13}C CP/MAS NMR spectroscopy was employed (Figure IV-4). In the DES-FSNCs spectrum, the signals for the aromatic carbons of DES (around 140 ppm) clearly existed, as well as the propyl carbon peaks (8, 22 and 42 ppm). MIFSNCs, however, showed no significant peaks of DES indicating the successful extraction of DES. The single peak still remaining at around 138 ppm was assigned to fullerene.[19] In addition, a residual peak at around 50 ppm displayed the presence of carbon-oxygen-silica linkages (C-O-Si).

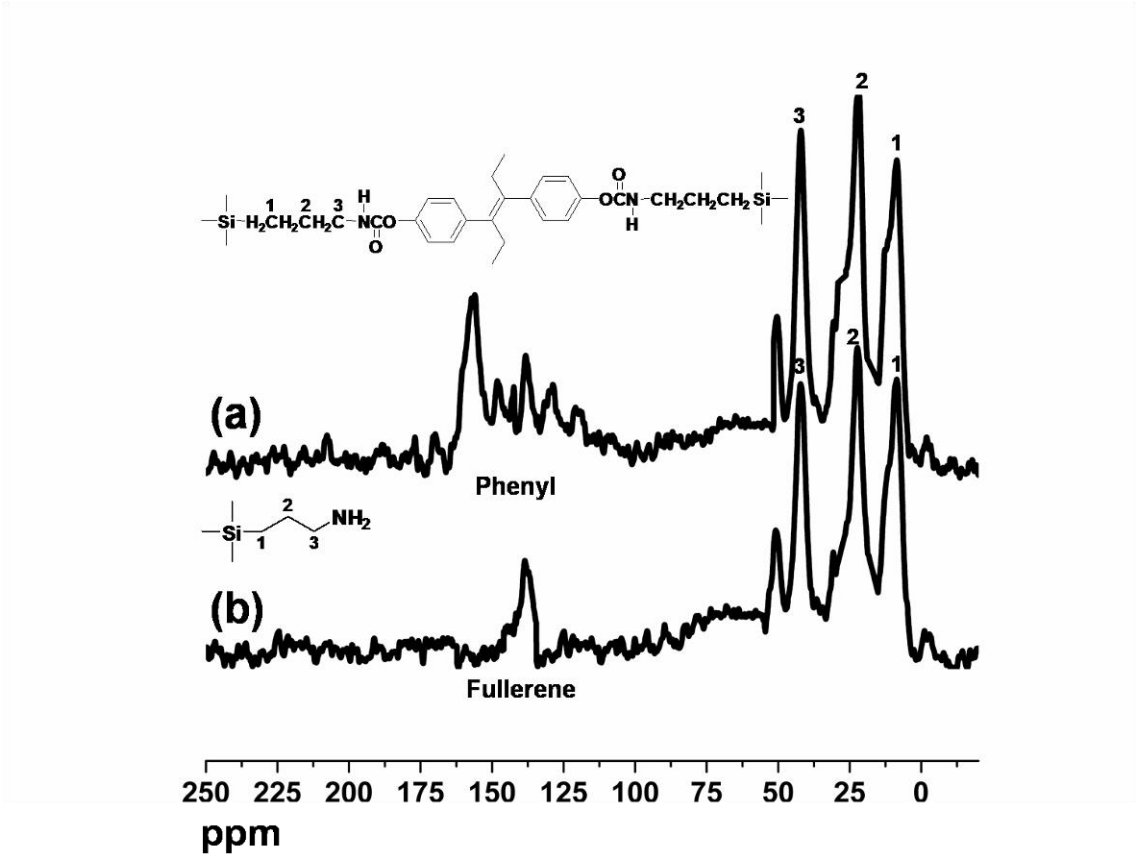

Figure IV-4. Solid-state ^{13}C CP/MAS NMR spectra of (a) DES-FSNCs and (b) MIFSNCs.

IV-3-2. Photophysical Properties of MIFSNCs

DES has a characteristic absorption around 270 nm and MIFSNCs has two peak absorptions around 230 and 275 nm as shown in Figure IV-5. Under excitation at 270 nm, MIFSNCs showed a broad fluorescence emission spectrum with peak maxima at around 600 nm with the Rayleigh scattering peaks at 270 and 540 nm. This characteristic emission is related to the highest occupied molecular orbitals (HOMO) - the lowest occupied molecular orbitals (LUMO) transitions in fullerene. the HOMO of C_{60} molecules is fivefold-degenerate, h_u and the LUMO is threefold-degenerate, t_{1u}. The

optical transitions between the h_u-derived valence band the the t_{1u}-derived conduction band are forbidden in general according to the momentum selection rules. However, these transitions can be allowed by interactions with environments or aggregation of fullerene molecules, that is, the selection rules of the forbidden h_u - t_{1u} transitions are broken and a radiative recombination across the relaxed forbidden gap occurs.[13] Fullerene molecules can exist as a small cluster or individually in the imprinted silica matrix to give rise to quantum confinement effects. Accordingly, they can be considered as carbon quantum dots, producing the intense visible PL.

The kinetic binding performance of MIFSNCs toward the target analyte was investigated. MIFSNCs were added to a solution of DES (200 ng mL^{-1}) in ethanol under stirring and the fluorescence spectrum was obtained at an interval of 10 min (Figure IV-6). The dramatic decrease in the fluorescence intensity was observed at the first stage up to 20 min. The adsorption equilibrium was reached after incubation for 60 min. These results showed that MIFSNCs had a fast kinetic binding property and a high sensitivity for DES.

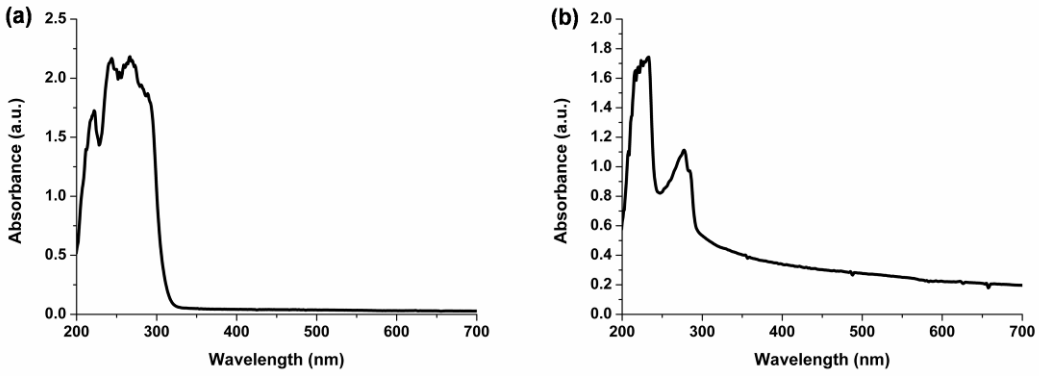

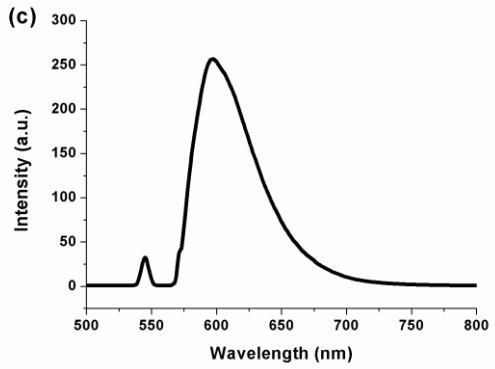

Figure IV-5. (a) UV-vis absorption spectrum of diethylstilbestrol. (b) UV-vis absorption and (c) emission spectra of MIFSNCs dispersed in ethanol (λ_{ex} = 270 nm).

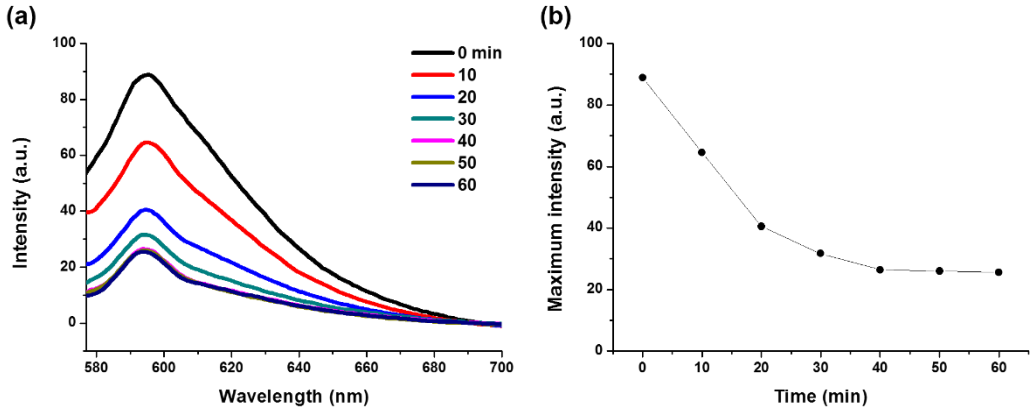

Figure IV-6. (a) Fluorescence spectra of MIFSNCs (100 μg mL^{-1}) in the presence of DES (200 ng mL^{-1}) after incubating for 0 - 60 min. (b) Influence of time periods of incubation on the maximum fluorescence intensity of MIFSNCs.

IV-3-3. Sensitivity and Competitive Rebinding Performance of MIFSNCs

As shown in Figure IV-7a, the fluorescence intensity of MIFSNCs decreased as the concentration of the target analyte increased. However, CS-MIFSNCs showed weak and

random PL quenching with increasing DES concentration (Figure IV-7b). This result could be attributed to the fact that the proximity for the charge transfer between fullerene in silica network and bound DES was not satisfied due to the thickness of the shell.

To confirm that the binding sites of MIFSNCs had high selectivity for the target molecule, binding tests for several structural analogs of DES, including bisphenol-A, β-estradiol and hexestrol were performed (Figure IV-8). These structural analogs of DES are also known to have high high toxicity.[20-23] Much smaller fluorescence quenching of MIFSNCs was observed for the analogs compared to DES, demonstrating the specific binding property of MIFSNCs for the template molecule. Non-imprinted fullerene-silica nanoparticles (NIFSNCs) were prepared in the same manner as described for MIFSNCs except that APTES was used instead of TES-DES. NIFSNCs showed much smaller fluorescence quenching than MIFSNCs in the rebinding test for DES (Figure IV-8e) because they had no specific binding sites for DES. It seemed that non-specific binding of the template molecule was not sufficient to cause effective fluorescence quenching.

For the quantitative evaluation of the selectivity of MIFSNCs toward the imprinted molecule, the Stern-Volmer equation was employed.[24]

$$F_0/F = 1 + K_{SV}[C]$$

where F_0 and F are the fluorescence intensities of MIFSNCs in the absence and presence of an analyte, respectively. [C] is the concentration of an analyte and K_{SV} is the Stern-Volmer quenching constant. As shown in Figure IV-8f, MIFSNCs exhibited a linear Stern-Volmer relationship for all analytes. The imprinting effect was evaluated from the Stern-Volmer quenching constant (K_{SV}) determined from the estimated slopes of the Stern-Volmer plots. The largest quenching constant of MIFSNCs was observed for DES (Figure IV-9). It was about five times higher than that for DES analogs, clearly implying the

highly selective recognition toward DES. NIFSNCs exhibited far lower K_{SV} than MIFSNCs; the imprinting factor ($K_{SV,MIFSNCs}$ / $K_{SV,NIFSNCs}$) was estimated to be 4.8.

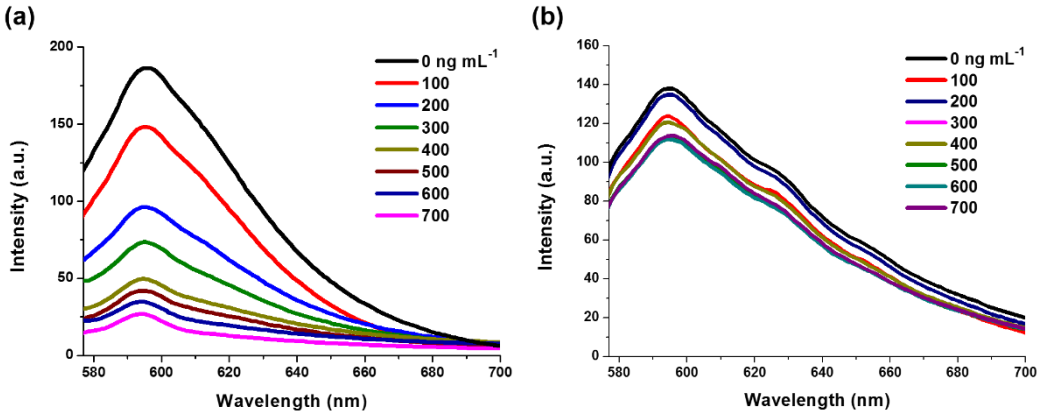

Figure IV-7. Fluorescence emission quenching of (a) MIFSNCs and (b) CS-MIFSNCs (λ_{ex} = 270 nm). Experimental conditions: concentration of MIFSNCs and CS-MIFSNCs, 100 μg mL^{-1}; concentration of DOX, 100-700 ng mL^{-1}; temperature 25 ^{0}C.

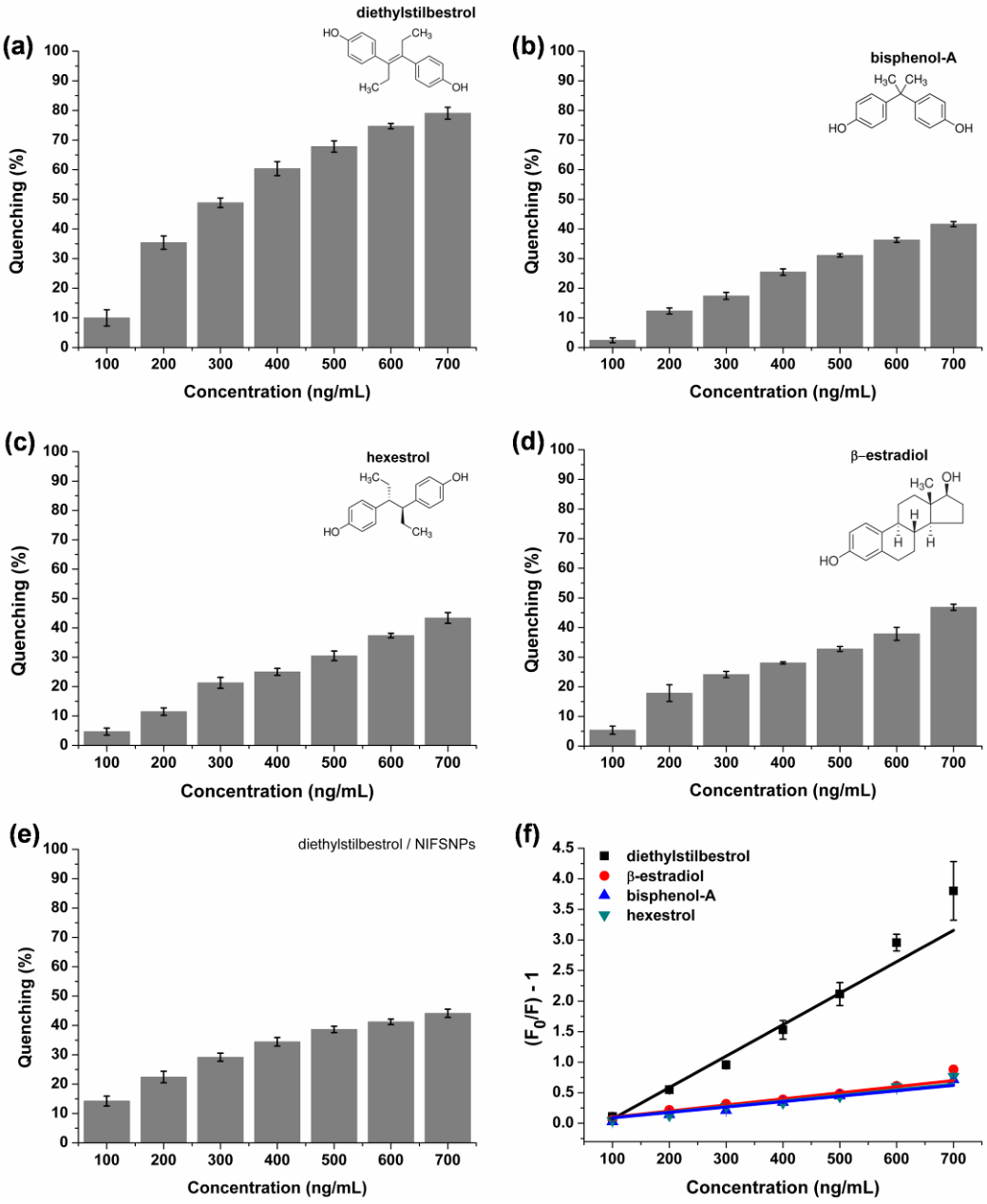

Figure IV-8. PL quenching % [= (1 - F/F_0)100] of MIFSNCs (100 µg mL^{-1}) computed with the sequential increment in concentration of (a) DES, (b) BPA, (c) hexestrol and (d) *β*-estradiol in ethanol. (e) PL quenching % of NIFSNCs (100 µg mL^{-1}) computed with the increasing concentration of DES in ethanol. (f) Estimated Stern-Volmer plots obtained from MIFSNCs.

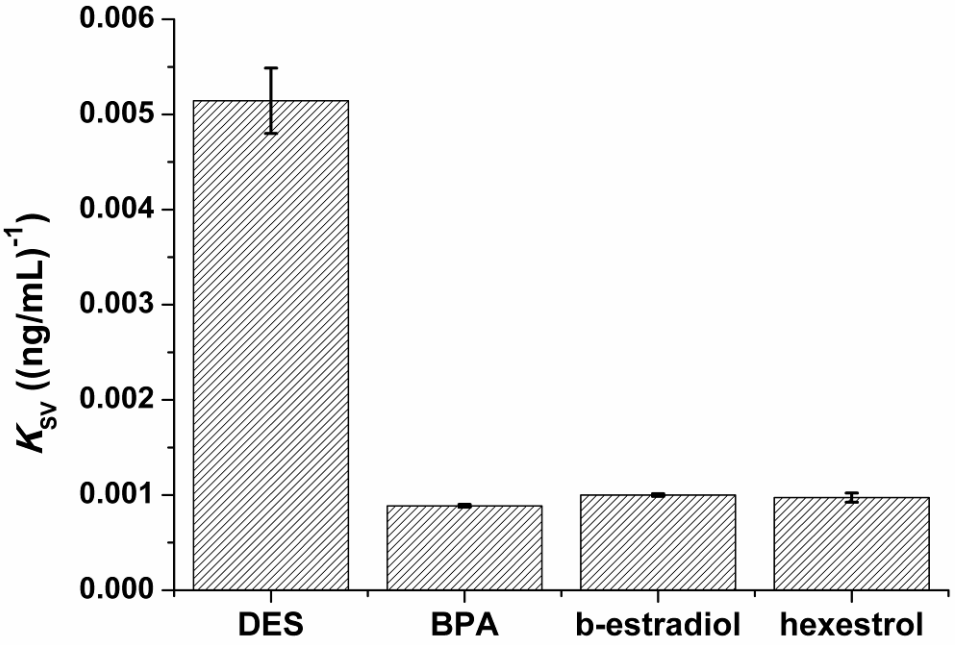

Figure IV-9. Stern-Volmer quenching constants of MIFSNCs by different kinds of target molecules.

IV-4. Conclusions

A facile fluorescent sensing assay of diethylstilbestrol was developed by fabricating a novel molecularly imprinted fullerene-silica nanocomposites (MIFSNCs). MIFSNCs showed bright PL which is caused by the quantum confinement effect of fullerene in the form of small clusters (carbon dot state). Selective binding sites for DES were introduced into the fullerene-silica network by the molecular imprinting technique. MIFSNCs exhibited high molecular recognition properties toward DES in terms of both sensitivity and selectivity. Based on the adequate proximity of the recognition sites to the fullerene in the silica network, a notable, concentration-sensitive fluorescence quenching derived from the charge transfer from MIFSNCs to DES could be observed.

IV-5. References

1. Haupt, K.; Mosbach, K. *Chem. Rev.* **2000**, 100, 2495-2504.

2. Xu, S.; Lu, H. *Chem. Commun.* **2015**, 51, 3200-3203.

3. Wan, W.; Biyikal, M.; Wagner, R.; Sellergren, B.; Rurack, K. *Angew. Chem. Int. Ed.* **2013**, 52, 7023-7027.

4. Tong, A.; Dong, H.; Li, L. *Anal. Chim. Acta* **2002**, 466, 31-37.

5. Kim, H.; Kim, Y.; Chang, J. Y. *J. Polym. Sci. A Polym. Chem.* **2012**, 50, 4990-4994.

6. Zheng, X. T.; Ananthanarayanan, A; Luo, K. Q.; Chen, P. *Small* **2015**, 11, 1620-1636.

7. Liang, F.; Chen, B. *Curr. Med. Chem.* **2010**, 17, 10-24.

8. Chen, Y.; Qu, K.; Zhao, C.; Wu, L.; Ren, J.; Wang, J.; Qu, X. *Nat. Commun.* **2012**, 3, 1074-1086.

9. Tu, R.; Liu, B.; Wang, Z.; Gao, D.; Wang, F.; Fang, Q.; Zhang, Z. *Anal. Chem.* **2008**, 80, 3458-3465.

10. Abdellatif, M. M.; Nomura, K. *ACS Macro Lett.* **2012**, 1, 423-427.

11. Maggini, M.; Scorrano, G. *J. Am. Chem. Soc.* **1993**, 115, 9798-9799.

12. Mandal, P.; Bardhan, M.; Ganguly, T. *J. Photochem. Photobiol. B.* **2010**, 99, 78-86.

13. Innocenzi, P.; Brusatin, G. *Chem. Mater.* **2001**, 13, 3126-3139.

14. Jun, S.; Lei, Z.; Jue, W.; Yufen, L.; Xiang, W. *Chin. Phys. Lett.* **1995**, 12, 693-696.

15. Ma, G.; Yang, Y.; Chen, G. *Mater. Lett.* **1998**, 34, 377-382.

16. Jeong, J.; Jung, J.; Choi, M.; Kim, J. W.; Chung, S. J.; Lim, S.; Lee, H.; Chung, B. H. *Adv. Mater.* **2012**, 24, 1999-2003.

17. Jeong, J.; Cho, M.; Lim, Y. T.; Song, N. W.; Chung, B. H. *Angew. Chem. Int. Ed.* **2009**, 48, 5296-5299.

18. Palmer, J. R.; Wise, L. A.; Hatch, E. E. *Cancer Epidemiol. Biomarkers Prev.* **2006**, 15, 1509-1514.

19. Jung, B. M.; Kim, M. S.; Kim, W. J.; Chang, J. Y. *Chem. Commun.* **2010**, 46, 3699-3701.

20. Lofgreen, J. E.; Moudrakovski, I. L.; Ozin, G. A. *ACS Nano* **2011**, 5, 2277-2287.

21. Porwal, S.; Diwedi, A.; Kamal, M. *Intl. J. Org. Chem.* **2012**, 2, 377-386.

22. Paris, F.; Balaguer, P.; Terouanne, B.; Servant, N.; Lacoste, C.; Cravedi, J.-P.; Nicolas, J.-C.; Sultan, C. *Mol. Cell. Endocrinol.* **2002**, 193, 43-49.

23. Rosenfeldt, E. J.; Linden, K. G. *Environ. Sci. Technol.* **2004**, 38, 5476-5483.

24. Ho, S.-M.; Tang, W.-Y.; de Frausto, J. B. *Cancer Res.* **2006**, 66, 5624-5632.

25. Cavalieri, E.; Rogan, E. *Ann. N. Y. Acad. Sci.* **2006**, 1089, 286-301.

26. Wang, H.-F.; He, Y.; Ji, T.-R.; Yan, X.-P. *Anal. Chem.* **2009**, 81, 1615-1621.

Chapter V.

Preparation of Highly Luminescent AIE Chromophore-Grafted Molecularly Imprinted Mesoporous Silica Nanoparticles for Fluorescent Sensing of Diethylstilbestrol

V-1. Introduction

The immobilization of fluorescent materials into inorganic matrices such as silica, aluminosilicate or transition metal oxides (ZrO_2, TiO_2) has drawn great attention as a powerful tool for the construction of hybrid materials with attractive photoluminescence properties.[1-4] Recently, luminescent metal organic frameworks (MOFs) made up of diverse building components and organic or inorganic fluorophores were reported as promising optical functional materials.[5,6] The fluorescent hybrid materials are used in drug delivery, optoelectronics, and biomedical devices and have a great potential for sensing applications.[7-12] Various organic-inorganic hybrid sensors have been developed and in particular, the fluorescent sensor based on molecularly imprinted hybrid materials are notable for their favorable features such as high sensitivity, selectivity, simplicity, rapid response time, and reproducibility.[13-17]

Molecular imprinting methodology is considered as an efficient way to produce synthetic receptors.[18] Molecularly imprinted materials have desirable features as a

receptor such as high mechanical and chemical stability, ease of processing and functioning under harsh conditions compared to natural enzymes or antibodies.[19-21] Molecularly imprinted materials are traditionally prepared in the form of monolithic particles by mechanical grinding of bulk materials, but they suffer from poor binding site accessibility. Surface imprinting technique alleviates this accessibility problem, which allows the dominant formation of binding sites on the surface of the imprinting materials.[22-25]

Imprinting into porous materials with high surface areas is another approach to overcome the accessibility problem. For example, mesoporous silica nanoparticles with a highly cross-linked rigid structure, high pore volume and nano-sized wall thickness allow the delicate formation of binding sites near the surface.[26-28] Moreover, their inner and outer surfaces can be selectively functionalized[29,30], which facilitates their application as a fluorescent sensor.[31-33]

Herein, a novel fluorescent sensor based on aggregation-induced emission (AIE) chromophore-grafted molecularly imprinted mesoporous silica nanoparticles was fabricated. AIE materials as a fluorescent probe have several advantages compared to quantum dots, such as high internal quantum yields, high photostability and large Stoke's shifts with low cytotoxicity.[34,35] In addition, the emission may not be affected by aggregation (no aggregation caused quenching) or incorporation into the solid materials.[36,37] Tetraphenylethylene (TPE) is a representative AIE-active dye.[38] The conventional TPE core, for example, H_4TCPE (tetrakis(4-carboxyphenyl)ethylene) shows a high internal quantum yield but its emission is too close to blue (λ_{em} = 480 nm).[39] In this study, the TPE-cored tetraaldehyde (1,1,2,2-tetrakis(4-formyl-(1,1'-biphenyl))ethene, TFPE) was synthesized and used as a fluorescent probe. An AIE

chromophores-grafted, molecularly imprinted mesoporous silica nanoparticles were fabricated as a fluorescent sensor showing excellent molecular recognition performance towards the target molecule.

V-2. Experimental Section

Materials. Tetraphenylethylene, Iodine, 4-formylphenylboronic acid, 3-(triethoxysilyl)propyl isocyanate, dibutyltin dilaurate, cetyltrimethylammonium bromide (CTAB), dienestrol (DN) were obtained from Tokyo Chemical Industry. Tetrakis(triphenylphosphine)palladium(0), tetraethyl orthosilicate (TEOS), 3-aminopropyl triethoxysilane (APTES), diethylstilbestrol (DES), bisphenol A (BPA), and 4,4'-biphenol (4BP) were obtained from Aldrich. [Bis(trifluoroacetoxy)iodo]benzene and dimethyl sulfoxide (DMSO) were obtained from Acros Organics. Toluene was distilled from sodium with benzophenone as color reagent. All chemicals were used without any purification.

Measurements. ^{1}H NMR spectrum was obtained on a Bruker Avance DPX-300 (300 MHz) spectrometer. Solid-state ^{13}C CP/MAS NMR spectra were recorded on a Bruker Avance DSX-400 (100 MHz) spectrometer equipped with a CP-MAS probe. Samples were spun in air at approximately 7 kHz. FT-IR spectra were recorded on a Thermo Scientific Nicolet 6700 spectrometer. Scanning electron microscopy (SEM) images were measured by using a JEOL JSM-6700F microscope. High Resolution Transmission electron microscopy (HRTEM) images were obtained by JEM-3010 operating at 300 kV. TEM samples were dispersed in methanol and a drop of mixture was placed on a carbon-coated copper TEM grid. Brunauer-Emmet-Teller (BET) surface area was measured by using a Belsorp-Max (BEL Japan. Inc.) analyzer. Ultra-high purity grade nitrogen (N_2) was used for all adsorption-desorption measurements. Pore size distribution was obtained

by using Barret-Joyner-Halenda (BJH) model on the adsorption branch. Powder X-ray diffractograms were obtained with the use of a Rigaku SmartLab Small Angle X-Ray Scattering system (Cu Kα radiation, λ = 1.54 Å). UV-vis spectrum was measured with a spectrophotometer SCINCO S-3150. Fluorescence spectra were measured using a Shimadzu RF-5301PC spectrofluorometer.

Synthesis of Triethoxysilane-template (diethylstilbestrol) complex (TES-DES). This compound was synthesized according to our previous reported procedure.[26]

Synthesis of Tetrakis(4-iodophenyl)ethylene (TIPE). This compound was prepared according to the reported procedure.[40]

Synthesis of 1,1,2,2-tetrakis(4-formyl-(1,1'-biphenyl))ethene (TFPE). This compound was synthesized according to the reported procedure.[41]

Preparation of DES embedded silica particles (DES-Si). An aqueous NaOH solution (2.0 M, 3.5 mL) was added to a solution of CTAB (0.94 g, 2.6 mmol) in distilled water (480 mL). A solution of TEOS (5.12 g, 24 mmol) and TES-DES (0.34 g, 0.45 mmol) in THF (20 mL) was added dropwise. The reaction mixture was stirred at 70 ^{0}C for 3 h. The precipitated product was filtered, washed with distilled water, methanol and acetone, and dried in *vacuo* at 30 ^{0}C for 3 days.

Preparation of DES embedded mesoporous silica particles (DES-MS). DES-Si (2.0 g) were stirred for 24 h in a mixed solution of HCl (35 wt%, 10 g) and methanol (200 g) at room temperature. The product was isolated by filtration, washed with distilled water and methanol, and dried in vacuum oven at 25 ^{0}C for 3 days.

Preparation of DES imprinted mesoporous silica particles (DIMS). DES-MS (2.0 g) was stirred in a mixture of distilled water (20 g) and 1,4-dioxane (145 g) at 110 ^{0}C for 24 h. The product was filtered, washed with 1,4-dioxane, methanol and acetone, and dried in *vacuo* at 50 ^{0}C for 3 days.

Preparation of -NH_2 functionalized DIMS (DIMS-NH_2). DIMS (1.0 g) was dehydrated under *vacuo* at 120 ^{0}C and added into a two-neck flask sealed with a rubber septum, then anhydrous toluene (20 mL) and APTES (3.0 mL) were mixed and injected into the flask at room temperature. The mixture was refluxed with stirring under N_2 protection for 6 h and filtered, washed with methanol and acetone, and dried under vacuum at 50 ^{0}C for 24 h.

Preparation of AIE chromophore-grafted, DES imprinted mesoporous silica particles (TFPE-DIMS). DIMS-NH_2 (1.0 g) was dispersed in DMSO (20 mL) and TFPE (5 mg, 0.0067 mmol) was dissolved in DMSO (10 mL). They were mixed and few drops

of acetic acid (3 mol/L, in DMSO) was added. The reaction mixture was stirred at 80 ^{0}C for 24 h, then the product was filtered, washed with methanol for several times and dried under *vacuo* overnight. The product was subjected to Soxhlet extraction with THF for 48 h to remove molecules that did not participate in the reaction and dried under vacuum at 30 ^{0}C for 2 days.

Preparation of AIE chromophore-grafted, non-imprinted mesoporous silica particles (TFPE-NIMS). TFPE-NIMS was prepared by adopting the same procedure as for TFPE-DIMS except that no TES-DES was added.

Kinetic binding test. TFPE-DIMS (2.0 mg) was dispersed in a solution of DES (500 ng mL^{-1}) in methanol (20 mL) and the fluorescence spectrum was measured every 10 min.

Rebinding test. In each vial, TFPE-DIMS or TFPE-NIMS (2.0 mg) was dispersed in different concentrations of DES solutions (100 - 700 ng mL^{-1}) in methanol (20 mL). After stirring for 10 min, the fluorescence spectrum of each solution was measured.

Selectivity test. Dienestrol, bisphenol A, and 4,4'-biphenol were selected as analogs of DES. TFPE-DIMS or TFPE-NIMS (2.0 mg) was dispersed in solutions of different concentrations of these analogs (100 - 700 ng mL^{-1}) in methanol (20 mL). After stirring for 10 min, the fluorescence spectrum of each solution was obtained.

Recyclability. TFPE-DIMS (2.0 mg) was dispersed in a solution of DES (100 ng mL^{-1}) in methanol (20 mL) and the fluorescence spectrum of the mixture was measured after stirring for 30 min. The initial fluorescence intensities of TFPE-DIMS in the absence of histamine were also recorded during each cycle. After evaporation of methanol, the solid residue was subjected to Soxhlet extraction with methanol for 24 h. TFPE-DIMS was isolated by filtration, dried and reused for the rebinding test.

V-3. Results and Discussion

V-3-1. Synthesis and Characterization

The schematic strategy to the preparation of AIE chromophore-grafted, DES imprinted mesoporous silica particles in which the silica framework and the inner surface were selectively functionalized was described in Scheme V-1. The AIE chromophore 1,1,2,2-tetrakis(4-formyl-(1,1'-biphenyl))ethene (TFPE) with four aldehyde groups was synthesized according to the literature.[41] TFPE had a longer conjugation length and thereby a narrower HOMO-LUMO energy gap than TPE, which promoted a large red shift of the emission peak.[42] DES was selected as a target molecule, which is classified as an endocrine disruptor whose rapid and sensitive detection is needed.[43-48] Two terminal hydroxyl groups of DES were reacted with two isocyanate groups of 3-(triethoxysilyl)propyl isocyanate *via* urethane bonds to produce a triethoxysilane-template complex (TES-DES). A previous report suggested that the urethane bond was thermally reversible and dissociated into a hydroxyl and an isocyanate group at elevated temperatures.[49,50]

DES embedded, mesoporous silica particles (DES-Si) were prepared through co-condensation of TES-DES with tetraethyl orthosilicate (TEOS) in the presence of cetyltrimethylammonium bromide (CTAB). The structure-directing surfactant, CTAB having amphiphilic character formed a micellar structure in an aqueous solution in which hydrophobic parts of surfactants were located inside the pore. The extraction of CTAB yielded DES embedded, mesoporous silica particles (DES-MS). The complete disappearance of the FT-IR absorption bands of CTAB at 3000-2800 cm^{-1} showed the successful removal of CTAB (Figure V-1). The extraction of template molecules in DES-

MS could be conducted by a reflux of DES-MS in a mixture of 1,4-dioxane and water. By the reflux process, DES which were embedded between pores of the silica framework were removed through the dissociation of thermally reversible urethane bonds to form delicate recognition cavities.

DES imprinted mesoporous silica particles (DIMS) were functionalized with amino groups by post-grafting reaction with 3-aminopropyltriethoxysilane (APTES).[51.52] TFPE was introduced into the pore of DIMS-NH_2 *via* the condensation reaction of an amine and an aldehyde to yield TFPE-grafted, DES imprinted mesoporous silica particles (TFPE-DIMS). In the FT-IR spectrum of TFPE-DIMS, the stretching absorption band of newly formed C=N bonds appeared at around 1656 cm^{-1} and the stretching absorption band of C=O at 1699 cm^{-1} disappeared (Figure V-1).[41]

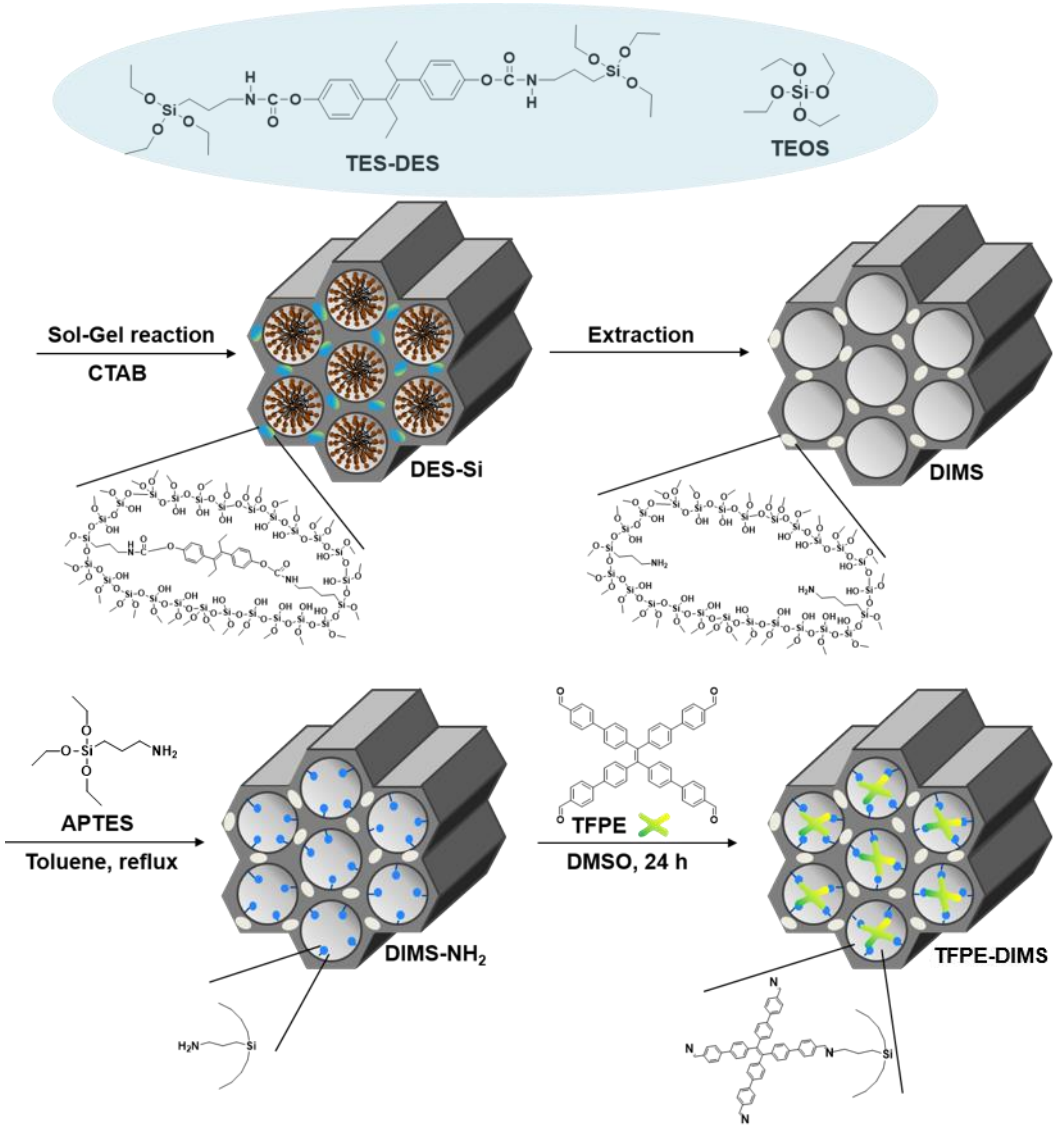

Scheme V-1. Schematic route of the preparation of AIE-active chromophore-grafted, DES imprinted mesoporous silica particles (TFPE-DIMS).

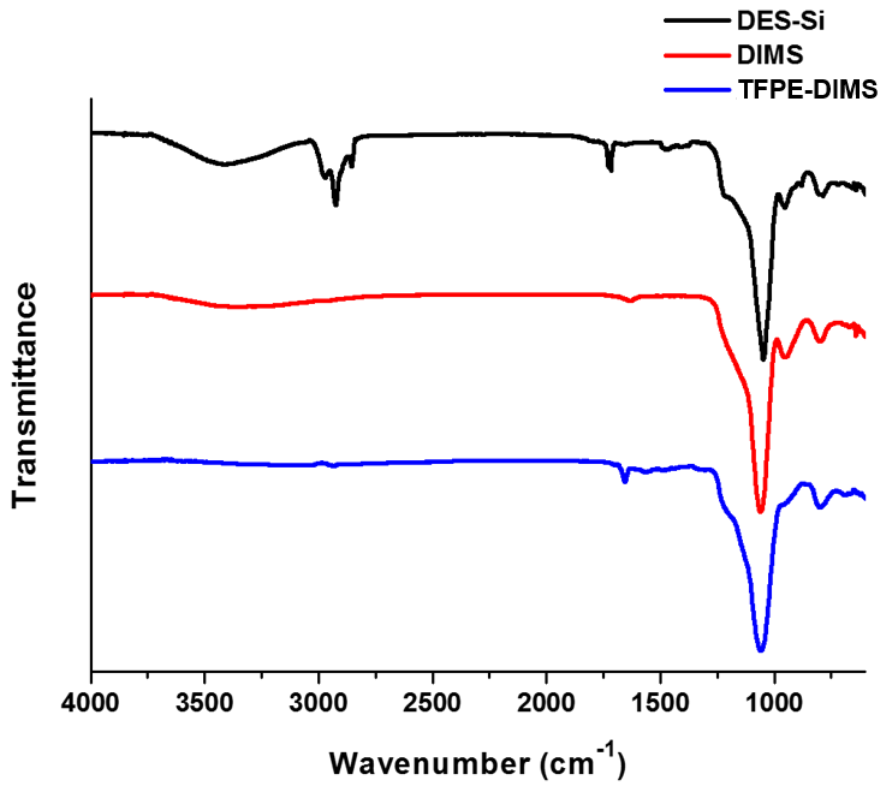

Figure V-1. FT-IR spectra of DES embedded silica (DES-Si), DES imprinted mesoporous silica (DIMS), and TFPE-grafted, DES imprinted mesoporous silica nanoparticles (TFPE-DIMS).

V-3-2. Structural and Morphological Analysis of Mesoporous Silica Nanoparticles

Chemical structures of DES-MS, DIMS-NH_2 and TFPE-DIMS were characterized by solid state ^{13}C CP/MAS NMR spectroscopy (Figure V-2). The spectrum of DES-MS showed broad peaks at around 140 ppm owing to phenyl carbons of DES.[26] After the removal of the template molecule, these peaks were completely disappeared. In the spectrum of TFPE-DIMS, the peak corresponding to imine groups formed by the condensation reaction between the amine and the aldehyde showed up at 160 ppm and no peak for unreacted aldehyde species around 180 ppm was observed.[53] The peaks for TPE core carbons appeared at around 140, 131 and 127 ppm.[54] The peaks at 8, 22 and 42 ppm

were assigned to the anchoring propyl carbons bonded to Si.[27]

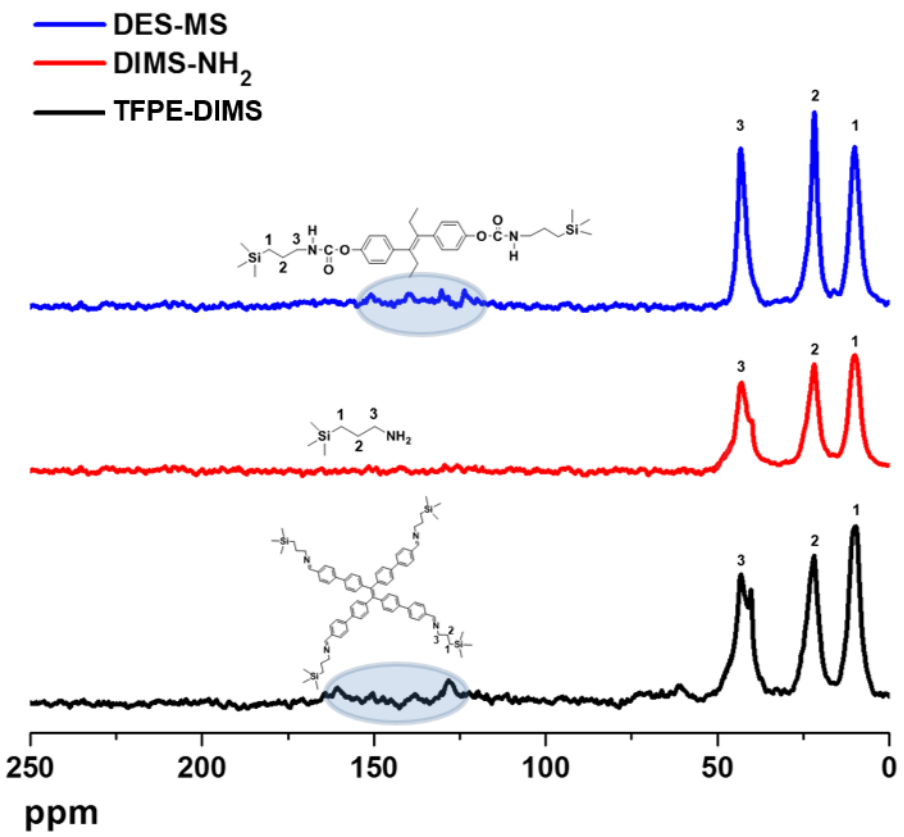

Figure V-2. Solid-state ^{13}C CP/MAS NMR spectra of DES embedded mesoporous silica (DES-MS), DIMS-NH_2, and TFPE-DIMS.

Figure V-3 shows the SEM and HRTEM images of DIMS-NH_2 and TFPE-DIMS. The silica particle had nano-sized spherical shapes as seen in the SEM images. The HRTEM image of DIMS-NH_2 presented a well-ordered mesoporous structure with an average pore size of about 3 nm and a distance between the pores of about 5 nm (Figure V-3c). TFPE-DIMS also showed organized pore structure with a uniform pore size. (Figure V-3d).

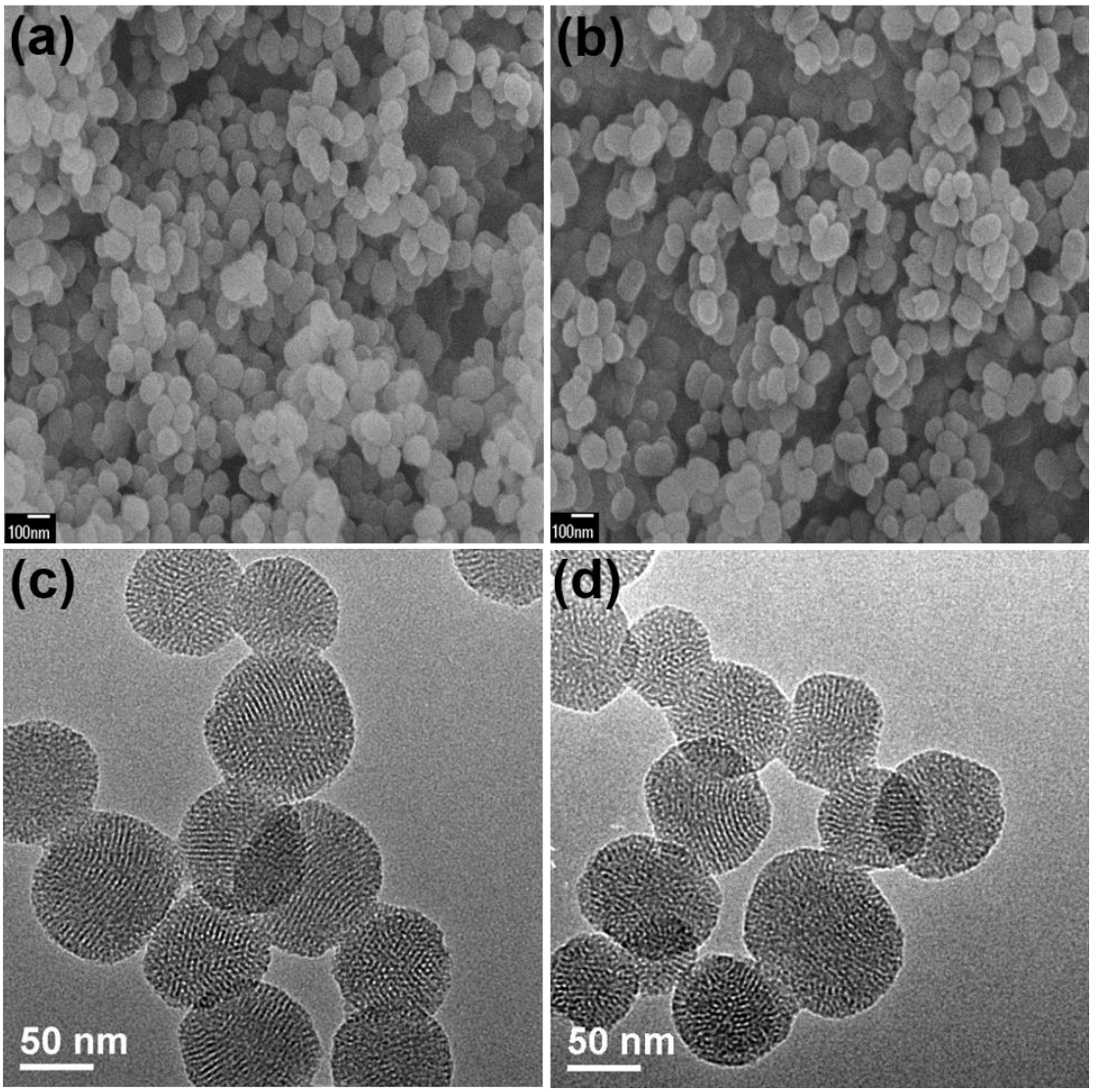

Figure V-3. SEM images of (a) DIMS-NH_2 and (b) TFPE-DIMS. HRTEM images of (c) DIMS-NH_2 and (d) TFPE-DIMS.

The N_2 adsorption/desorption isotherm for DIMS-NH_2 are presented in Figure V-4a. DIMS-NH_2 exhibited type IV isotherms of typical mesoporous materials. The Brunauer-Emmett-Teller (BET) surface area of DIMS-NH_2 was 843 $m^2 g^{-1}$. The average pore size of 2.9 nm was estimated by the BJH method, which was close to that observed by HRTEM. The grafting of TFPE onto DIMS-NH_2 was assessed by N_2 adsorption/desorption (Figure V-4b). TFPE-DIMS also showed type IV isotherms, whereas the adsorbed volume of N_2

obviously decreases, indicating that TFPE molecules were introduced into the mesopores. The result was further confirmed from the decrease in the BET surface area (671 m^2 g^{-1}) and the BJH pore diameter (2.2 nm) after TFPE grafting.[55]

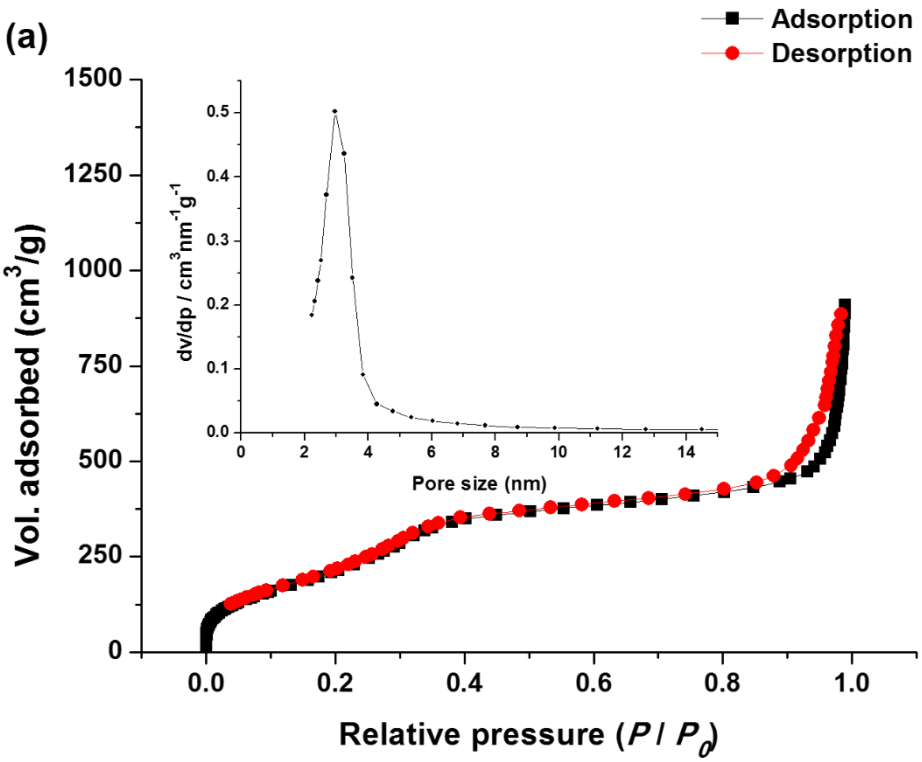

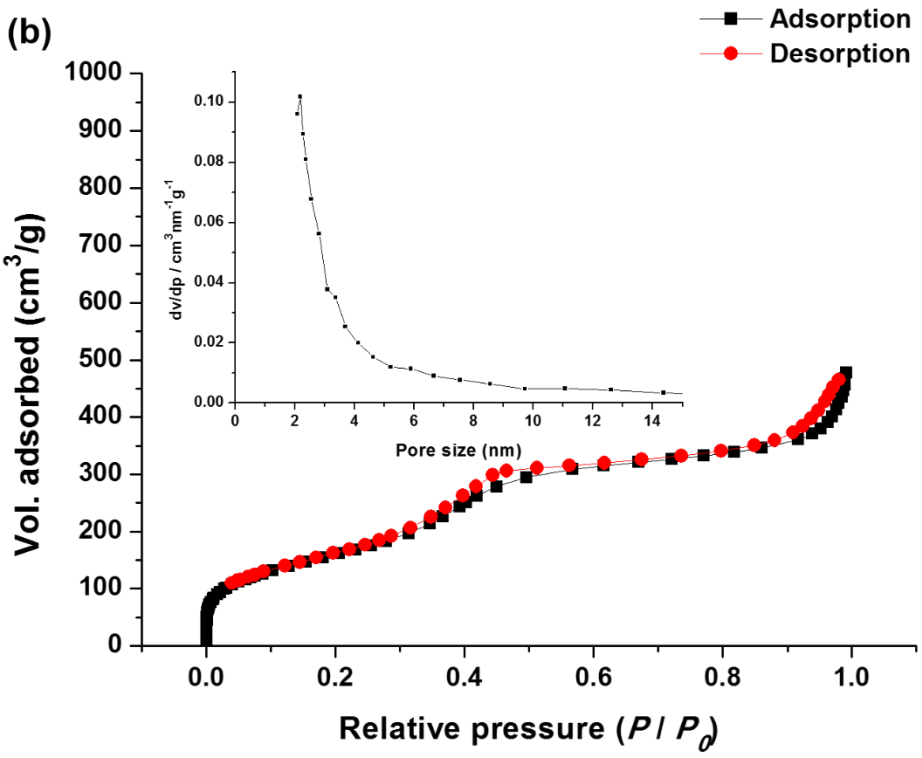

Figure V-4. N_2 adsorption-desorption isotherms of (a) DIMS-NH_2 and (b) TFPE-DIMS (inset: corresponding pore size distribution plots).

The ordered mesoporous structure of DIMS-NH_2 and TFPE-DIMS was studied by the small angle powder X-ray diffractogram (XRD). As depicted in Figure V-5, both DIMS-NH_2 and TFPE-DIMS diffractograms exhibited three well resolved peaks that were indexed as (100), (110) and (200) reflections of a 2D hexagonal (P6mm) structure.[56] The XRD pattern of DIMS-NH_2 showed intense peak at 2θ = 1.9°, corresponding to the d-spacing of 4.6 nm and a lattice parameter of a_0 = 5.3 nm. The XRD pattern of TFPE-DIMS showed intense peak at 2θ = 2.3°, corresponding to the d-spacing of 3.8 nm and a lattice parameter of a_0 = 4.4 nm. The pore wall thickness of DIMS-NH_2 between the pores can be estimated using the following expression[57] $a_0 = t + D_{BJH}$ where a_0 and t are a lattice parameter and a pore wall thickness, respectively. D_{BJH} is the average pore size obtained by Barrett-Joyner-Halenda (BJH) analysis. The wall thickness of DIMS-NH_2

was about 2.4 nm. The optimized lengths of the template (DES) and TFPE subjected to an initial geometric optimization using a Polymer Consistent Force Field (pcff) method were 1.5 nm and 2.2 nm, respectively.[58] Given the results of the wall thickness and the lengths of DES and TFPE, I assumed that the template molecule was incorporated in the silica framework between the pores and TFPE was grafted onto the pore wall. The slight peak shift towards a higher angle was observed in the TFPE-DIMS diffractogram,[59-61] but the overall mesostructural ordering was preserved.

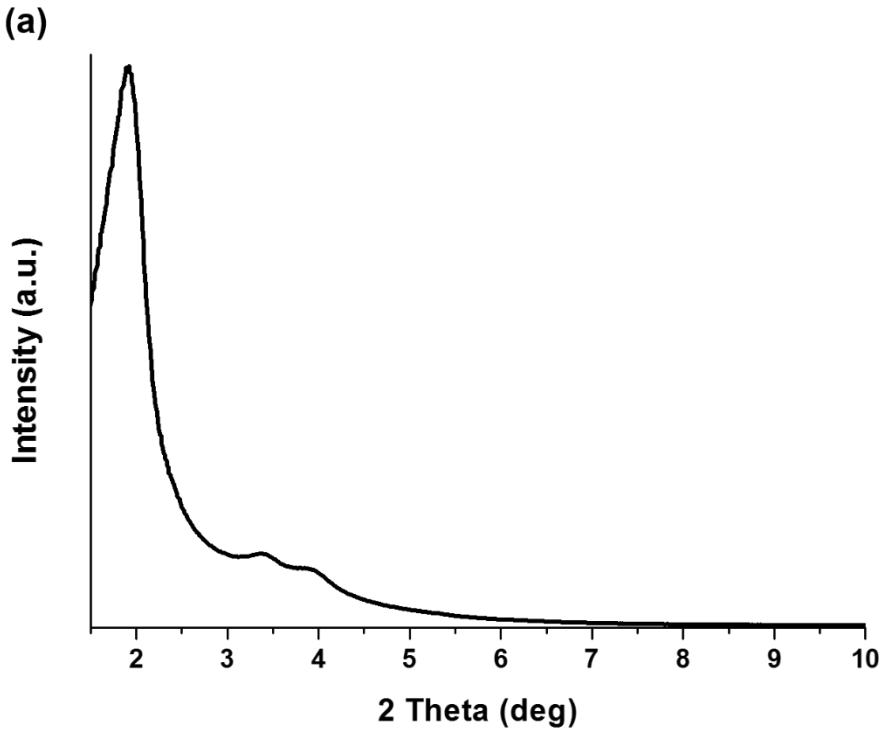

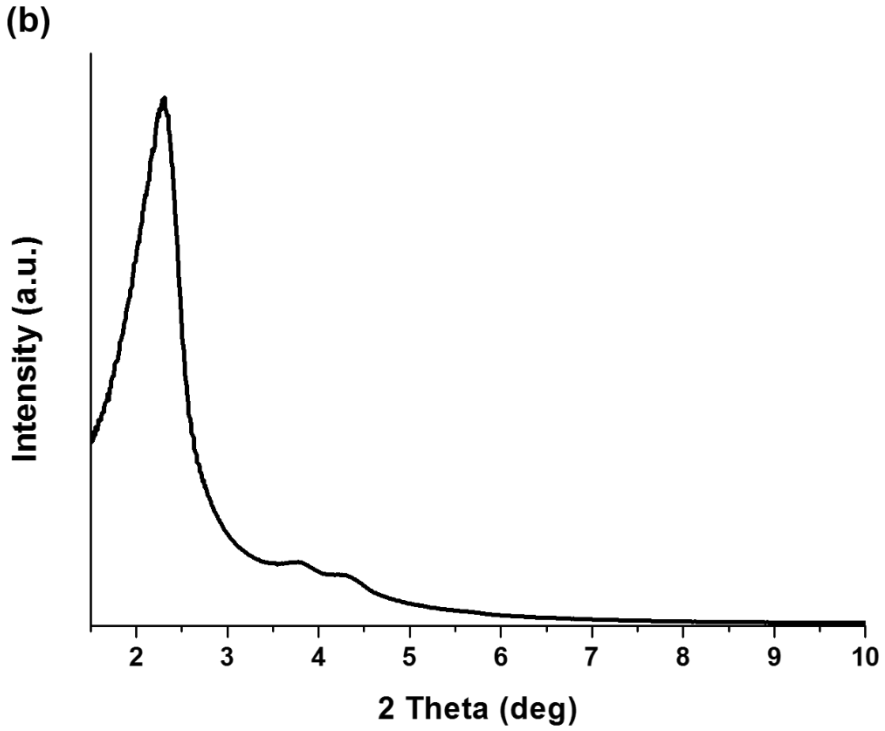

Figure V-5. Small angle XRD patterns of (a) DIMS-NH_2 and (b) TFPE-DIMS.

V-3-3. Photophysical Properties

Room temperature emission measurements were performed to investigate the optical properties of TFPE and TFPE-DIMS. Fluorescence spectra of a solution of TFPE and suspension of TFPE-DIMS in DMSO were measured by dissolving TFPE and dispersing TFPE-DIMS with the same molar quantities of chromophores in DMSO (Figure V-6a). The solution of TFPE in DMSO was nearly non-emissive. In the dilute DMSO solution, TFPE had intramolecular rotational freedom and nonradiative deactivation occurred dominantly after it was excited.[62-65] However, TFPE-DIMS showed a strong yellow-green fluorescence peak at 530 nm where TFPE molecules were covalently grafted onto the pore walls of the mesoporous silica. DIMS-NH_2 containing no chromophores was nonfluorescent. Figure V-6b presents the photographs of the DMSO solution of TFPE and

the suspensions of DIMS-NH_2 and TFPE-DIMS taken upon the irradiation with a UV lamp. The suspension of DIMS-NH_2 showed no fluorescence under the UV illumination. An extremely feeble fluorescence was observed for the solution of TFPE, while intense yellow and green light was emitted from TFPE-DIMS. These results suggested that immobilizing a TPE-cored AIE chromophores, especially with four aldehyde groups, into the pores of rigid silica matrix largely restricted intramolecular rotation, vibration, and torsion of the chromophore. This inhibited non-radiative relaxation channel and facilitated the radiative decay, thus improving the overall fluorescence.[66]

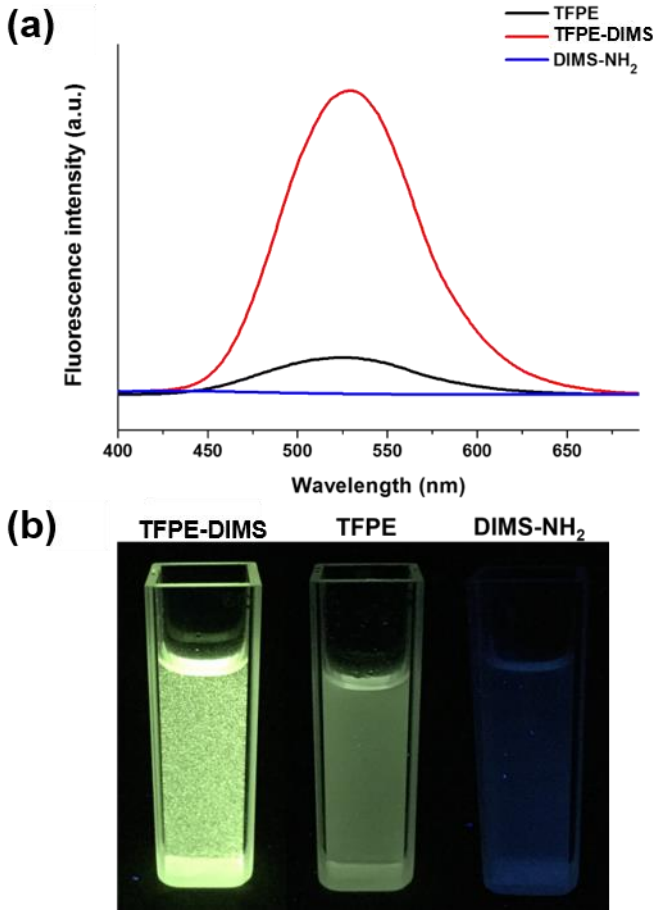

Figure V-6. (a) Fluorescence spectra of TFPE-DIMS and TFPE in DMSO. The spectrum of DIMS-NH_2 is measured for comparison. Concentration of AIE chromophore (TFPE): 10^{-5} M. Excitation wavelength (λ_{ex}): 350 nm. (b) Photographs of dispersions of TFPE-

DIMS and DIMS-NH_2, and solution of TFPE in DMSO; photographs taken upon irradiation with a UV light of 365 nm.

As depicted in Figure V-7a, the UV-vis spectrum of TFPE showed the broad absorption bands in the range of 250-450 nm. When excited at 350 nm in methanol, TFPE-DIMS exhibited a clear intense emission peak at around 530 nm in addition to the Rayleigh scattering peaks at 350 and 700 nm (Figure V-7b). A large Stokes shift of TFPE in TFPE-DIMS compared to that of TPE (λ_{em} = 480 nm) would be advantageous in sensing, which could minimize the influence of excitation light.[67]

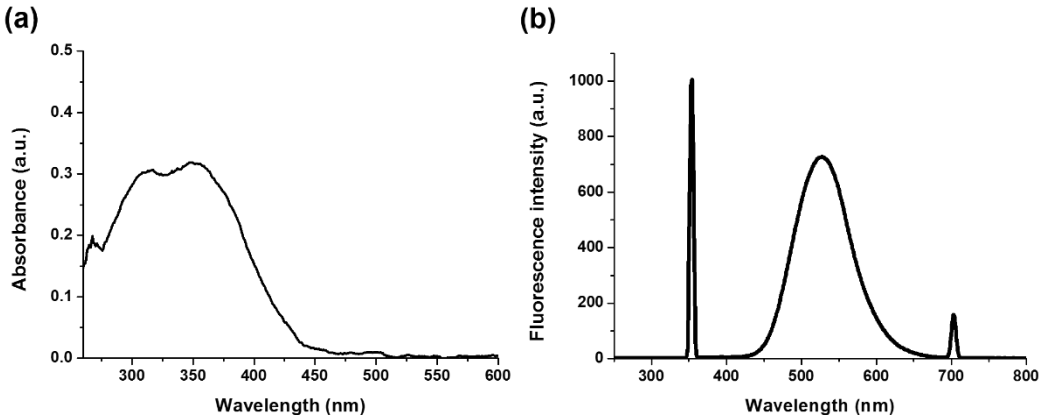

Figure V-7. (a) UV-vis absorption spectrum of TFPE; (b) emission spectrum of TFPE-DIMS dispersed in methanol (λ_{ex} = 350 nm).

V-3-4. Kinetic Binding Study of TFPE-DIMS

The kinetic binding study of TFPE-DIMS was conducted to measure its recognition ability for the target molecule, DES (Figure V-8). TFPE-DIMS (2.0 mg) were dispersed in a solution of DES (500 ng mL^{-1}) in methanol (20 mL) with stirring and the fluorescence spectrum was recorded at 10 min intervals. The maximum fluorescence intensity was

rapidly quenched with time up to the first 10 to 20 min. The equilibrium quenching reached within 60 min, suggesting that the template molecules could access the binding sites easily.

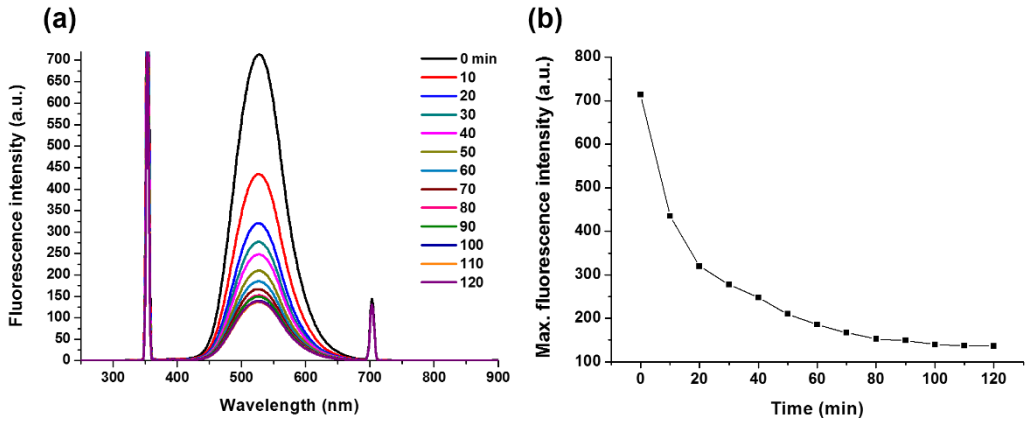

Figure V-8. (a) Kinetic binding profile of emission spectra of TFPE-DIMS (100 μg mL^{-1}) in the presence of DES (500 ng mL^{-1}) recorded after incubating for constant periods of time in methanol (λ_{ex} = 350 nm); (b) Plot of the maximum fluorescence intensity with respect to incubation time.

V-3-5. Molecular Recognition Properties of TFPE-DIMS

Fluorescence quenching of TFPE-DIMS and TFPE-NIMS as a function of the concentration of DES was investigated. Fluorescence spectra of TFPE-DIMS were collected 10 min after stirring TFPE-DIMS with a solution of DES in methanol. Upon increasing concentrations of DES (100 to 700 ng mL^{-1}), the fluorescence intensity of TFPE-DIMS rapidly decreased (Figure V-9a), but much smaller degrees of quenching was observed with TFPE-NIMS (Figure V-9b), demonstrating that the specific binding of DES to the imprinted cavities occurred.

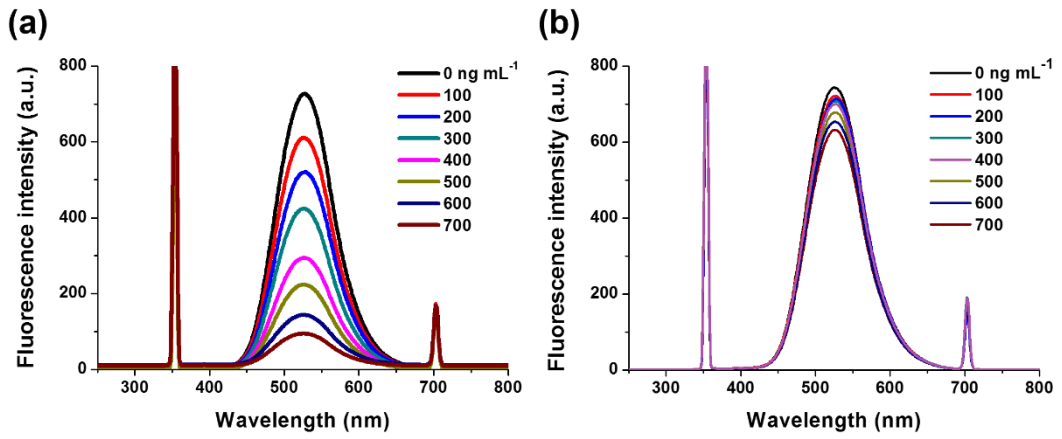

Figure V-9. Fluorescence emission spectra of (a) TFPE-DIMS (100 μg mL^{-1}) and (b) TFPE-NIMS recorded after 10 min stirring upon a gradual increase on the concentration of DES in methanol (λ_{ex} = 350 nm).

To further study the selectivity of TFPE-DIMS, its fluorescence quenching behavior was tested in the presence of structural analogs of DES, including dienestrol (DN), bisphenol A (BPA) and 4,4'-biphenol (4BP).[68] The selectivity test was carried out in the same manner as described above. As shown in Figure V-10a, only a slight fluorescence quenching of TFPE-DIMS occurred for these analogs.

The fluorescence quenching response can be further evaluated by the Stern-Volmer equation[69]

$$F_0/F = 1 + K_{SV}[C]$$

where F and F_0 are the fluorescence intensities of TFPE-DIMS in the presence and absence of an analyte, respectively. [C] is the corresponding concentration of an analyte and K_{SV} is the Stern-Volmer quenching constant. This equation can be used for the quantitative analysis toward the target molecule. Linear Stern-Volmer plots of both TFPE-DIMS and TFPE-NIMS for DES and its structural analogs were obtained (Figure V-10b and V-10c). The Stern-Volmer quenching constant (K_{SV}) determined by the slopes of the

Stern-Volmer plots can be used to evaluate the selectivity of TFPE-DIMS. As depicted in Figure V-11, K_{SV} of TFPE-DIMS for DES was more than ten times higher than that for DES analogs. The imprinting factor (IF) which is the ratio of quenching constants of the imprinted and non-imprinted particles (i.e., IF = $K_{SV,\text{AIE-DIMS}}/K_{SV,\text{AIE-NIMS}}$) was 15.7.

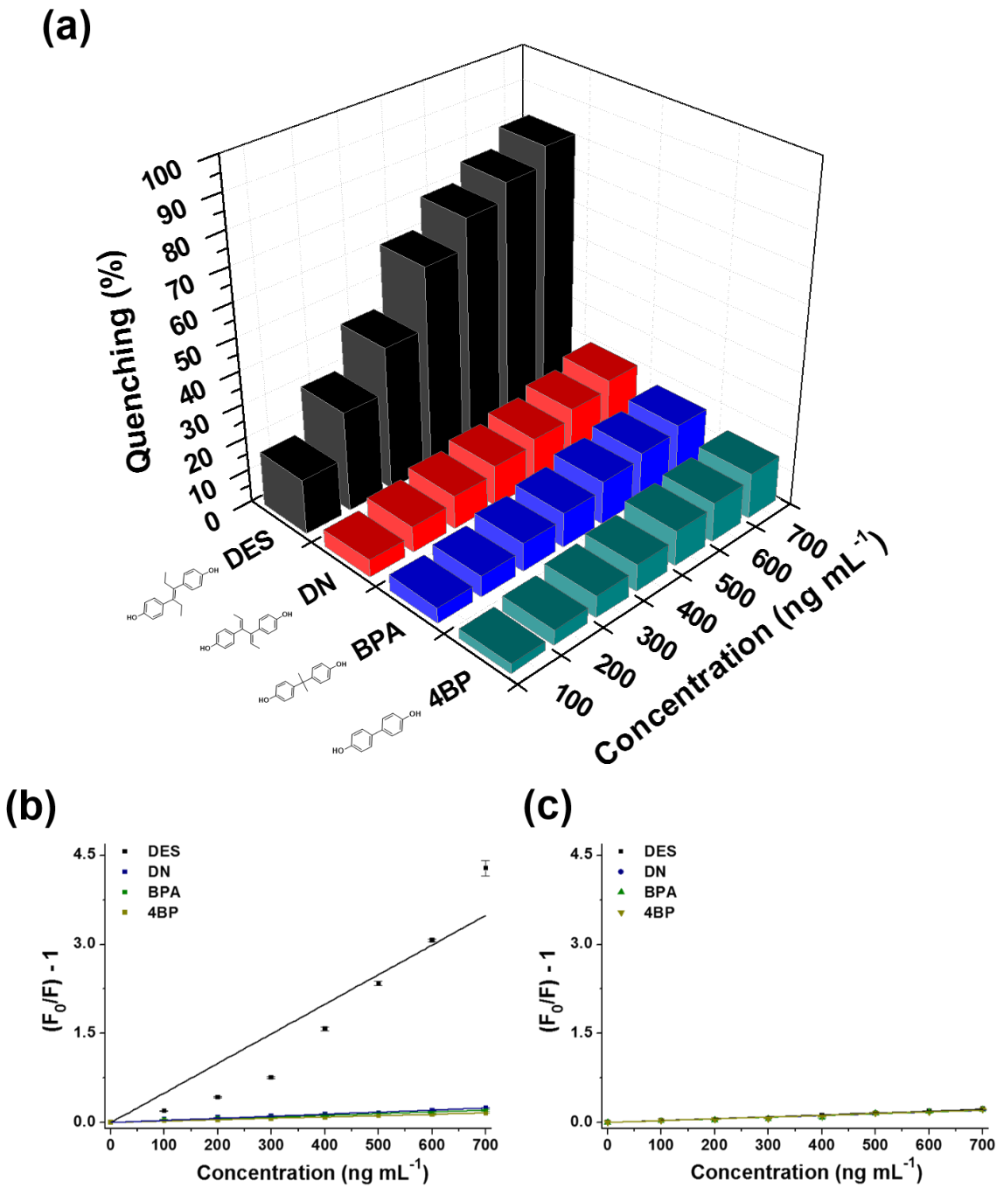

Figure V-10. (a) Cross-selectivity profile for DES and structurally related analogs in TFPE-DIMS (100 μg mL^{-1}) measured after 10 min stirring with an increase on the concentration of DES, DN, BPA and 4BP in methanol. Degree of quenching calculated as

Quenching (%) = $(1 - F/F_0)100$. Stern-Volmer plots estimated from (b) TFPE-DIMS and (c) TFPE-NIMS.

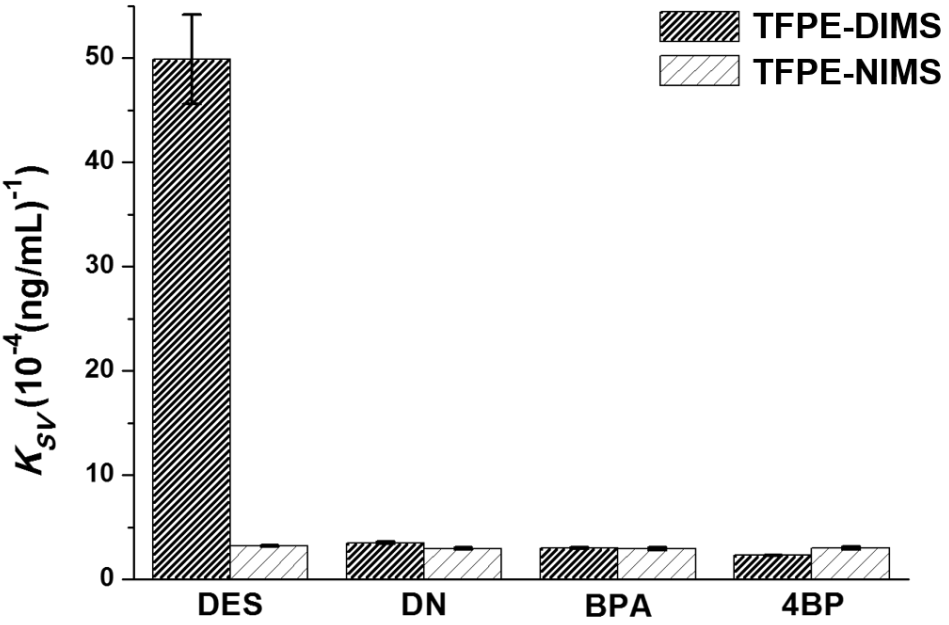

Figure V-11. Estimated Stern-Volmer quenching constants (K_{SV}) of TFPE-DIMS and TFPE-NIMS in relation to different analytes. For all the experiments, the excitation wavelength was 350 nm.

V-3-6. Recycability Test

The reusability of TFPE-DIMS was examined by consecutive binding, extraction and rebinding experiments. TFPE-DIMS (2.0 mg) was dispersed in a solution of DES (100 ng mL^{-1}) in methanol (20 mL) with stirring for 30 min, allowing most binding sites to be filled with the template molecule and the subsequent extraction of the bound DES after the evaporation of methanol was carried out. TFPE-DIMS nearly maintained its initial

fluorescence intensity and showed the almost same fluorescence quenching behavior in the extraction-rebinding process. During the repetition of the extraction-rebinding cycles seven times, the overall fluorescence intensity of TFPE-DIMS decreased by ca. 6% compared to that of as-prepared TFPE-DIMS (Figure V-12).

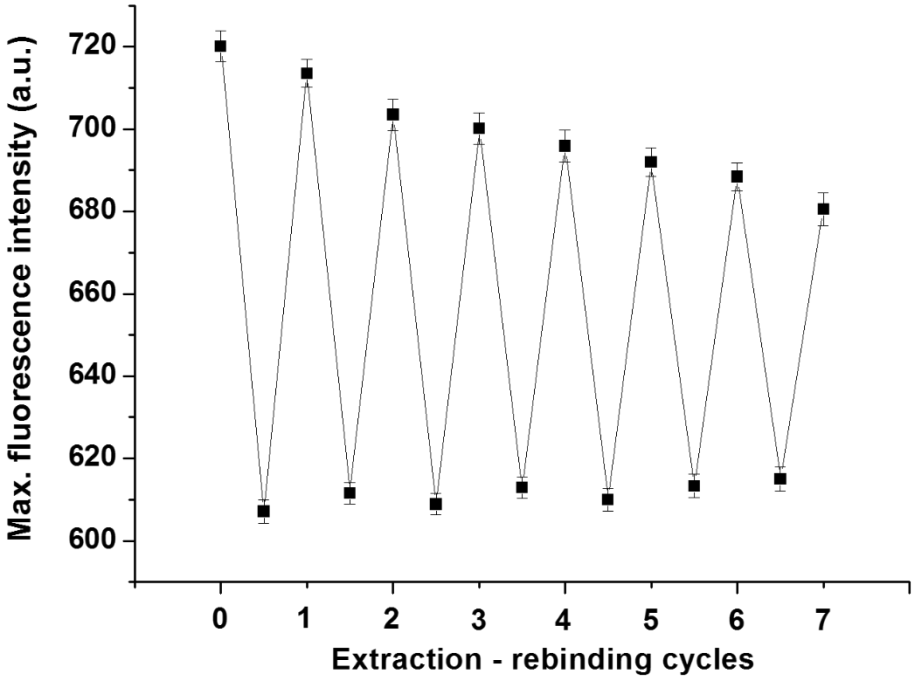

Figure V-12. Recovery of the fluorescence intensity upon the repeated cycles of extraction and rebinding of DES in the dispersion medium of TFPE-DIMS.

V-4. Conclusions

In summary, AIE-active chromophores (TFPE)-grafted molecularly imprinted mesoporous silica nanoparticles (TFPE-DIMS) were fabricated as a fluorescent DES sensor. The silica framework between the pores was used for a molecular imprinting matrix in which the delicate two-point binding sites were formed. An AIE chromophore (TFPE) was introduced onto the pore walls of the imprinted mesoporous silica as a fluorescent probe. TFPE-DIMS displayed excellent sensitivity and selectivity in fluorescent sensing of the target analyte. A concentration-sensitive fluorescence quenching of TFPE-DIMS was observed due to a close proximity of the bound template to TFPE.

V-5. References

1. Wu, C.; Zheng, J.; Huang, C.; Lai, J.; Li, S.; Chen, C.; Zhao, Y. *Angew. Chem. Int. Ed.* **2007**, 46, 5393-5396.

2. Minkowski, C.; Pansu, R.; Takano, M.; Calzaferri, G. *Adv. Funct. Mater.* **2006**, 16, 273-285.

3. Watanabe, H.; Kunitake, T. *Chem. Mater.* **2008**, 20, 4998-5004.

4. Palomares, E.; Martinez-Diaz, M. V.; Torres, T.; Coronado, E. *Adv. Funct. Mater.* **2006**, 16, 1166-1170.

5. Wei, Z.; Gu, Z.-Y.; Arvapally, R. K.; Chen, Y.-P.; McDougald, Jr., R. N.; Ivy, J. F.; Yakovenko, A. A.; Feng, D.; Omary, M. A.; Zhou, H.-C. *J. Am. Chem. Soc.* **2014**, 136, 8269-8276.

6. Li, H.-Y.; Wei, Y.-L.; Dong, X.-Y.; Zang, S.-Q.; Mak, T. C. W. *Chem. Mater.* **2015**, 27, 1327-1331.

7. Heck, J. G.; Napp, J.; Simonato, S.; Möllmer, J.; Lange, M.; Reichardt, H. M.; Staudt, R.; Alves, F.; Feldmann, C. *J. Am. Chem. Soc.* **2015**, 137, 7329-7336.

8. Kwak, S.-Y.; Kim, N. R.; Lee, K.; Yi, J.; Kim, J. H.; Bae, B.-S. *J. Sol-Gel Sci. Technol.* **2011**, 60, 137-143.

9. Taranekar, P.; Qiao, Q.; Jiang, H.; Ghiviriga, I.; Schanze, K. S.; Reynolds, J. R. *J. Am. Chem. Soc.* **2007**, 129, 8958-8959.

10. Maitra, U.; Jain, A.; George, S. J.; Rao, C. N. R. *Nanoscale* **2011**, 3, 3192-3197.

11. Mansur, A. A. P.; Mansur, H. S.; Soriano-Araújo, A.; Lobato, Z. I. P. *ACS Appl. Mater. Interfaces* **2014**, 6, 11403-11412.

12. Wang, S.; Kang, Y.; Wang, L.; Zhang, H.; Wang, Y.; Wang, Y. *Sens. Actuators B* **2013**,

182, 467-481.

13. Wang, H.; Yi, J.; Velado, D.; Yu, Y.; Zhou, S. *ACS Appl. Mater. Interfaces* **2015**, 7, 15735-15745.

14. Jalili, R.; Amjadi, M. *RSC Adv.* **2015**, 5, 74084-74090.

15. Zhang, Z.; Li, J.; Wang, X.; Shen, D.; Chen, L. *ACS Appl. Mater. Interfaces* **2015**, 7, 9118-9127.

16. Kim, H.; Kim, Y.; Chang, J. Y. *Macromol. Chem. Phys.* **2014**, 215, 1274-1285.

17. Ton, X.-A.; Tse Sum Bui, B.; Resmini, M.; Bonomi, P.; Dika, I.; Soppera, O.; Haupt, K. *Angew. Chem. Int. Ed.* **2013**, 52, 8317-8321.

18. Haupt, K.; Mosbach, K. *Chem. Rev.* **2000**, 100, 2495-2504.

19. Wulff, G. *Chem. Rev.* **2002**, 102, 1-27.

20. Whitcombe, M. J.; Vulfson, E. N. *Adv. Mater.* **2001**, 13, 467-477.

21. Ye, L.; Mosbach, K. *Chem. Mater.* **2008**, 20, 859-868.

22. Lai, J.-P.; Yang, M.-L.; Niessner, R.; Knopp, D. *Anal. Bioanal. Chem.* **2007**, 389, 405-412.

23. Dvorakova, G.; Haschick, R.; Chiad, K.; Klapper, M.; Müllen, K.; Biffis, A. *Macromol. Rapid Commun.* **2010**, 31, 2035-2040.

24. Yu, S.; Luo, A.-q.; Biswal, D.; Hilt, J. Z.; Puleo, D. A. *Talanta* **2010**, 83, 156-161.

25. Ma, Y.; Pan, G.; Zhang, Y.; Guo, X.; Zhang, H. *Angew. Chem. Int. Ed.* **2013**, 52, 1511-1514.

26. Jung, B. M.; Kim, M. S.; Kim, W. J.; Chang, J. Y. *Chem. Commun.* **2010**, 46, 3699-3701.

27. Lofgreen, J. E.; Moudrakovski, I. L.; Ozin, G. A. *ACS Nano* **2011**, 5, 2277-2287.

28. Kim, Y.; Jeon, J. B.; Chang, J. Y. *J. Mater. Chem.* **2012**, 22, 24075-24080.

29. Kim, M. S.; Chang, J. Y. *J. Mater. Chem.* **2011**, 21, 8766-8771.

30. Kim, M. S.; Jeon, J. B.; Chang, J. Y. *J. Mater. Chem.* **2012**, 22, 20713-20718.

31. Li, L.-L.; Sun, H.; Fang, C.-J.; Xu, J.; Jin, J.-Y.; Yan, C.-H. *J. Mater. Chem.* **2007**, 17, 4492-4498.

32. Wang, Y.; Li, B.; Zhang, L.; Liu, L.; Zuo, Q.; Li, P. *New J. Chem.* **2010**, 34, 1946-1953.

33. Gomes, R.; Bhaumik, A. *Micropor. Mesopor. Mater.* **2015**, 207, 71-77.

34. Qin, W.; Li, K.; Feng, G.; Li, M.; Yang, Z.; Liu, B.; Tang, B. Z. *Adv. Funct. Mater.* **2014**, 24, 635-643.

35. Zhang, Y.; Wang, J.-H.; Zheng, J.; Li, D. *Chem. Commun.* **2015**, 51, 6350-6353.

36. Banal, J. L.; White, J. M.; Ghiggino, K. P.; Wong, W. W. H. *Sci. Rep.* **2014**, 4, 1-5.

37. Zhao, Z.; Chan, C. Y. K.; Chen, S.; Deng, C.; Lam, J. W. Y.; Jim, C. K. W.; Hong, Y.; Lu, P.; Chang, Z.; Chen, X.; Lu, P.; Kwok, H. S.; Qiu, H.; Tang, B. Z. *J. Mater. Chem.* **2012**, 22, 4527-4534.

38. Tong, H.; Hong, Y.; Dong, Y.; Häussler, M.; Li, Z.; Lam, J. W. Y.; Dong, Y.; Sung, H. H.-Y.; Williams, I. D.; Tang, B. Z. *J. Phys. Chem. B* **2007**, 111, 11817-11823.

39. Shustova, N. B.; McCarthy, B. D.; Dincă, M. *J. Am. Chem. Soc.* **2011**, 133, 20126-20129.

40. Sengupta, S. *Synlett* **2004**, 7, 1191-1194.

41. Luo, W.; Zhu, Y.; Zhang, J.; He, J.; Chi, Z.; Miller, P. W.; Chen, L.; Su, C.-Y. *Chem. Commun.* **2014**, 50, 11942-11945.

42. Hu, Z.; Huang, G.; Lustig, W. P.; Wang, F.; Wang, H.; Teat, S. J.; Banerjee, D.; Zhang, D.; Li, J. *Chem. Commun.* **2015**, 51, 3045-3048.

43. Soto, A. M.; Sonnenschein, C. *Nat. Rev. Endocrinol.* **2015**, 11, 507-508.

44. Rezg, R.; El-Fazaa, S.; Gharbi, N.; Mornagui, B. *Environ. Int.* **2014**, 64, 83-90.

45. Gibson, D. A.; Saunders, P. T. K. Endocr.-Relat. *Cancer* **2014**, 21, T13-T31.

46. Rubin, B. S. *J. Steroid Biochem. Mol. Biol.* **2011**, 127, 27-34.

47. Potter, J. D. *Cancer Epidemiol. Biomarkers Prev.* **2011**, 20, 574-577.

48. Soto, A. M.; Sonnenschein, C. *Nat. Rev. Endocrinol.* **2010**, 6, 363-370.

49. Ki, C. D.; Oh, C.; Oh, S.-G.; Chang, J. Y. *J. Am. Chem. Soc.* **2002**, 124, 14838-14839.

50. Lee, K.; Ki, C. D.; Kim, H.; Chang, J. Y. *Macromolecules* **2004**, 37, 5544-5549.

51. Luan, Z.; Fournier, J. A.; Wooten, J. B.; Miser, D. E. *Micropor. Mesopor. Mater.* **2005**, 83, 150-158.

52. Tonlé, I. K.; Diaco, T.; Ngameni, E.; Detellier, C. *Chem. Mater.* **2007**, 19, 6629-6636.

53. Modak, A.; Mondal, J.; Aswal, V. K.; Bhaumik, A. *J. Mater. Chem.* **2010**, 20, 8099-8106.

54. Chen, Q.; Wang, J.-X.; Yang, F.; Zhou, D.; Bian, N.; Zhang, X.-J.; Yan, C.-G.; Han, B.-H. *J. Mater. Chem.* **2011**, 21, 13554-13560.

55. Miao, C.; Li, D.; Zhang, Y.; Yu, J.; Xu, R. *Microporous Mesoporous Mater.* **2014**, 196, 46-50.

56. Choi, M.; Heo, W.; Kleitz, F.; Ryoo, R. *Chem. Commun.* **2003**, 1340-1341.

57. Zhao, D.; Feng, J.; Huo, Q.; Melosh, N.; Fredrickson, G. H.; Chmelka, B. F.; Stucky, G. D. *Science* **1998**, 279, 548-552.

58. Dey, A.; Kirchner, M. T.; Vangala, V. R.; Desiraju, G. R.; Mondal, R.; Howard, J. A. K. *J. Am. Chem. Soc.* **2005**, 127, 10545-10559.

59. Cagnol, F.; Grosso, D.; Sanchez, C. *Chem. Commun.* **2004**, 1742-1743.

60. Nicole, L.; Boissière, C.; Grosso, D.; Hesemann, P.; Moreau, J.; Sanchez, C. *Chem. Commun.* **2004**, 2312-2313.

61. Quach, A.; Escax, V.; Nicole, L.; Goldner, P.; Guillot-Noël, O.; Aschehoug, P.; Hesemann, P.; Moreau, J.; Gourier, D.; Sanchez, C. *J. Mater. Chem.* **2007**, 17, 2552-2560.

62. Luo, J.; Xie, Z.; Lam, J. W. Y.; Cheng, L.; Chen, H.; Qiu, C.; Kwok, H. S.; Zhan, X.;

Liu, Y.; Zhu, D.; Tang, B. Z. *Chem. Commun.* **2001**, 1740-1741.

63. Tracy, H. J.; Mullin, J. L.; Klooster, W. T.; Martin, J. A.; Haug, J.; Wallace, S.; Rudloe, I.; Watts, K. *Inorg. Chem.* **2005**, 44, 2003-2011.

64. Tong, H.; Dong, Y.; Häußler, M.; Hong, Y.; Lam, J. W. Y.; Sung, H. H.-Y.; Williams, I. D.; Kwok, H. S.; Tang, B. Z. *Chem. Phys. Lett.* **2006**, 428, 326-330.

65. Ning, Z.; Chen, Z.; Zhang, Q.; Yan, Y.; Qian, S.; Cao, Y.; Tian, H. *Adv. Funct. Mater.* **2007**, 17, 3799-3807.

66. Li, D.; Yu, J.; Xu, R. *Chem. Commun.* **2011**, 47, 11077-11079.

67. Ghosh, B.; Masuda, Y.; Wakayama, Y.; Imanaka, Y.; Inoue, J.-i.; Hashi, K.; Deguchi, K.; Yamada, H.; Sakka, Y.; Ohki, S.; Shimizu, T.; Shirahata, N. *Adv. Funct. Mater.* **2014**, 24, 7151-7160.

68. Nakagawa, Y.; Tayama, S. *Arch. Toxicol.* **2000**, 74, 99-105.

69. Wang, J.; Wang, D.; Miller, E. K.; Moses, D.; Bazan, G. C.; Heeger, A. J. *Macromolecules* **2000**, 33, 5153-5158.

국문 요약

분자날인법은 사용이 용이하고 비용이 적게 드는 장점을 가져 분자 인식 재료의 실용적인 제조 방법으로 평가되고 있다. 본 연구에서는 다양한 형광 발광 물질들을 신호 전달체로 이용하여 분자 날인된 나노재료들을 기반으로 한 형광센서들을 제조하였다.

CdSe 양자점을 신호전달체로, 메조포러스 실리카 나노 입자를 분자 인식 재료로 이용하여 높은 감응도를 갖는 분자 날인된 형광센서를 제조하였다. 내분비계교란물질로 알려진 비스페놀 A를 주형분자로 이용하였다. 분자날인된 결합자리를 기공들 사이의 실리카에 선택적으로 형성하였고, CdSe 양자점들은 기공 내부에 도입하였다. 양자점이 도입된, 분자날인된 메조포러스 실리카 나노 입자는 감도와 선택도 면에서 우수한 분자인식능력을 보였다. 분자인식자리와 양자점 간의 가까운 거리로 인하여 CdSe 양자점의 형광이 비스페놀 A의 농도에 따라 민감하게 감소하였다. 또한 주형분자에 대해 선형의 Stern-Volmer 그래프를 보였으며, 주형분자와 구조적으로 유사한 분자들에 비해 열 배가 넘는 우수한 Stern-Volmer 발광감소 상수를 보였다.

유기젤 상태 중합반응을 이용하여 분자인식 고분자 나노파이버를 합성하고 이를 형광센서의 제조에 응용하였다. 신호전달체로는 CdSe/ZnS 양자점을 이용하였다. 아크릴기와 디아세틸렌기, 두 종류의 중합기를 갖는 다기능성 젤화제를 합성하고 다기능성 젤화제와 구조가 유사하고 주형분자와 복합체를 이루는 기능성 단량체를 합성하였다. 히스타민(주형분자), 기능성 단량

체, 양자점, 디비닐벤젠(가교제), 광개시제, 젤화제가 포함된 유기젤을 데칸에서 제조하고 유기젤 상태에서 광중합을 진행한 후, 주형분자를 제거하여 히스타민이 분자날인된 고분자 나노파이버를 제조하였다. 나노파이버 형태의 형광센서는 히스타민을 빠르고 정량적으로 인식하였으며 재사용이 가능하였다.

풀러린을 함유하는 분자인식 실리카 나노복합체를 제조하였다. 디에틸스틸베스트롤을 주형분자로 선택하였다. 계면활성제의 도움으로 마이크로 에멀션 안에 존재하는 풀러린을 TEOS와 주형분자인 디에틸스틸베스트롤이 결합된 실리카 전구체의 졸-젤 반응을 통하여 실리카에 도입하였다. 제조된 분자날인 풀러린-실리카 나노복합체는 높은 파장에서 광발광 현상을 나타내었고, 다양한 주형분자 농도에서 빠르고 정량적인 광발광 감소 효과를 보였다.

Aggregation induced emission(AIE) 성질을 나타내는 테트라페닐에텐(TPE)계 발광물질을 도입한 분자인식 메조포러스 실리카 나노입자를 제조하였다. 주형분자인 디에틸스틸베스트롤과 실리카 전구체가 열가역적 우레탄 결합으로 연결된 주형분자 복합체인 TES-DES를 합성하였다. AIE 발광물질이 기공 내부에 도입되고, 디에틸스틸베스트롤이 날인된 메조포러스 실리카 나노입자(TFPE-DIMS)를 TES-DES와 TEOS의 졸-젤 반응과 주형분자의 제거를 통하여 제조하였다. TFPE-DIMS는 주형분자에 대해 우수하고 빠른 분자인식능을 보였으며, Stern-Volmer 발광감소 상수를 비교하여 TFPE-DIMS가 주형분자를 선택적으로 인식하는 것을 확인하였다. 또한 반복적인 주형분자 제거와 결합에도 광발광 감소 효율이 크게 줄어들지 않았다.

주요어: 분자인식, 메조포러스 실리카, 유기젤, 풀러린, 양자점, 형광, 발광, 센서.

학번: 2011-30182

List of Publications

(1) Hyungwoo Kim, Youngdo Kim and Ji Young Chang, "Preparation of a molecularly imprinted polymer containing europium(III) ions for luminescent sensing", *J. Polym. Sci. A Polym. Chem.* **2012**, 50, 4990-4994.

(2) Youngdo Kim, Jae Bum Jeon and Ji Young Chang, "CdSe quantum dot-encapsulated molecularly imprinted mesoporous silica particles for fluorescent sensing of bisphenol A", *J. Mater. Chem.* **2012**, 22, 24075-24080.

(3) Hyungwoo Kim, Youngdo Kim and Ji Young Chang, "Polymers for luminescent sensing applications", *Macromol. Chem. Phys.* **2014**, 215, 1274-1285.

List of Presentations

(1) 2012년 10월, 추계 한국고분자학회, “CdSe quantum dot-encapsulated molecularly imprinted mesoporous silica particles for fluorescent sensing of bisphenol A”

(2) 2013년 4월, 춘계 한국고분자학회, “CdSe quantum dot-encapsulated molecularly imprinted mesoporous silica particles for fluorescent sensing of bisphenol A”

(3) 2013년 10월, 추계 한국고분자학회, “Fullerene-appended molecularly imprinted polymer for highly sensitive and selective recognition of doxorubicin”

(4) 2014년 4월, 춘계 한국고분자학회, “Molecularly imprinted fullerene-silica composite nanoparticles for highly sensitive and selective recognition of diethylstilbestrol”

(5) 2015년 10월, 추계 한국고분자학회, “CdSe/ZnS quantum dots embedded molecularly imprinted organogel nanofiber”